Shallow geothermal energy in district heating and cooling: a potential solution for decarbonising heating and cooling

Li, Xiang

UNIVERSITÉ DE GENÈVE **FACULTÉ DES SCIENCES**
Département F.-A. Forel Professeur M. K. Patel
des sciences de l'environnement et de l'eau
Institut des sciences de l'environnement

Shallow geothermal energy in district heating and cooling: a potential solution for decarbonising heating and cooling

THÈSE

présentée à la Faculté des sciences de l'Université de Genève
pour obtenir le grade de Docteur ès sciences, mention sciences de l'environnement

par

Xiang LI

de

Wenzhou (Chine)

Thèse N°5797

GENÈVE

Repromail – Université de Genève

2024

UNIVERSITÉ DE GENÈVE

FACULTÉ DES SCIENCES

DOCTORAT ÈS SCIENCES, MENTION SCIENCES DE L'ENVIRONNEMENT

Thèse de Madame Xiang LI

intitulée :

«Shallow Geothermal Energy in District Heating and Cooling: a Potential Solution for Decarbonising Heating and Cooling»

La Faculté des sciences, sur le préavis de Monsieur M..K. PATEL, professeur ordinaire et directeur de thèse (Département F.-A. FOREL des sciences de l'Environnement et de l'Eau), Monsieur J. CHAMBERS, docteur (Institut des sciences de l'environnement), Monsieur U. PERSSON, professeur (Innovation and Sustainability, School of Business, Halmstad University, Halmstad, Sweden), Monsieur P. ALBERG ØSTERGAARD, professeur (Department of Sustainability and Planning, University of Aalborg, Aalborg, Denmark), Madame S. YILMAZ, professeure (Faculté des géosciences et de l'environnement, Université de Lausanne, Lausanne) et Monsieur M. SULZER, professeur (Urban Energy System, Department of Engineering Sciences, Swiss Federal Laboratories for Materials Science and Techology, Dübendorf), autorise l'impression de la présente thèse, sans exprimer d'opinion sur les propositions qui y sont énoncées.

Genève, le 6 février 2024

Thèse - 5797 -

Le décanat

N.B. - La thèse doit porter la déclaration précédente et remplir les conditions énumérées dans les "Informations relatives aux thèses de doctorat à l'Université de Genève".

Abstract

To meet their climate neutrality objectives and effectively mitigate climate change, governments worldwide must urgently transition towards a sustainable, affordable, and reliable energy system. Heating and cooling play an essential role in this transition, as they currently account for more than half of the global total energy consumption, with cooling demand expected to surge in the coming decades. Immediate actions are imperative to replace the dominant use of fossil fuels for heating and cooling with renewable energy sources. District heating and cooling (DHC) has emerged as an enabler of large-scale penetration of renewable energy, projected to play a fundamental role in the future sustainable energy system. While numerous studies have explored the potential of district heating to decarbonise building heating demand, insufficient attention has been directed to growing cooling demand. Decarbonising cooling presents both a challenge and an opportunity. Waste heat generated by cooling applications can be used as a thermal source for heating purposes. Recent advancements in DHC technologies, including fourth-generation district heating (4GDH) and fifth-generation district heating and cooling (5GDHC), provide possibilities for exploiting these synergies. Shallow geothermal energy stands out as one of the most abundant renewable energy sources ideally suited for integration in DHC, given its versatility in supplying heating, cooling, and seasonal storage. Despite sufficient evidence showing the effectiveness of DHC and shallow geothermal energy for decarbonising heating and cooling, there is limited understanding about how to facilitate their massive deployment. Further research and methodological development are essential to fully understand and exploit their potential as integrated part of future sustainable energy systems.

This thesis introduces Geographic information system (GIS) based modelling frameworks to assess future cooling demand and investigate the potential role of DHC and shallow geothermal energy in addressing this growing cooling demand alongside heating demand. A data-driven building stock model is developed for detailed mapping of current and future space cooling demand in the service sector, focused on building-level analysis of space cooling diffusion and cooling systems characteristics. The space cooling demand, defined as the heat removed by the cooling appliances, is estimated to be 900 ± 200 GWh/year in the Swiss service sector in 2015. It is projected to increase by 400% - 600% by 2050 under climate scenarios of The Intergovernmental Panel on Climate Change (representative concentration pathway 2.6, 4.5, and 8.5), primarily driven by rising cooling system adoption under climate change. Next, a scalable modelling framework is proposed to quantify the technical potential of shallow geothermal energy for synergetic combined heating and cooling, considering seasonal

regeneration through re-injection of waste heat from space cooling. This approach integrates spatial analysis to account for spatial proximity constraints on resource allocation in scenarios for local heat exchange and for DHC. A case study in the Swiss cantons Vaud and Geneva reveals that shallow geothermal potential could cover up to 71% of service-sector cooling demand and up to 55% of heat demand in 2050 through local heat exchange, which increases to 87% and 85% when DHC is employed. Furthermore, a comprehensive investigation has been conducted to assess the economic, environmental, and technical performance of 5GDHC. This approach integrates spatial-temporal analysis of DHC systems and techno-economic assessment. The 5GDHC under examination connects decentralised heat pumps to shallow geothermal energy (serving as borehole thermal energy storage, BTES) to unlock the potential synergy of heating and cooling. Special attention is given to scenarios with balanced yet asynchronous heating and cooling loads and to assess the implications of increasing cooling load relative to heating. Results from a case study in the canton of Geneva show that 5GDHC integrated with BTES facilitates seasonal balancing of heating and cooling demands, leading to lower levelized cost of energy, reduced greenhouse gas emission, decreased exergy consumption, and lower electricity peak load compared to the stand-alone air source heat pump system. However, the higher upfront costs of such system, mainly attributed to borehole drilling and heat pump installation, might be a barrier to its adoption. The applicability of 5GDHC with BTES across various conditions, especially considering rising cooling loads, is explored through global sensitivity analysis. Results indicate that the cooling adoption rate is the most dominating factor deciding whether 5GDHC with BTES economically outperforms alternative systems, such as stand-alone air source heat pump system. Cooling adoption rates that maintain a balanced cooling and heating demands are more likely to lead to the better economic performance of 5GDHC with BTES. This advantage arises from the reduced borehole drilling requirements due to long-term equilibrium of the ground when utilized for well-balanced heating and cooling demands.

Overall, this thesis has advanced the understanding of the crucial role of DHC based on shallow geothermal energy in decarbonising heating and cooling, with a particular focus on understanding and addressing the future growth of cooling energy demand. This work lays the foundation for comprehensive methodologies to evaluate the potential of DHC and shallow geothermal energy, bridging critical knowledge gaps, and providing essential data to support the future deployment of these systems that can effectively meet both heating and cooling demands in the future. The developed modelling frameworks are scalable and adaptable for application in other countries, which can be used by policy makers, energy utilities, and researchers to assess and implement future sustainable energy solutions.

Résumé

Pour atteindre leurs objectifs de neutralité climatique et atténuer efficacement le changement climatique, les gouvernements du monde entier doivent passer d'urgence à un système énergétique durable, fiable et peu coûteux. Le chauffage et la climatisation jouent un rôle essentiel dans cette transition, car ils représentent actuellement plus de la moitié de la consommation totale d'énergie dans le monde, et la demande de climatisation devrait augmenter dans les décennies à venir. Il est impératif de prendre des mesures immédiates pour remplacer l'utilisation dominante des combustibles fossiles pour le chauffage et la climatisation par des sources d'énergie renouvelables. Les réseaux de chaleur et de froid à distance, ou réseaux thermiques (RTs), sont apparus comme un moyen de favoriser la pénétration à grande échelle des énergies renouvelables et devraient jouer un rôle fondamental dans le futur système énergétique durable. Alors que de nombreuses études ont exploré le potentiel de la chaleur à distance (CAD) pour décarboniser la demande de chauffage des bâtiments, la demande croissante de froid n'a pas fait l'objet d'une attention suffisante. La décarbonisation de la climatisation représente à la fois un défi et une opportunité. La chaleur résiduelle générée par les systèmes de refroidissement peut être utilisée comme source de chaleur à des fins de chauffage. Les progrès récents des technologies RTs , y compris les réseaux de chaleur à distance de quatrième génération et les réseaux thermiques de cinquième génération (dits 5GDHC pour fifth-generation district heating and cooling, en anglais), offrent des possibilités d'exploitation de ces synergies. La géothermie de faible profondeur fournit l'une des sources d'énergie renouvelable les plus abondantes et les mieux adaptées à l'intégration dans les systèmes de chauffage et de climatisation, étant donné sa polyvalence en matière de chauffage, de refroidissement et de stockage saisonnier. Bien qu'il y ait suffisamment de preuves de l'efficacité des RTs et de la géothermie de faible profondeur pour décarboniser le chauffage et la climatisation, comment faciliter leur déploiement massif reste une question à explorer. Il est essentiel de poursuivre la recherche et le développement méthodologique afin de comprendre et d'exploiter pleinement leur potentiel en tant que partie intégrante des futurs systèmes énergétiques durables.

Cette thèse présente des cadres de modélisation basés sur des systèmes d'information géographique (SIG) pour évaluer la demande future de refroidissement et étudier le rôle potentiel des RT et de la géothermie de faible profondeur pour répondre à cette demande croissante de climatisation parallèlement à la demande de chauffage. Un modèle de parc immobilier basé sur des données est développé pour cartographier en détail les besoins actuels

et futurs en climatisation du secteur tertiaire, en se concentrant sur l'analyse de la diffusion et des caractéristiques des systèmes de climatisation à l'échelle des bâtiments. Le besoin en refroidissement des locaux dans le secteur tertiaire suisse, défini comme la chaleur extraite par les installations de climatisation, est estimé à 900 ± 200 GWh/an en 2015. Ce chiffre devrait augmenter de 400 % à 600 % d'ici 2050 selon les scénarios climatiques du Groupe d'experts intergouvernemental sur l'évolution du climat (Trajectoires représentatives de concentration RCP 2.6, 4.5 et 8.5), principalement en raison de l'adoption croissante de systèmes de climatisation dans un contexte de changement climatique. Ensuite, un cadre de modélisation évolutif est proposé pour quantifier le potentiel technique de la géothermie de faible profondeur combinant le chauffage et la climatisation en synergie, compte tenu de la régénération saisonnière par la réinjection de la chaleur extraite pour la climatisation des locaux. Cette approche intègre l'analyse spatiale pour tenir compte des contraintes de proximité sur l'allocation des ressources dans les scénarios d'échange de chaleur local et de RTs. Une étude de cas dans les cantons suisses de Vaud et de Genève révèle que la géothermie de faible profondeur pourrait couvrir jusqu'à 71 % de la demande en climatisation du secteur tertiaire et jusqu'à 55 % de la demande en chaleur d'ici 2050 grâce à l'échange direct de chaleur, ce chiffre passant à 87 % et 85 % si des RTs sont déployés.

En outre, une enquête complète a été menée pour évaluer les performances économiques, environnementales et techniques du 5GDHC. Cette approche intègre l'analyse spatio-temporelle des RTs et l'évaluation techno-économique. Le 5GDHC examiné relie les pompes à chaleur décentralisées à l'énergie géothermie de faible profondeur (servant de stockage de l'énergie thermique en puits SETP) pour libérer le potentiel de synergie entre le chauffage et la climatisation. Une attention particulière est accordée aux scénarios avec des besoins de chauffage et de climatisation équilibrés mais asynchrones et à l'évaluation des implications de l'augmentation du besoin en climatisation par rapport à celui en chauffage. Les résultats d'une étude de cas dans le canton de Genève montrent qu'un système 5GDHC relié à du SETP facilite l'équilibrage saisonnier des demandes de chauffage et de refroidissement, ce qui permet de réduire le coût actualisé de l'énergie (en anglais Levelized Cost of Energy – LCOE), les émissions de gaz à effet de serre, la consommation d'exergie et la charge de pointe de l'électricité par rapport à un système de pompe à chaleur indépendant. Toutefois, les coûts initiaux plus élevés d'un tel système 5GDHC, principalement attribuables au forage géothermique et à l'installation d'une pompe à chaleur centralisée, pourraient constituer un obstacle à son adoption. L'applicabilité de systèmes 5GDHC avec SETP dans diverses conditions, en particulier en tenant compte de l'augmentation du besoin de refroidissement, est étudiée au moyen d'une analyse de sensibilité globale.

Les résultats suggèrent que, lorsque le taux d'adoption de systèmes de climatisation est le facteur déterminant de l'efficacité économique d'un système 5GDHC avec SETP par rapport à les

systèmes alternatifs, tels que les systèmes de pompe à chaleur indépendants. Les taux d'adoption de systèmes de climatisation qui maintiennent un équilibre entre la demande de climatisation et de chauffage ont plus de chances d'entraîner de meilleures performances économiques pour 5GDHC avec SETP. Cet avantage est dû à la réduction des besoins de forage en raison de l'équilibre à long terme du sol lorsqu'il est utilisé pour répondre à des demandes de chauffage et de climatisation bien équilibrées. Dans l'ensemble, cette thèse a permis de mieux comprendre le rôle crucial des RTs basés sur la géothermiqe de faible profondeur dans la décarbonisation du chauffage et de la climatisation, avec un accent particulier sur la compréhension et la réponse à la croissance future des besoins de climatisation. Ce travail pose des bases pour établir des méthodologies complètes pour évaluer le potentiel crucial des RTs basés sur la géothermiqe de faible profondeur, en comblant des lacunes importantes en matière de connaissances et en fournissant des données essentielles pour soutenir le déploiement futur de ces systèmes qui sont susceptibles de répondre efficacement à la fois aux demandes de chauffage et de climatisation à l'avenir. Les cadres de modélisation développés sont évolutifs et adaptables à d'autres pays. Ils peuvent être utilisés par les instances politiques, les distributeurs d'énergie et le monde académique pour évaluer et mettre en œuvre de futures solutions énergétiques durables.

Acknowledgements

Firstly, I would like to express my sincere gratitude to Prof. Martin Patel for offering me this extraordinary opportunity to pursue my lifelong dream of becoming a scientist, and for his continuous guidance, support, and invaluable feedback. I am equally thankful to my co-supervisors, Dr. Jonathan Chambers and Prof. Selin Yilmaz, for their dedication to guiding my research and supporting my personal development. They always made time to address my questions about my research, academic writing, or any other challenges I encountered at every stage of my PhD. They have served as role models in numerous aspects of my professional and personal life. Additionally, I extend my sincere thanks to my thesis committee members, Prof. Matthias Sulzer, Prof. Urban Persson, Prof. Poul Alberg Østergaard, for their keen interest, insightful comments, and encouragement. Their constructive feedback has been instrumental in refining my work and broadening my perspectives.

I am also deeply grateful for the funding provided by Future Energy Efficient Buildings & Districts (SCCER-FEEB&D) and SWiss Energy research for the Energy Transition (SWEET) project DeCarbCH (Decarbonisation of Cooling and Heating in Switzerland).

I am fortunate to have collaborated with excellent researchers, Dr. Alina Walch, Dr. Nahid Mohajeri, and Prof. Jean-Louis Scartezzini, in the field of shallow geothermal energy. Our fruitful and inspiring collaboration has significantly enriched this thesis and my academic journey as a whole. Special thanks go to my dear officemates, Stefano, Francesco, for the fruitful exchange of ideas during our coffee breaks and lunches. I am also thankful to my colleagues and close friends, Ruchi, Xin, Kai, Navdeep, Mart, Imane, Thomas, Arven, Julien, Mohammad-Reza, Mostafa, for their professional support and unforgettable adventures we have shared in and around Geneva.

To my friends in Geneva, thank you for making me feel at home in a place far from where I started. A heartfelt thanks to my best friend and PhD buddy, Yi, for sharing emotions and thoughts through every peak and valley of this journey.

Last but not least, I thank my parents, brother, and extended family for their strong support and belief in my pursuits. And to my partner, Zhenglyu, your unconditional love and encouragement have been a constant source of strength during the most challenging times.

Table of Contents

List of figures

List of tables

List of Acronyms

3GDH	Third generation district heating
4GDH	Fourth generation district heating
5GDHC	Fifth generation district heating and cooling
AIC	Akaike's Information Criterion
ASHP	Air-source heat pumps
BAU	Business-As-Usual
BHE	Borehole heat exchanger
BHP	Booster heat pump
BTES	Borehole thermal energy storage
CDD	Cooling degree days
COP	Coefficient of performance
D	Scenario with district heating and cooling
DC	District cooling
DH	District heating
DHC	District heating and cooling
DHW	Domestic hot water
DOC	Demand overlap coefficient
EU	European Union
FC	Full cooling
GIS	Geographic information system
GSHP	Ground-source heat pump
HDD	Heating degree days
HGSHP	Hybrid ground-source heat pump
HP	Heat pump
HX	Heat exchanger
IPCC	The Intergovernmental Panel on Climate Change
LTDH	Low-temperature district heating
NC	Scenario of no cooling
ND	Scenario without district heating and cooling

O&M	Operation and maintenance
PC	Scenario of partial cooling
R^2	Coefficient of determination
RCP	Representative concentration pathway
RegBL	Swiss building registry *(Registre fédéral des bâtiments et des lodgements)*
SAO	Spatial allocation with optimisation
SC	Space cooling
SH	Space heating
STES	Seasonal thermal energy storage
TLM	Topographic landscape model
VIF	Variance inflation factor
WCP	Water circulation pump

1 Introduction

1.1 Background

Climate change represents one of most significant challenges for humanity in the 21st century, primarily driven by greenhouse gas (GHG) emissions from fossil fuels combustion, where the energy is used in industry, transport and building sector. Numerous countries have set GHG emission reduction goals as part of their commitments under the 2015 Paris Agreement [1]. For instance, the European Union (EU) committed itself to reduce its GHG emission by at least 55% by 2030 compared with the 1990 level [2]. Switzerland aims to achieve climate neutrality by 2050 [3]. To fulfil these pledges, an urgent transition to a sustainable, affordable, and reliable energy system is required in the coming decades.

Decarbonizing the heating and cooling sector is critical in this energy transition. Heating and cooling account for approximately half of the EU's energy demand [4], and 35% of Switzerland's total energy use is attributed to heating and cooling [5]. Moreover, the demand for cooling is projected to surge due to factors such as rising heat waves caused by climate change and increasing expectations for thermal comfort [6]. Despite its importance, the role of renewable heating and cooling has received limited attention from policy makers. By the end of 2022, only 29 countries, mainly in Europe, had announced targets for renewable heating and cooling, while 135 countries have national targets for renewable power generation [7]. As a result, the heating and cooling sector still heavily relies on fossil fuels today, with a limited renewable share of 11%. In contrast, the renewable share of global electricity achieved a steady growth and reached 28% in 2021 [7]. Urgent actions are needed to replace fossil fuels for heating and cooling with renewable energy sources.

Various renewable energy sources are available for decarbonising heating and cooling, such as biomass, solar energy, geothermal energy, and ambient heat (e.g., from air, soil, water bodies) [8]. Apart from reducing GHG emissions, renewables heating and cooling provides other benefits including improved air quality and strengthened energy security due to increased and more efficient use of local resources [9]. However, multiple barriers slow down the adoption of renewable heating and cooling [10]. One important technical challenge is that most renewable thermal energy sources are geospatially bounded. Unlike electricity, transporting thermal energy is subject to considerable losses, making it necessary to be consumed in proximity. Another technical barrier relates to temperature compatibility between renewable energy source

and demands. Some low-temperature renewable resources (e.g., geothermal energy, ambient heat) may not be able to fully meet the temperature required by specific users (e.g., poorly insulated houses).

District heating and cooling (DHC) has been identified as an enabler of large-scale penetration of renewable energy and is projected to play a fundamental role in the future sustainable energy system. DHC uses a pipe network to deliver thermal energy (for heating or cooling) to multiple consumers in the residential, commercial, or industrial sector, allowing to integrate local available renewable energy into the energy mix. Despite their substantial potential for renewable integration, the current share of heating and cooling supplied by DHC is low and its penetration is slow [11]. To speed up the transition to renewable energy, accelerated deployment of DHC is needed, which forms a cornerstone of decarbonization strategies in countries like Denmark [11], Germany[12], and Switzerland [13]. Comprehensive planning is key for local, regional, and national development of DHC. More research is imperative to provide adequate data, knowledge, and methodologies for assessing the potentials of DHC to decarbonizing the heating and cooling sector.

1.2 Review of district heating and cooling

1.2.1 Renewable-based DHC

DHC is a well-established approach to for addressing building heating and cooling demand in urban environment. District heating systems (DH) have been widely used in North America, China, Scandinavia and Eastern Europe. In Europe, they cover 12% of total heat demand [14]. In contrast, district cooling systems (DC) are much less utilised than their equivalent for heating, mainly deployed in the Middle East and sparingly present in Europe [11]. Most DHC are supplied by fossil fuel today, with renewable energy accounting for only 8% of energy use in DHC in 2018 [15]. Nevertheless, a growing number of DHC projects across Europe have successfully integrated a wide range of renewable energy sources. Biomass is one of the largest renewable energy sources in district heating system [11]. It includes wood chips, agricultural residue, and food waste. Given their compatibility with boilers or cogeneration plants [16], biomass-based district heating systems are widely used in countries with abundant forest resources, like Sweden, Finland, and Austria [17]. Solar thermal collectors installed on rooftops or open spaces capture solar radiation for heating. Solar thermal based district heating have shown notable development in countries like Denmark and Germany [18]. Geothermal energy has contributed significantly to district heating systems, especially in Iceland [19]. Geothermal drilled wells and geothermal heat pumps are used to provide year-round heat production from subsurface. Free cooling for space cooling can be implemented using water from sea, lake, or rivers. Heat exchangers are used to transfer

heat from the building to the natural environment. District cooling based on free cooling can be found in France [20] and Switzerland [21].

Despite the significant potential of these renewable energy sources to supply DHC, they remain largely untapped. Adequate planning is crucial to speed up the deployment of renewable based DHC. Due to the local nature of thermal energy utilization, mapping and quantification of heating and cooling demand and local available thermal sources are a vital step for DHC planning and design. Several European-wide projects have been conducted to provide essential datasets on heating and cooling demands and renewable supplies to support strategic heating and cooling planning. HotMaps developed open-source tool for estimating heating and cooling energy as well as local renewable and waste heat potentials in GIS layers [22]. The considered renewable sources include biomass, waste heat, shallow geothermal, wind, and solar energy. The Pan-European Thermal Atlas (Peta) project provides mapping and quantification of heating and cooling demands at the hectare level and identifies the availability of waste heat resource as well as geothermal, solar thermal and biomass [23]. Heat RoadMap Europe use the thermal atlas developed by Peta to assess district heating potentials [24]. The results demonstrate that district heating can cost-effectively provide more than half of the heating demand in studied European countries by 2050 while significantly reducing GHG emissions.

1.2.2 Evolution of DHC technology

Traditionally, district heating systems use a pipe network to deliver heat from a central generation plant to various buildings within a district. The first generation DH relied on steam as the heat carrier. The second generation DH introduced the use of superheated water at temperatures exceeding 100°C, with increased efficiency and reliability. The third generation, 3GDH, lowered the supply temperature to below 100°C. This reduction in temperature allowed to reduce distribution losses and to utilise combined heat and power (CHP) and high-temperature industrial excess heat. The first three generations of DH predominantly relied on fossil fuels for their heat supply [25].

In response to the imperative challenge of transitioning to a sustainable energy system, Lund et al. [25,26] introduced the concept of the fourth generation district heating (4GDH):

> "The 4th Generation District Heating (4GDH) system is consequently defined as a coherent technological and institutional concept, which by means of smart thermal grids assists the appropriate development of sustainable energy systems. 4GDH systems provide the heat supply of low-energy buildings with low grid losses in a way in which the use of low-temperature heat sources is integrated with the operation of smart energy systems. The concept involves the development of an institutional and organisational framework to facilitate suitable cost and motivation structures."

In contrast to earlier generations, 4GDH further reduces the supply temperature to the lowest temperature that allows direct heating of the connected buildings, often below 70°C. This lower supply temperature not only minimizes distribution losses but also enables the integration of additional waste heat sources and some forms of renewable energy (e.g., solar energy) which provide lower temperatures. Moreover, the evolution of district heating extends to ultra-low temperature DH (ULTDH), where supply temperatures can be as low as 50°C [27,28].

Similar evolution can be observed for DC. The first generation relied on refrigerants as the carrier fluid. The second generation DC transitioned to the use of cold water from large compression chillers, while the third generation introduced various cooling sources, including absorption chillers and free cooling from natural water bodies. In line with the 4GDH concept, Østergaard et al. [20] introduced the concept of fourth generation district cooling (4GDC):

> "4GDC consists of systems operating in synergy with other energy sectors, such as electricity and heating sectors, using centralised and/or decentralised technologies such as electric heat pumps, absorption heat pumps, ambient sources and cold storage facilities for fulfilling residential, commercial and industrial cooling demands. The principal drivers are smart energy systems integration and exploitation of the combined heating and cooling synergy."

In recent years, a novel concept in the field of district energy systems addressing both heating and cooling demands has emerged in countries like Germany, Switzerland, and Italy [29,30]. They are known as '5th Generation District Heating and Cooling' (5GDHC), although different terms like 'cold district heating' ('Kalte Fernwärme' in German) [31] and 'anergy network' ('Anergienetz' in German) are also used [32]. Several review papers [29,33,34] have attempted to define the concept by examining existing installations around the world. The primary characteristics that distinguish 5GDHC from conventional district heating systems can be outlined as follows:

- Operation at ambient temperature. 5GDHC typically functions within the temperature range of 0-30°C, close to the ground, which ensures minimal heat losses and facilitates the integration of low-grade renewable thermal sources. Importantly, the close-to-ground temperature minimises the barrier to recover waste heat generated during cooling processes (e.g., data centre cooling).
- Bidirectional energy flow. 5GDHC allows simultaneous supply of both heating and cooling via the same network. Buildings connected to the network act as prosumers, capable of extracting or injecting heat according to their energy demands (e.g., space heating, space cooling, domestic hot water). 5GDHC typically has two pipes, and in some cases, a single pipe can serve as the thermal reservoir. In contrast, traditional district thermal systems rely on separated networks for heating and cooling (i.e., four pipes). This bidirectional functionality permits compensation of concurrent heating and cooling demands. The degree of overlap between heating and cooling demands within and among buildings is proven to contribute to improved system efficiency.

- Decentralized heat pumps. Since the operation temperature of 5GDHC is not suitable for direct heating, decentralized heat pumps are required at buildings for temperature modulation. In comparison to 4GDH, 5GDHC show strong adaptability to diverse temperature requirements, capable of accommodating modern efficient buildings and historical buildings in the building stock.

Considering these distinguishing attributes, it is important to recognise 5GDHC as a complementary technology to 4GDH, rather than the succeeding generation [35].

1.2.3 Shallow geothermal energy

Among the various renewable thermal sources, geothermal energy stands out due to its versatility and abundant potential to supply humanity's energy needs. Geothermal energy, by definition, refers to the heat stored below the surface of the solid earth [36]. It is a sustainable energy source available nearly everywhere throughout the year, independent from weather conditions. Additionally, its localized nature aligns with environmentally conscious practices. Geothermal energy is generally categorized into two groups: deep geothermal and shallow geothermal. Deep geothermal accesses rock structures at depths exceeding 400 meters, where temperature is suitable for electricity generation or direct feed into district heating network [37]. In contrast, shallow geothermal refers to depths up to 400 meters into the earth and harnesses heat at temperatures generally below 30°C [38].

In European countries, shallow geothermal energy is primarily used for heating purposes (e.g. space heating, domestic hot water) in the form of ground source heat pump (GSHP), where heat pumps (HP) are coupled with vertical borehole heat exchangers (BHE) or horizontal ground heat exchangers (GHE) to extract heat from the ground [39]. Leveraging the higher temperature in the subsoil, GSHPs achieves higher efficiency compared to air source heat pump (ASHP). Shallow geothermal is also suitable for cooling purposes through GSHP or direct cooling, making it very attractive for urban areas [40]. When shallow geothermal energy is harnessed for both heating and cooling, these hybrid systems provide multiple benefits. Firstly, they provide heating and cooling through renewable and local source, effectively mitigating the carbon footprint. Secondly, the re-injection of excess heat from space cooling usage into the ground reduces impacts on the shallow subsurface from heating usage, an effect termed 'seasonal regeneration', enhancing the overall system efficiency [41]. Another application of shallow geothermal energy is thermal storage, often realized through BHEs, knows as Borehole Thermal Energy Storage (BTES) systems [42]. BTES store surplus thermal energy during periods of abundance for retrieval when demand arises. This technology is commonly utilized in the form of seasonal thermal energy storage.

Existing 5GDHC installations reveal that shallow geothermal energy naturally complements 5GDHC, especially in situations where heating and cooling demands do not align and cannot be balanced out. Multiple 5GDHC projects highlight the advantages of employing the ground as seasonal thermal energy storage, offering efficient and sustainable heating solutions to urban areas and contributing to reduce energy consumption carbon footprint [29]. In the Anergy Grid installed in Zurich, Switzerland, borehole fields are utilized as the energy source, as well as seasonal storage to exploit the synergy between heating and cooling demands [32]. Shallow geothermal energy also supports the use of solar energy. Solar district heating and cooling system integrated with BTES are found to significantly enhance the exploitation of solar energy, reshaping the landscape of sustainable heating and cooling [43]. Another study demonstrates that the integration of GSHPs within a solar-driven 5GDHC significantly enhances the system efficiency [44].

1.3 Research Gaps

While some research has attempted to provide data for the strategic planning of DHC, a number of key gaps remain. Insufficient attention has been given to assessing the future challenges of growing cooling demand. With the rising urbanization, climate change, and increased thermal comfort expectations, cooling demand is expected to soar in Europe [45]. However, existing studies typically overlook the emerging need for space cooling, since it currently represents a minor share of energy consumption compared to heating demand. There is a need for additional research to examine the future growth of cooling demand.

Currently, the fulfillment of space cooling primarily relies on individual compression chiller units (i.e., air conditioner). Further exploration is required to identify renewable sources to fulfil future cooling demand sustainably. While most research has focused on the availability of renewable sources for heating, the potential of renewable sources for cooling purpose is underresearched. Another significant research gap is the limited research on exploiting the synergies between heating and cooling. Addressing future cooling demand represents not only a challenge, but also presents opportunities. When the consideration of cooling decarbonisation is aligned with the decarbonisation of heating, the potential for synergies becomes evident. By integrating heating and cooling, waste heat generated during cooling process can be effectively recycled and utilized to meet heating demands.

Shallow geothermal is an attractive sustainable energy source for both heating and cooling. Its capacity for thermal storage offers the key to unlock these synergies. However, existing knowledge predominantly focuses on small-scale applications of shallow geothermal. There is

limited understanding regarding the large-scale exploitation of shallow geothermal resources. A comprehensive methodology needs to be developed to quantify the full potential of shallow geothermal energy. This involves data collection, detailed spatial analysis of available spaces, ground modelling, as well as accounting for hybrid use for heating and cooling.

DHC is another promising solution for synergetic coupling of heating and cooling. To date, majority of the studies investigate district heating or district cooling in isolation. However, there has been a growing interest in 5GDHC in recent years, which provides combined heating and cooling in the same network [29]. This enables compensation of simultaneous heating and cooling, helping achieve significant energy saving and improved system efficiency [46]. Further research is needed to fully understand and explore the technical feasibility and economic viability of implementing combined heating and cooling in DHC. To address these research gaps, comprehensive studies and analyses are required to assess the future growth in cooling demand and sustainable provision of cooling in DHC.

1.4 Research questions and objectives

This thesis contributes to the understanding of how DHC based on renewable energy sources can provide sustainable solutions for heating and cooling, with a particular focus on understanding and addressing the future growth of cooling energy demand. It aims to address research gaps regarding the techno-economic assessment of the combined provision of heating and cooling through DHC.

To achieve the defined research aims, this thesis is guided by the following main research questions:

- To what extent will the cooling demand of the Swiss service sector increase, and what are the main drivers of this increase?
- What are the technical potentials of shallow geothermal energy usable by DHC?
- What is the technical and economic performance of a 5GDHC integrated with shallow geothermal energy?
- What are the main factors that influence the applicability of 5GDHC integrated with shallow geothermal energy?

This thesis is divided into four main studies, each addressing a specific topic outlined in Table **1.1**.

Table 1.1 - Overview on research topics covered in this thesis with related method and publication.

Research topics	Methods	Publication*	Status
1. Quantification of space cooling demand in the service sector			
1.1 Cooling demand in the Swiss service sector	Monte Carlo simulation	J1	Published
1.2 Spatial distribution of cooling demand	Geospatial analysis	C1	Published
2. Availability of shallow geothermal energy and waste energy sources for DHC			
2.1 Method for optimal spatial allocation of resource	Geospatial analysis + optimisation	J2	Published
2.2 Technical potential of shallow geothermal energy for DHC	Analytical modelling + geospatial analysis	J3	Published
2.3 Technical potential of industrial excess heat for DH	Spatial-temporal analysis	C2	Published
3. Techno-economic performance of 5GDHC			
3.1 Technical and economic performance of 5GDHC based on shallow geothermal energy	Techno-economic analysis	J4	Published
4. Applicability of 5GDHC			
4.1 Potential heating-cooling synergies in 5GDHC with respect to growth in cooling demand.	Sensitivity analysis	C3	Accepted

* J denotes journal paper. C denotes conference paper.

This thesis represents a significant contribution by providing essential data, methodologies, and knowledge to support the successful deployment of renewable-based DHC that can effectively meet both heating and cooling demands in the future. Techno-economic analysis of 5GDHC based on shallow geothermal energy is a practical approach to assess its potential. The present work develops novel methods and models integrating knowledge from several engineering and computational science disciplines, including probabilistic methods (Monte Carlo methods), graph theory and transport theory, and geospatial information systems. In summary, this work lays the foundation for a comprehensive approach to assess the potential of DHC, bridging

significant knowledge gaps and providing valuable insights for the future deployment of sustainable heating and cooling solutions.

This thesis is structured as follows:

Chapter 1 provided an overview of the background and context in which this thesis has been developed and defines the research questions that will be addressed.

Chapter 2 quantifies the future growth trends of cooling demand in the service sector, focusing on the case study of Switzerland. It assesses the drivers behind this growth.

Chapter 3 presents a developed method for the optimal allocation of thermal sources among multiple DHC systems. It applies this method to investigate the technical potential of shallow geothermal energy and industrial excess heat (IEH) for supplying DHC.

Chapter 4 proposes a method for evaluating the technical and economic feasibility of implementing 5GDHC coupled with geothermal energy.

Chapter 5 explores the general applicability of 5GHDC and investigates its potential in leveraging the synergies of coupled heating and cooling.

Chapter 6 summarize the findings and provides an outlook for future developments in the field.

2 Quantification of space cooling demand

Research question 1: To what extent will the cooling demand of the Swiss service sector increase, and what are the main drivers of this increase?

To address this research question, a building stock model combined with Monte Carlo method was developed to estimate the current and future space cooling demand in the Swiss service sector. In-depth analysis was conducted on building level aspects of space cooling diffusion, as well as cooling systems characteristics, and their potential evolution under climate change. This bottom-up approach allows mapping of space cooling demand with high geospatial precision, laying the foundation for further exploration for solutions to address this demand.

I have prepared two publications based on this work: one journal paper published in *Energy & Buildings* and one conference paper presented at 21st Status Seminar; 3–4 September 2020; Aarau, Switzerland.

Journal paper 1:

Xiang Li, Jonathan Chambers, Selin Yilmaz, and Martin K Patel. 'A Monte Carlo Building Stock Model of Space Cooling Demand in the Swiss Service Sector under Climate Change'. *Energy & Buildings* 233 (2021).

Conference paper 1:

Xiang Li, Jonathan Chambers, Selin Yilmaz, and Martin K Patel. 'GIS-Based Analysis of Space Cooling Demand in the Swiss Service Sector'. *21. Status-Seminar*, no. September 2020 (2020): 112–18.

2.1 A Monte Carlo building stock model of space cooling demand in the Swiss service sector under climate change

2.1.1 Introduction

The global mean temperature is likely to rise between 0.3-4.8 °C in the 21st century, together with a higher frequency and longer duration of heat waves [47]. This, in combination with increasing thermal comfort expectations, affordability of cooling systems, and potentially higher internal loads, is expected to cause a rapid growth of cooling demand in buildings [45,48–50]. However, studies on the energy demand for space cooling in Europe are scarce, mainly due to the relatively immature cooling market [49] and the practice of not separately reporting cooling device consumption and total electricity consumption [51]. Knowledge of space cooling demand is essential to model the future energy systems and design policies, since space cooling is expected to become one of the largest end-uses in European countries [52].

The European cooling saturation rate (i.e., share of floor area cooled) is low. Total space cooling consumption is dominated by the service sector [53], with a saturation rate in the EU (European Union) 15 estimated to be 30% compared to 4% in the residential sector [54]. Several studies estimated energy demand for cooling in the EU service sector in the range of 145-375 TWh/y [51,55–57] , and that of Switzerland in the range of 734-2677 GWh/y [50,58,59]. However, these studies depend heavily on assumptions of national aggregated figures such as cooling market development status and national average cooling energy intensity and do not come to a consensus. Other studies focus on regional case studies and are not representative for the national level [60,61].

To address the lack of research on current and future space cooling demand of the Swiss service sector, this paper aims to estimate the space cooling demand in terms of useful energy[1] at building level, thereby taking into account building characteristics, future climate scenarios as well as socioeconomic factors. In this paper, the service sector is comprised of offices, trade, hotels, and health-related services; other subsectors are not covered due to lack of data. A data driven Monte Carlo bottom-up model of the Swiss building stock for offices, wholesale and retail trade, hotels, and health was developed based on cooling systems data from the canton of Geneva. The novelty of this model lies in that it a) uses logistic regression to predict probabilities of presence of space cooling equipment based on building characteristics; b) applies a model of

[1] Useful energy is the energy service provided by the appliances (not to be confused with final or primary energy) [62]. In the case of space cooling, the useful energy represents the removed heat (thermal energy).

the building stock to project the development in the building stock's size and composition; and c) estimates the diffusion of space cooling equipment at building level under climate change.

The remainder of this paper is structured as follows: Section 2.1.2 presents the background and relevant literature on methods for modelling space cooling demand in the service sector, building stock modelling, and impact of climate change on future cooling demand. Section 2.1.3 presents the input data acquired. Section 2.1.4 presents the methods chosen, including the Monte Carlo model and calculations performed to forecast the future space cooling demand. Section 2.1.5 presents the results of probability distributions of cooling characteristics, as well as current and future space cooling demand. Sections 2.1.6 presents a discussion of findings, comparisons to other studies, policy implications, and limitations of the method developed. Finally, Section 2.1.7 concludes the paper.

2.1.2 Background

2.1.2.1 Modelling space cooling demand in the service sector

A range of research has assessed the space cooling demand for European service sector, but this has been limited by data availability. Studies for the EU-28 service sector have used demand data from existing cooling projects [51] or from the USA as a proxy for Europe [55]. However, in the latter case, the large difference in climates and lower indoor temperature in the USA [63] cast doubt on the validity of applying dependence of useful cooling demand intensity on cooling degree days (CDD) determined in USA to European countries. There are very few studies on space cooling demand in Swiss service sector [50,64]. These studies relied on rough estimates of cooling related parameters at national level (e.g., saturation rate, average cooling energy intensity), which are under-investigated and hence poorly understood in most European countries including Switzerland. Another drawback of these studies is that only aggregated cooling demand at national scale was given, lacking detailed information at building level, making them not applicable to model the impact of age, technology options, or policy measures.

Approaches to model the energy demand at building level can be divided into two categories [65]: physics-based approach and data-driven approach. The basis of physics-based approach is the energy consumption of end uses, heat transfer, and energy balance, facilitating the simulation of energy load with high temporal resolution. The complexity of models can vary from simplified steady-state energy balance equations [66] to advanced dynamic energy simulation tools [67]. Physics-based approaches require extensive data to model high levels of detail. Input information includes building geometry, building characteristics, internal loads, weather conditions, and further detailed information describing end-uses schedules and occupant behaviours are necessary [68]. Given the heterogeneity of the service sector relative to the residential sector [69–71], applications of physics-based approach have been limited to

building level or district level case studies [60,61,65]. The spatial scale of physics-based model is expanding thanks to growing computational resources and advances in modelling. For instance, a physic-based model was scaled up to country level by weighting the results of simulations of very large representative samples [72].

The data-driven approach on the other hand relies on historical information to model the energy demand, that requires relatively fewer input parameters. Studies using data-driven approach demonstrated that factors such as building characteristics, appliance usage, outdoor environment, and occupant behaviours significantly affect building energy use [73,74], among which building characteristics are the most significant predictors [75]. Several studies have also explored the effect of macroeconomic and socioeconomic factors on cooling energy demand, which is generally not covered in physics-based models [76,77]. The main limitation of data-driven approach is that historical energy consumption information of representative samples and of potential explanatory factors are required. The amount of inputs required by data-driven approach is nevertheless less than the physics-based approach [78].

Chambers et al. [79] developed a Monte Carlo model of the Swiss office building stock to estimate cooling and lighting electricity demand and the saving potential of electrochromic glazing. However, the missing cooled floor area were assumed to be equivalent to service area in that study, which could overestimate the cooled floor area and thus total cooling demand, since the saturation rate of cooling market in Europe is quite low [49]. Nevertheless, the estimated total yearly electricity demand for cooling can be considered to represent the potential of cooling demand when the Swiss cooling market is saturated (i.e., there is essentially no additional demand for cooling systems). Furthermore, the model was developed only for offices, while different characteristics may be observed in other subsectors. For instance, the likelihood of cooling being used was assumed to be linearly correlated to number of floors, which may be more likely for offices than for hotels. Finally, the model only considered current climate conditions (for 2015) and therefore did not take into account increasing cooling demand due to global warming.

2.1.2.2 Building stock modelling

Building stock modelling has been widely applied for estimating energy consumption at national scale [80–82]. Although extensive studies have focused on estimating space heating demand or electricity demand [83,84], few studies have adopted building stock modelling to investigate space cooling demand. To account for changes in the stock, dynamic material flow analysis principles and the underlying drivers can be introduced to the stock model [85,86]. In [87] and [88], a model of the building stock was developed and applied to 11 European countries to simulate the long-term development in dwelling stock composition.

In [87] and [88], a model of the building stock was developed and applied to 11 European countries to simulate the long-term evolution of the dwelling stock. The key principles of the model are to firstly estimate the annual demand for dwellings based on population. The demolished dwellings per year are then estimated by applying a demolition probability function. Finally, the construction activity for each year is equal to the sum of demolished dwellings and additional demand.

2.1.2.3 Impact of climate change on future space cooling demand

Climate change increases ambient temperature, which strongly influences space cooling demand [50,89]. CDD is widely used in building cooling demand estimation as a simple and efficient indicator for weather conditions and climate [55,90,91]. CDD is defined as the sum of degrees that a daily average temperature is above a predefined threshold:

$$CDD = \sum_{day=1}^{365} max\left(0,\ T_{avg} - T_{CDD}\right) \qquad (2.1)$$

Many studies assume that space cooling demand is proportional to CDD, given relatively constant building properties [92,93]. Previous studies have demonstrated a substantial increase in CDD in Switzerland for the 21st century [64,94,95].

Climate change is arguably one of the drivers for diffusion of space cooling equipment. Several studies (including cross-country analyses) suggest that this diffusion in residential and service sectors is closely linked to climate and economic factors [54,55,96–98]. For the economic factors, Isaac and Vuuren [98] showed that space cooling equipment is widely available when there is sufficient wealth, as is the case in Switzerland (i.e. there are not concerns about affordability of cooling systems). Some studies have attempted to model the saturation rate or share of buildings cooled as a function of local CDD [55,96]. However, this approach results in fluctuations in projected market diffusion level. Historical maximum CDD is a more appropriate climate indicator, as proposed by Bird et al. [97]. They argue that adoption of space cooling is triggered by years with high CDD and is rarely removed once it has been adopted. Therefore, the maximum yearly CDD experienced historically at a given location should be a better predictor of space cooling adoption than mean CDD. They demonstrated that the saturation rate in European countries is a linear function of historical maximum CDD.

2.1.3 Input data

The model is developed based on data from Swiss building registry (RegBL) [99], Geneva cooling system permits [79], current regional CDDs [79], future climate scenarios [100], and projected

change in GDP [101]. An overview of the input data is presented in Table **2.1**. Every building in Switzerland is included in the RegBL with some building metadata.

In the canton of Geneva, every space cooling system needs to be authorized prior to installation Tight regulation was moreover introduced to minimize the use of comfort space cooling in this canton [102]. An installation used to evacuate thermal energy including compression or absorption refrigeration machines is subject to authorization. The air-conditioned space must meet requirements provided by national standards [103,104], such as good insulation, high thermal inertia, and external sun protection, etc. Therefore, in general, only a fraction of the building's total floor area is actively cooled. Similar authorization process is also required in other cantons [105,106].

The three RCP scenarios were defined by the IPCC [47], which range from a mitigation scenario with substantial emissions reduction (RCP 2.6) to unabated emissions throughout the 21st century (RCP 8.5). Historical maximum CDD is used as a more appropriate climate indicator. Median of CDDs and historical maximum CDDs of the ensemble of 68 simulations, respective to the RCP 2.6, RCP 4.5, and RCP 8.5, are calculated for year 2035 and 2050 as model inputs by adapting the procedure used in [94]. Contrary to the approach in [94], we apply a 30-year moving average after calculating CDD from weather data, to avoid peak flattening and underestimating CDD.

The number of buildings in RegBL and the Geneva cooling system permits are listed in Table **2.2**.

Table 2.1 - Overview of input datasets.

Dataset	Information contained	Description
Swiss building registry (RegBL)	EGID (unique building identifier, used to link data from RegBL and Geneva cooling system permits), location, canton, construction year, building category, ground area, number of floors, total area (the product of ground area and number of floors), residential area, service area (calculated by subtracting residential area from total area)	All Swiss buildings (including offices, health, trade, residential etc.) Among them, buildings assigned to offices, trade, hotels, and health-related services are covered in this study.
Geneva cooling system permits	EGID, cooling service (useful energy), cooled floor area, coefficient of performance (COP, defined as the ratio of useful cooling provided to work required), operating hours	Installation of space cooling systems is subject to authorisation in the canton of Geneva. This dataset contains cooling system permits up to 2019.
Mean regional CDDs	Mean yearly CDDs (18.3 °C is used as the reference temperature [64,107]) for each canton	Mean CDDs for period 1990-2015 are used to represent the current climate for each canton
Future climate scenarios	Mean daily temperature in gridded 2 km resolution	Ensemble of 68 climate change simulations based on three RCPs: RCP 2.6 (12 simulations), RCP 4.5 (25 simulations), RCP 8.5 (31 simulations). Available for the period 1981-2099
Projected change in GDP	Annual percentage change in real GDP for Switzerland	Until 2050

Table 2.2 - Number of samples in the RegBL and the Geneva cooling system permits.

Subsector	Number of buildings in RegBL	Number of buildings in Geneva cooling system permits
Office	12,891	334
Trade	7152	71
Hotel	4256	59
Health	2144	35
Total	26,443	499

2.1.4 Methods

The model presented in this section is an extension of Chambers' previous work [79]. We implemented this model using the Python libraries SciPy [108] and Statsmodels [109].

2.1.4.1 Monte Carlo modelling of space cooling demand

To estimate the space cooling demand of each service sector building, the following data characterizing the space cooling equipment is required: presence of space cooling equipment (whether the building is being actively cooled), cooled floor area, cooling power intensity (defined in terms of cooled floor area), operating hours (equivalent full-load hours), and COP. The cooling characteristics data provided by Geneva cooling system permits cover a small portion of the Swiss service building stock, while comprehensive data on building characteristics (e.g., number of floor, service area) are available in RegBL. Therefore, a Monte Carlo simulation is applied to randomly assign cooling characteristics from approximated probability distributions, which are regressed on building characteristics. The workflow of the model is explained in Figure **2.1**. In order to compare the different preferences in cooling characteristics among subsectors the model is separately applied to offices, trade, hotels, and health-related services.

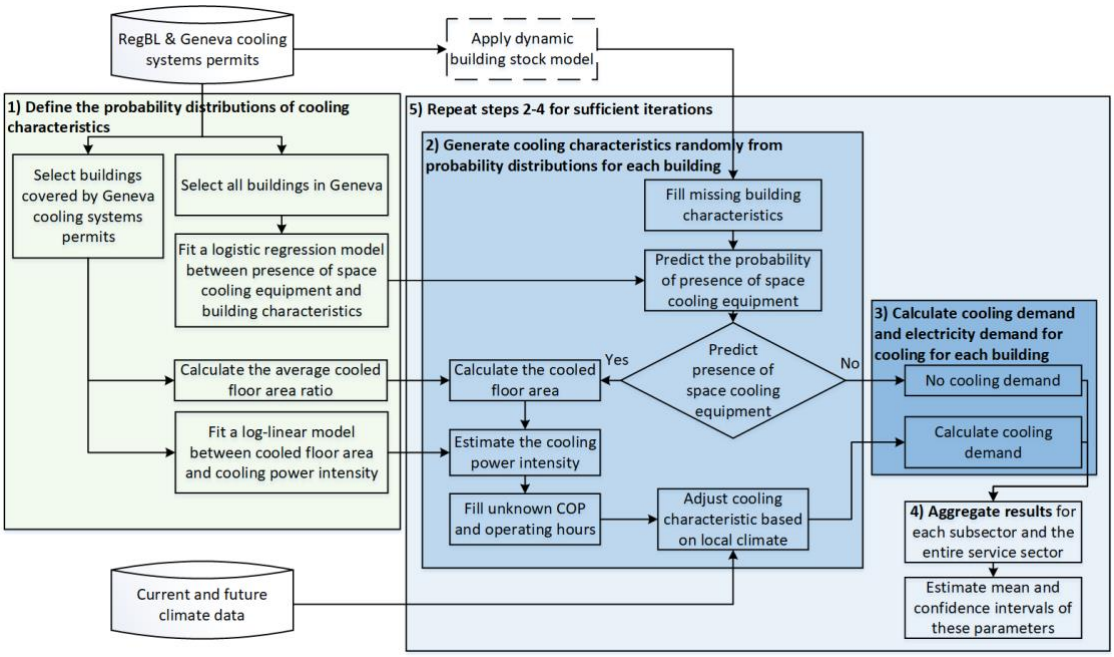

Figure 2.1 - Monte Carlo building stock model for estimating space cooling demand in Swiss service sector.

Step 1) Define the probability distributions of cooling characteristics

In this step, statistical analyses of empirical cooling data are performed to define probability distributions for each cooling characteristic. In cases where a dependence of a cooling characteristic on building characteristics is identified, the dependence is implemented in the probability distribution. Table **2.3** summarizes the cooling characteristics, the respective probability distributions, and parameters. These variables are explained in detail below.

Table 2.3 - Overview of key cooling characteristics.

Cooling characteristic	Approximated probability distribution	Relevant parameters
Presence of space cooling equipment (δ)	Bernoulli distribution	$P(\delta = 1) = Pr$, where Pr is modelled by a logistic function of building characteristics
Cooled floor area (A_{cooled})	Proportional to the service area $A_{service}$	$A_{cooled} = \varphi \times A_{service}$
Cooling power intensity ($p_{cooling}$)	Log-normal distribution	$\log p_{cooling} \sim N(a + b \log A_{cooled}\,,\, s^2)$
Number of operating hours (NH)	Empirical distribution	-
Coefficient of Performance (COP)	Empirical distribution	-

To prepare the data from which the probability distributions are derived, the RegBL building data for the Canton of Geneva is combined with the Geneva cooling system permits data using the unique building identifier (EGID). As the cooling permits are compulsory in Geneva, we may assume that all buildings in Geneva for which a cooling permit exists have space cooling equipment installed and those without permit have no space cooling. This allows us to define a variable for the presence or absence of space cooling. The presence of space cooling equipment δ is modelled as a Bernoulli distribution, which takes value 1 (presence) with probability Pr and 0 (absence) with probability $1 - Pr$. The probability of presence of space cooling equipment Pr, which is predicted by a binary logistic regression model, is assumed to depend on building characteristics. The logistic regression model is fitted based on the service building stock in Geneva. Building characteristics selected as possible predictor variables are building age, $\log_{10}$ of ground area ($log_{10}\ A_{ground}$), number of floors, $\log_{10}$ of total area ($log_{10}\ A_{total}$), and $\log_{10}$ of service area ($log_{10}\ A_{service}$). Building age is a 6-category variable and is converted to 5 dummy variables: AgeA – 1919 to 1945, AgeB – 1946 to 1960, AgeC – 1961 to 1980, AgeD – 1981 to 2000, AgeE – later than 2000. Buildings constructed before 1919 serve as the reference category, where all 5 dummy variables are set to 0. Each of the dummy variable becomes 1 when the building was constructed in the corresponding range, and becomes 0 otherwise. Multicollinearity is tested by investigating the variance inflation factors (VIF) of predictor variables. Predictor variables selection is done via Akaike's Information Criterion (AIC), which measures the trade-off between the goodness of fit and the number of variables included in the model.

For the remaining parameters, we only use data for buildings which have space cooling. We have both the service area from the RegBL and the cooled floor area from the cooling permits. This implies that when a building has space cooling, not the entire service area is actively cooled. The

cooled floor area is assumed to be proportional to service area of the building. The cooled floor area ratio φ is estimated by the following equation:

$$\varphi = \frac{\sum_{i=1}^{n} A_{cooled}}{\sum_{i=1}^{n} A_{service}} \tag{2.2}$$

The relation between cooling power intensity and cooled floor area is modelled by a log-linear model:

$$log\, p_{cooling} = a + b\, log\, A_{cooled} + Noise \tag{2.3}$$

Parameters in equation 2.3 are estimated by applying a linear regression with logarithmic transformations [79]. The logarithmic transformation of cooling power intensity is found to be optimal according to the Box-Cox Test [110] as shown in Figure A.**1**. 1 in Appendix. The transformation on cooled floor area is selected via AIC among several commonly used transformations: no transformation, square root, logarithm, and reciprocal.

A noise term is added to the cooling power intensity to model the unidentified diversity among buildings, i.e., thermal insulation level, occupant behaviours, etc.:

$$Noise \sim N(0,\, s^2) \tag{2.4}$$

$$s = \sqrt{\frac{\sum\left(p_{cooling} - a * A_{cooled}^{b}\right)^2}{n-2}} \tag{2.5}$$

The number of operating hours NH is sampled from the empirical distribution of values recorded in the cooling permits. The cooling system's Coefficient of Performance (COP) is also sampled from the empirical distribution of COP of the cooling systems present in the cooling permits. No correlation was found between NH or COP and other building characteristics.

Step 2) Generate cooling characteristics randomly from probability distributions

Before generating cooling characteristics for all buildings in the service sector, missing building characteristics are filled by randomly sampling from existing values, such as service area and number of floors. For each building, the presence of space cooling equipment is firstly assigned by randomly sampling from the Bernoulli distribution, which takes the value 1 (presence) with probability of presence *Pr* predicted by the logistic regression model. Then, only for buildings predicted to have δ values equal to 1 (i.e., presence of space cooling equipment), the characteristics required for calculating space cooling demand, such as cooled floor area, cooling power intensity, operating hours, and COP, are generated from probability distributions defined in step 1).

The variation of climate among cantons is also integrated in the model. Since we have cooling data only for the canton of Geneva, the probabilities of presence of space cooling equipment is scaled according to local historical maximum CDD:

$$Pr' = Pr \times \frac{c + d \times CDD_{max,local}}{c + d \times CDD_{max,Geneva}} \quad (2.6)$$

And the cooling energy intensity (product of cooling power intensity $p_{cooling}$ and number of operating hours NH) is scaled according to local CDD:

$$q'_{cooling} = p_{cooling} \times NH \times \frac{CDD_{local}}{CDD_{Geneva}} \quad (2.7)$$

Step 3) Calculate building specific annual cooling demand, annual electricity cooling demand.

The following equation is used to calculate the annual cooling demand for each building:

$$Q_{cooling} = q'_{cooling} \times A_{cooled} \quad (2.8)$$

The following equation is used to calculate the annual electricity demand for space cooling:

$$E_{cooling} = \frac{Q_{cooling}}{COP} \quad (2.9)$$

Values for NH and COP originate from the Genevan permit data.

Step 4) Aggregate the results of space cooling demand.

To estimate the space cooling demand of service sector, building specific cooling demand are first aggregated for each subsector and second for the entire service sector. Parameter aggregates are calculated as described below and shown in equations 10-13: total service area equals sum of $A_{service}$; total cooled floor area equals sum of A_{cooled}; saturation rate SR equals total cooled area divided by total service area; total space cooling demand equals sum of $Q_{cooling}$; average cooling energy intensity $q_{cooling,avg}$ equals total space cooling demand divided by total cooled floor area; total electricity demand for cooling equals sum of $E_{cooling}$; average electricity intensity for cooling $e_{cooling,avg}$ equals total electricity demand for cooling divided by total cooled floor area; and average coefficient of performance COP_{avg} equals total electricity demand for cooling divided by total space cooling demand.

$$SR = \frac{\sum_{i=1}^{N} A_{cooled}}{\sum_{i=1}^{N} A_{service}} \quad (2.10)$$

$$q_{cooling,avg} = \frac{\sum_{i=1}^{N} Q_{cooling}}{\sum_{i=1}^{N} A_{cooled}} \quad (2.11)$$

$$e_{cooling,avg} = \frac{\sum_{i=1}^{N} E_{cooling}}{\sum_{i=1}^{N} A_{cooled}} \quad (2.12)$$

$$COP_{avg} = \frac{\sum_{i=1}^{N} Q_{cooling}}{\sum_{i=1}^{N} E_{cooling}} \quad (2.13)$$

Step 5) Repeat for sufficient iterations.

In accordance with the Monte Carlo method, steps 2-4 are repeated for sufficient iterations to generate stable distributions of the aggregated sector level parameters. Mean and confidence interval are estimated.

2.1.4.2 Forecasting future space cooling demand

Climate change

To evaluate the impact of climate change on cooling demand, we estimate future cooling demand under three climate scenarios: RCP 2.6, RCP 4.5, and RCP 8.5. CDDs are calculated based on Equation 2.1, using 2km gridded climate simulation ensemble data and allocated to buildings in the service sector by mapping the building location. Building specific cooling demand are calculated according to future CDD scenarios[100]:

$$q_{cooling,future} = q'_{cooling} \times \frac{CDD_{future}}{CDD_{local}} \quad (2.14)$$

Diffusion of space cooling equipment

At building level, the diffusion of space cooling equipment is reflected in the probability of presence of space cooling equipment and potentially cooled floor area ratio (i.e. cooled floor area divided by total floor area). We assume cooled floor area ratio will remain the same in the future since stable average cooled floor area ratio was observed over the years in input data. Therefore, in this study we only consider the impact of changing probability of presence of space cooling equipment. This is modelled by the linear fit between the share of cooled buildings cooled and the historical maximum CDD observed in the Genevan permit data, following the work of Bird et al. [97]. Genevan permit data is used despite the small sample size because the data from literature is not readily usable due to the different scope compared to this study [55,96,98]. Further data collection is required to investigate the impact of climate change on the diffusion of space cooling.

The probabilities predicted by the logistic regression are scaled for each year up to the scenario time horizon (2050). The scaling is calculated using maximum CDD (derived from the future climate scenarios) experienced in the period up to and including the scenario year. The scaling is truncated by upper limit of 1 and lower limit of 0:

$$Pr_{future} = \begin{cases} 0, & if\ Pr' \times \frac{c + d * CDD_{max,future}}{c + d * CDD_{max,local}} < 0\ ; \\ 1, & if\ Pr' \times \frac{c + d * CDD_{max,future}}{c + d * CDD_{max,local}} > 1\ ; \\ Pr' \times \frac{c + d * CDD_{max,future}}{c + d * CDD_{max,local}}, & otherweise \end{cases} \quad (2.15)$$

Dynamic building stock

A model of the building stock developed in [87] and [88] is adopted to project the demolition of existing buildings and construction of new buildings. For each year, the probability that a building will be demolished is modelled by a Weibull distribution. The change in total service area is determined by predicted change in GDP, as we assume a constant floor area per GDP in Switzerland [111]. The rate of new construction is determined based on the change in total service area and the rate of demolished buildings. To model new buildings, these are sampled from existing buildings built after 2000 and added to the stock.

2.1.5 Results

2.1.5.1 Probability distributions of cooling characteristics

Probability of presence of space cooling equipment

Table **2.4** shows the VIF as the measure of the multicollinearity among predictor variables. We found significant multicollinearity between predictor variables $log_{10}\ A_{ground}$, $log_{10}\ A_{total}$, and $log_{10}\ A_{service}$ in all subsectors. In most service buildings, service area equals total area because there is no residential use, while total area is the product of ground area and number of floors. The presence of multicollinearity suggests that there is no clear physical meaning to the regression coefficients [112]. Nevertheless, the overall prediction accuracy of the model is not reduced [113–115]

Table 2.4 - VIF of predictor variables. If not collinear, VIF=1; VIF > 10 indicates the presence of multicollinearity [114].

Subsector	AgeA	AgeB	AgeC	Age D	AgeE	$log_{10}A_{ground}$	Number of floors	$log_{10}A_{total}$	$log_{10}A_{service}$
Office	1.31	1.40	1.78	1.55	1.33	34.0	9.37	197	151
Trade	1.4	1.79	2.34	1.75	1.76	50.2	10.8	140	91.6
Hotel	1.21	1.27	1.55	1.34	1.15	23.7	8.92	110	77.1
Health	1.54	1.42	2.22	2.02	1.87	30.1	8.53	218	165

The probability of presence of space cooling equipment is modelled by logistic regression; Table **2.5** lists the results for the predictor variables selected by AIC for the four subsectors. For offices and hotels, some multicollinearity was found between the predictor variables, but their inclusion is shown to improve prediction accuracy, indicating that they also introduced meaningful independent information. For this reason, the most meaningful predictor variables are retained. For trade and health, only one of the collinear predictor variables is selected by AIC. We proceed only with this variable (i.e., $A_{service}$ in both cases).

Figure **2.2** compares the estimated probabilities of presence of space cooling equipment with observed probabilities in Geneva's buildings. The representative data points are obtained by dividing samples into deciles (or grouping by number of floors) and then taking the mean of predictor variables and mean probabilities for each decile.

Table 2.5 - Logistic regression coefficients for the probability of presence of space cooling equipment, for predictor variables selected by AIC for the corresponding subsector.

Subsector	Predictor variable	Regression coefficient (95% confidence interval)	Standard error	p value	Odd ratio
Office	Constant	-6.18 (-7.11, -5.25)	0.48	< 0.001	-
	$log_{10}\ A_{ground}$	-2.24 (-3.02, -1.46)	0.40	< 0.001	0.106
	$log_{10}\ A_{total}$	3.30 (2.65, 3.96)	0.33	< 0.001	27.1
	AgeA	-0.21 (-0.77, 0.35)	0.29	0.46	0.811
	AgeB	-0.14 (-0.68, 0.40)	0.28	0.61	0.869
	AgeC	-0.40 (-0.82. 0.03)	0.22	0.07	0.670
	AgeD	0.04 (-0.41, 0.50)	0.23	0.84	0.961
	AgeE	0.56 (0.03, 1.10)	0.27	0.04	1.75
Trade	Constant	-4.98 (-6.26, -3.70)	0.65	< 0.001	-
	$log_{10}\ A_{service}$	1.03 (0.66, 1.41)	0.19	< 0.001	2.80
Hotel	Constant	-6.41 (-8.48, -4.35)	1.05	< 0.001	-
	$log_{10}\ A_{ground}$	-3.11 (-4.84, -1.37)	0.89	< 0.001	0.0446
	$log_{10}\ A_{service}$	4.06 (2.55, 5.58)	0.77	< 0.001	58.0
Health	Constant	-7.69 (-10.74, -4.63)	1.56	< 0.001	-
	$log_{10}\ A_{service}$	1.53 (0.74, 2.32)	0.40	< 0.001	4.62
	AgeA	0.74 (-1.35, 2.84)	1.07	0.49	2.10
	AgeB	1.00 (-1.12, 3.13)	1.08	0.35	2.72
	AgeC	-0.22 (-2.03, 1.58)	0.92	0.81	0.803
	AgeD	0.97 (-0.68, 2.62)	0.84	0.25	2.64
	AgeE	1.50 (-0.13, 3.13)	0.83	0.07	4.48

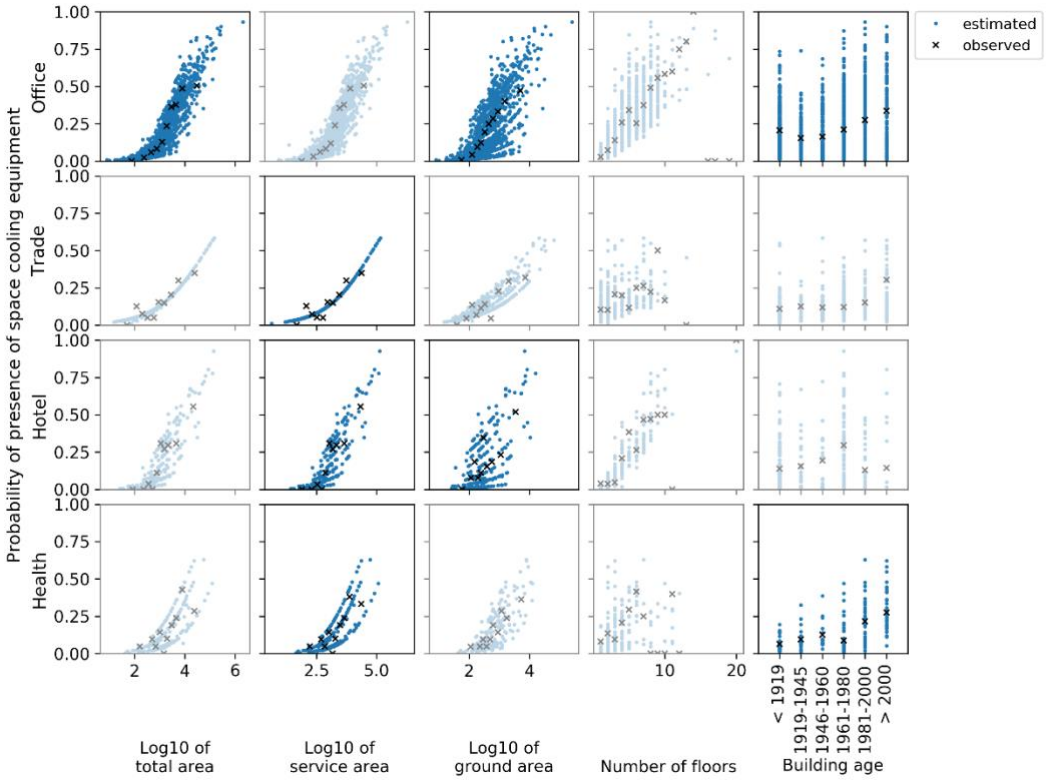

Figure 2.2 - Observed and estimated probabilities of presence of space cooling equipment. The chosen predictor variables are highlighted in black. Insignificant predictor variables are presented in grey.

Figure **2.3** presents the share of buildings cooled as a function of historical maximum CDD for year 1991-2015. Year 2003 was excluded as an outlier, due to the unprecedented heat wave in that year. The figure indicates that the share of cooled building grows as CDD hit new records. Since the linear function is fitted based on a limited number of data points, this finding should thus be treated with considerable caution.

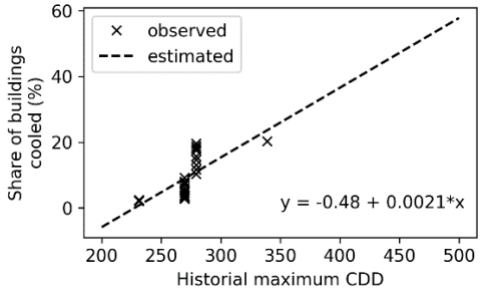

Figure 2.3 - Share of buildings cooled as a function of historical maximum CDD.

Cooled floor area ratio

Based on Equation 2.2, we calculate the average cooled floor area ratio of commercial offices in Geneva as 0.43 (highest average), where average cooled floor area ratios of trade, hotel, health

are 0.29, 0.22, and 0.34, respectively. The simulated distribution of cooled floor area is close to the observed distribution. A comparison of the observed and simulated values of cooled floor area in Geneva office buildings can be found in Figure A.**2**.

Cooling power intensity

We found a significant decreasing trend of cooling power intensity with increasing cooled floor area in all subsectors studied. Figure **2.4** shows the case of offices as an example. The simulated distribution of cooling power intensity is compared with the observed distribution and shows good agreement in Figure A.**3**.

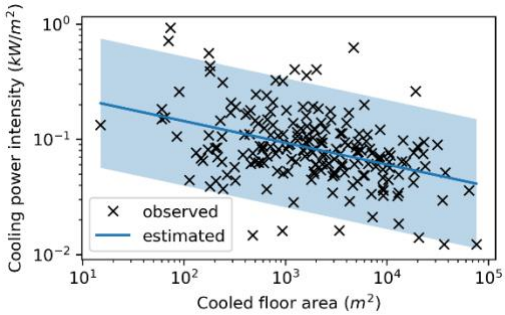

Figure 2.4 - Observed and estimated cooling power intensity as a function of cooled floor area in offices. Shaded area indicates 95% prediction interval.

In offices, the coefficient of determination (R^2) of the log-linear model fitted is only 0.17. Similarly, low R^2 values were found for other subsectors. This means that only a small portion of variation in cooling power intensity can be explained by changes in cooled floor area. The unexplained part of variation could be associated with other building characteristics not reflected in the RegBL, e.g., insulation level, equipment rate, internal gains, occupant density, and occupant behaviour. The unexplained variation in cooling power intensity is modelled by a noise term added to Equation 2.4 and Equation 2.5, which produces the broad prediction interval in Figure **2.4**. The fitted coefficients for Equation 2.3 and Equation 2.4 for all subsectors are listed in Table **2.6**.

Table 2.6 - Results of log-linear regression on cooling power intensity in kW/m² (A_{cooled} in m²).

Coefficient	*a*	*b*	*s*
Offices	0.34	-0.19	0.66
Trades	0.15	-0.07	0.51
Hotels	0.17	-0.10	0.49
Health	0.37	-0.20	0.83

Operating hours and COP

We found that operating hours and COP are independent of other variables, with no strong dependence on other building characteristics in any subsectors. Figure **2.5** presents this relation for offices as an example.

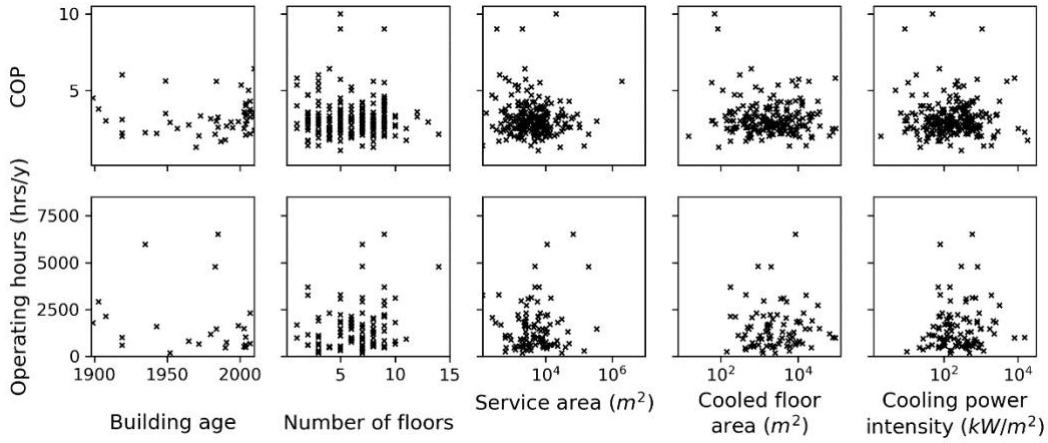

Figure 2.5 - Dependence of operating hours and COP on building characteristics and cooling characteristics.

2.1.5.2 Current space cooling demand

The Monte Carlo model was run on an HP Z8 workstation with a 28 core CPU (Xeon Gold 6132), 128GB RAM, and 512GB SSD. The number of iterations was 2,000 for a computational time of 10 mins.

Table **2.7** summarizes floor area, estimated space cooling demand, and electricity demand for space cooling by subsector. The total space cooling demand is decomposed into three components: total service area, saturation rate, and cooling energy intensity of cooled floor area. Figure **2.6** visualizes the total space cooling demand and the three components. The saturation rate of offices is the highest, reaching 12% ± 2%. Other subsectors have saturation rates around 5%. Trade, hotels, and health have a similar cooling energy intensity (100 - 110 kWh/m².y, with health featuring an extremely large range), while the values for offices are typically lower (90 ± 20 kWh/m².y, with a relatively very small range). The total cooling demand of the Swiss service sector is estimated to be 900 ± 200 GWh/y. Offices consume 70% of the cooling demand, while trade accounts for roughly 10%, hotel 10%, and health 10%.

Table 2.7 - Estimation of floor area, space cooling demand (useful energy) and electricity demand for current cooling needs in Switzerland by subsector.

Subsect-or	Floor area		Useful energy		Final energy		
	Total service area (Mm^2)	Saturation rate (%)	Average cooling energy intensity ($kWh/m^2.y$)	Cooling demand (GWh/y)	Average COP	Average electricity intensity for cooling ($kWh/m^2.y$)	Electricity demand for cooling (GWh/y)
Office	61.0 ± 0.5	12 ± 2	90 ± 20	600 ± 200	2.9 ± 0.3	30 ± 7	220 ± 50
Trade	23.5 ± 0.3	5 ± 2	110 ± 60	130 ± 90	2.9 ± 0.5	40 ± 20	50 ± 30
Hotel	11.2 ± 0.1	4 ± 1	110 ± 50	50 ± 30	3.0 ± 0.3	40 ± 20	20 ± 10
Health	11.6 ± 0.2	6 ± 4	100 ± 80	70 ± 70	3.1 ± 0.4	30 ± 30	20 ± 20
Total	107.3 ± 0.6	9 ± 1	90 ± 20	900 ± 200	2.9 ± 0.2	31 ± 7	310 ± 70

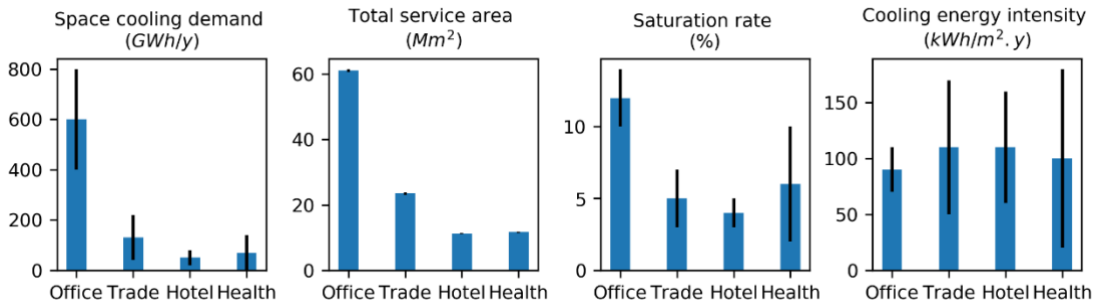

Figure 2.6 - Estimation of space cooling demand (useful energy) and its three components: total service area, saturation rate, and cooling energy intensity of cooled floor area, by subsector.

2.1.5.3 Future space cooling demand

Figure **2.7** presents the results of the modelling of the Swiss service building stock growth by 2050.

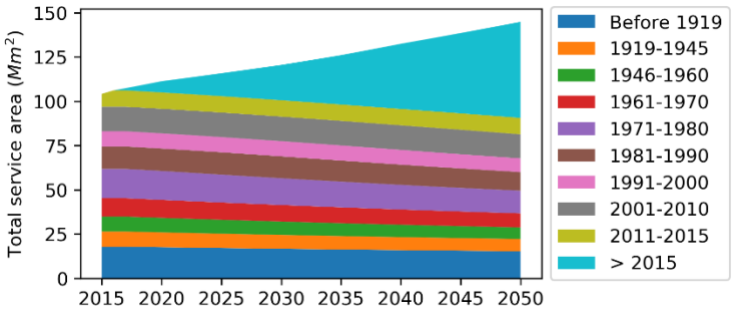

Figure 2.7 - Forecasted growth of the Swiss service building sector built area until 2050.

Figure **2.8** shows the national average CDD and historical maximum CDD for the climate change scenarios, both weighted by the service area. By 2050, area-weighted CDD will increase from current value of 150 to 202-274 (+ 34-83%), while area-weighted historical maximum CDD will increase from 270 to 385-415 (+ 42-53%).

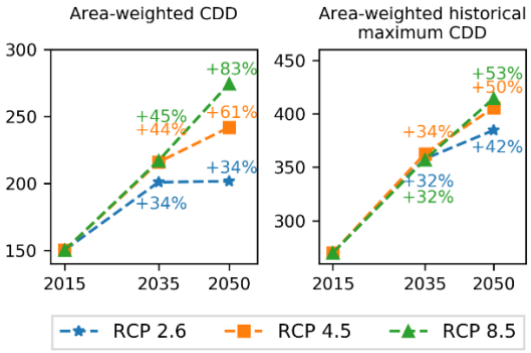

Figure 2.8 - Area-weighted CDD and historical maximum CDD in climate change scenarios: RCP 2.6, RCP 4.5, and RCP 8.5.

Figure **2.9** presents estimation of cooling demand (useful energy) and its three components: total service area, saturation rate, and cooling energy intensity of cooled floor area under climate change scenarios. Space cooling demand is expected to grow sharply in all three scenarios. In the most severe scenario RCP 8.5, space cooling demand will increase from 900 GWh/y to 6000 GWh/y (+ 600%) by 2050 with 35% caused by increase in total service area, 200% by increase in saturation rate, and 70% by increase in cooling energy intensity.

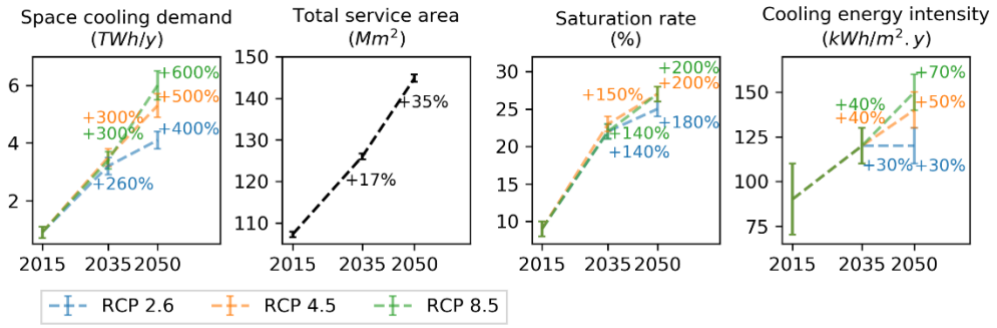

Figure 2.9 - Estimation of cooling demand (useful energy) and its three components: total service area, saturation rate, and cooling energy intensity of cooled floor area under climate change scenarios by 2050.

2.1.6 Discussion

2.1.6.1 Factors influencing probability of presence of space cooling equipment

The logistic regression found that the probability of presence of space cooling equipment increases with increase in ground area, total floor area, and service area in all subsectors analysed. This result may be explained by the fact that large commercial buildings tend to adopt a box-like structure and glass windows. Compared to traditional architecture with extensive perimeter exposure, these buildings are designed to rely on ventilation and cooling systems to remove heat from internal gains [116]. Interestingly, cooling power intensity decreases as cooled floor area increase. The observed decreasing trend might be explained by smaller surface-area-to-volume ratio and consequential less heat gain from the surface (solar gains and infrared radiation); to a lesser extent, pooling of the cooling equipment for non-simultaneous cooling needs and cold storage may play a role in large systems. Additionally, we found warmer climate contributes significantly to the diffusion of space cooling equipment. The linear regression on historical data of Geneva suggests that if historical maximum CDD increases from 300 to 500, the share of buildings cooled will increase from 15% to 58%. This finding is based on the assumption that the diffusion of space cooling equipment is more linked to most extreme warm weather rather than long-term average. It also raises intriguing questions regarding the drivers for adoption of space cooling equipment.

Furthermore, many variables not considered in this study might also play roles in adoption of space cooling equipment. For example, air conditioning has been increasingly implemented to tackle excessive solar gains in summer in all-glass buildings [117], which have become more popular over recent years.

2.1.6.2 Current space cooling demand in Swiss service sector

This study suggests that the space cooling demand (useful energy) in Swiss service sector is 900 ± 200 GWh/y. This result was compared with two other sources. Dumortier et al. [58] reported the demand to be 734-792 GWh/y (variation is due to divergent decomposition of the service sector), which is in agreement with this study. Another study [59] estimated that useful energy demand for space cooling in Switzerland was 2,677 GWh/y in 2012. The disagreement can be explained by the fact that Fleiter et al. [59] includes energy consumption of ventilation used for cooling.

In this study, the average cooling energy intensity was estimated at 90 ± 20 kWh/m².y, with electricity intensity for space cooling amounting to 31 ± 7 kWh/m².y. In accordance with the present results, a previous study [51] estimated the average cooling energy intensity in the service sector in 2010 to be 71 kWh/m².y in France and 74 kWh/m².y in Germany. The observed slightly higher average cooling energy intensity in Switzerland could be attributed to difference in year estimated (2015 versus 2010) as well as to the higher level of wealth in Switzerland. The saturation rate of space cooling in the Swiss service sector was determined to be 9 ± 1 %. To the best of our knowledge, there is no comprehensive study on the market diffusion of space cooling equipment in Switzerland. The service sector saturation in 2015 in France is approximately 22.5% and that of Germany is approximately 8.9% [118]. It reasonable that we estimated a relatively low saturation rate in Switzerland which can partly be explained by the colder climate (This study shows the area-weighted CDD in 2015 in Switzerland is 150. The CDD in 2015 in France is 236 and that of Germany is 118 [118]) and partly by tighter regulation [102,119].

Approximately 70% (220 ± 50 GWh/y) of the total electricity demand for space cooling of Swiss service sector (310 ± 70 GWh/y) is attributed to offices. Offices constitute 57% of the total service area, and have the highest saturation rate of 12.0%, while other subsectors range from 4% - 6%. This might be explained by these factors: the extensive use of glass façades in modern office buildings, high internal heat gains (generated from occupants and electrical equipment), and increased comfort level [120]. The average electricity intensity for cooling of offices was estimated to be 29.8 ± 7.3 kWh/m².y. By comparison, Chambers et al. [79] estimated electricity demand for cooling of offices at 180 ± 20 GWh/y, with electricity intensity for cooling equalling to 20 ± 0.6 kWh/m².y. Interestingly, although our result of national space cooling demand of offices is within the confidence interval of Chambers' result, detailed analysis of cantons reveals a different distribution of space cooling demand: this study estimated more cooling demand contributed by cantons with warmer climate, such as Geneva, Basel, and Ticino. For example, Chambers predicted similar saturation rate in offices for Zurich (39%) and Geneva (33%), while this study presents a much lower saturation rate in Zurich (7%) than Geneva (23%). The discrepancy is due to that in Chambers' model, the cooling presence model was fitted using

Geneva buildings and applied to other cantons, while this study scaled probabilities of space cooling use based on local climate, resulting in a lower saturation rate in Zurich than Geneva.

The confidence interval is approximately 20% of total space cooling demand, where most of uncertainty is attributed to cooling energy intensity estimation. The data availability is particularly limited in the health subsector. Our results show greater uncertainty in total space cooling demand than Chambers' model (11%) [79], due to the addition of the noise term (Equation 2.3) which allows to reflect the unidentified variation in cooling power intensity.

2.1.6.3 Trend in space cooling demand under climate change scenarios

This study highlights that the space cooling demand in Swiss service sector will increase by 400% in RCP 2.6, 500% in RCP 4.5, and 600% in RCP 8.5 between 2015 and 2050. By decomposing the space cooling demand into three components: total service area, saturation rate, and cooling energy intensity of cooled floor area, we identified the saturation rate as the most influential driver in cooling demand growth. For example, in RCP 8.5 scenario, saturation rate is projected to increase 200%, far more rapidly than increases in total service area (35%) and cooling energy intensity (70%).

Surprisingly, the results suggest that the growth in saturation rate will gradually slow down. A possible explanation for this result is that the new buildings installing space cooling triggered by warmer climate are likely to be smaller in size than early adopters. It is observed that currently more large buildings are cooled. When climate gets warmer, owners of smaller buildings begin to consider space cooling to deal with heatwaves. So, smaller buildings are usually lagging in cooling adoption. Therefore, the future growth in saturation rate (share of floor area cooled) can be expected to be slower than growth in share of buildings cooled, which agrees with model results (growth in share of building cooled is 300%, much more than the 200% growth in saturation rate).

An approach that can be applied to analyse future climate change implications is to study cities which currently have the climate that Swiss cities are expected to have in the future. The future climate of Bern in 2071-2100 was found to be like the current climate in Sicily, Italy [121]. The future climate of Switzerland in 2050 appears to be similar to current warm climate in Italy or Spain. The average cooling energy intensity of cooled area in the Swiss service sector in 2050 estimated by this study is in the range of 110-150 kWh/m².y, which is in agreement with values reported for Italy's and Spain's service sector today (126 kWh/m².y, 121 kWh/m².y). The current cooling saturation rate in the Italian and Spanish service sector are both about 73% [118]. This study estimated saturation rate in Swiss service sector to reach 25% - 27% by 2050 under climate change, which is much lower than the current figures of those two countries. The diffusion of space cooling equipment might be underestimated by this study. This is an important topic for future research.

The present study only considered the future space cooling demand in terms of useful energy. A discussion of future final energy consumption for space cooling is beyond the scope of this paper. This requires a comprehensive understanding and assessment of available cooling solutions including their efficiency, as well as regulation of cooling systems. These topics are recommended for future research.

2.1.6.4 Policy implications

The expected large increase in space cooling demand could be of interest to policy makers. Total space heating demand (useful energy) in Swiss service sector was about 12.2 TWh in 2012 [122], and is estimated to decrease almost half by 2050 [101,123]. This study found current space cooling demand in service sector is approximately 7% of space heating demand, but by 2050 space cooling demand will be equivalent to more than half of space heating demand in all three RCP scenarios. This should be of high importance to policy makers.

If all future space cooling demand are met by electric-powered air conditioning systems, more electricity generation capacity will be required [124], with increased greenhouse gas emissions if fossil fuel generation is used. Policy makers should evaluate the effectiveness of alternative cooling measures, such as night ventilation and district cooling networks, and develop adaption strategies to tackle the expanding demand for space cooling.

The adoption of air-conditioning could be substantially influenced by legislation. For example, in Geneva, in order to obtain a permit for air conditioner, the need has to be demonstrated and the system needs to fulfil certain requirements [102]. By contrast, installations of air conditioners are not subject to prior approval in EU [119]. The difference in legislation may partly explain the significant discrepancy in estimated future Swiss saturation rate (25% - 27%) and values of Italy and Spain (both about 73% [118]). Therefore, it would be advisable for policy makers to regulate the use of air conditioners in advance and promote environmentally friendly cooling solutions.

2.1.6.5 Limitations

This study is subject to a number of limitations. Data on cooling system characteristics were only obtained for Geneva and were assumed to be representative for all Switzerland. There is a potential bias which we were not able to test due to lack of comparable data for other Swiss locations. We approximated cooling intensities and probabilities of presence of cooling equipment in other cantons by scaling these values according to local climate. Furthermore, buildings in Switzerland were constructed under similar construction code and should have no significant difference. Moreover, the permit database does not include small moveable units (i.e. single-duct systems) which do not need to be installed by a professional. The energy consumed by this type of space cooling equipment is consequently not taken into account in this study. Future research should address this aspect, e.g. based on equipment sales. The Geneva cooling

permits dataset showed a low cooling saturation, given the relatively low CDD. The linear relation fitted between share of buildings cooled and historical maximum CDD is extrapolated and applied to future climate scenarios, which shows a higher range of CDD outside the sample dataset. This approach is rather speculative because we are not able to verify if the market diffusion follows the same path.

The impact of climate change on future cooling demand is not fully represented by CDD. For example, choice of whether to install a cooling system could be related to the frequency and duration of heat waves. Urban heat island effects may magnify the impacts of increasing temperatures. The model used in this study needs to be further justified and validated.

The proposed model estimates the space cooling demand in places where there is no reported data and it projects data into the future. By definition there is not a baseline against which to validate future projections. We therefore provide inductive evidence to verify our model, i.e. we ensure that the fundamental physical and data inputs are well understood and supported by existing literature, and therefore these support our conclusions. Despite these limitations, this study's estimation on current space cooling demand in Swiss service sector is consistent with the literature, in terms of average cooling energy intensity and saturation rate. It can thus be suggested that this result is robust within the estimated confidence interval. The estimated future space cooling demand and particularly saturation rate under climate change might be underestimated.

2.1.7 Conclusions

In this study, we estimated the current and future space cooling demand in Swiss service sector using a data-driven Monte Carlo model of the building stock. The model allows quantifying the changes of cooling system characteristics under climate change at building level and calculating the corresponding space cooling demand. The model was applied to current climate conditions (2015) and three future climate scenarios: RCP 2.6, RCP 4.5, RCP 8.5, until 2050. We found that the space cooling demand in Swiss service sector is 900 ± 200 GWh/year in 2015 and will increase to 4100 ± 300 GWh/year (+ 400%) in RCP 2.6, 5300 ± 400 GWh/year (+ 500%) in RCP 4.5, and 6000 ± 500 GWh/year (+ 600%) in RCP 8.5 by 2050. During the same period, growth in saturation rate (+ 180-200%) is the major driver for space cooling demand growth, far more than increases in total service area (+ 35%) and cooling energy intensity (+ 30-70%). A key policy priority should therefore be to plan for the considerable, potential increase of final energy consumption for space cooling in the future and formulate long-term strategy accordingly, e.g. by paying more attention to enhanced energy efficiency and permit conditions. Total floor area, service area, ground floor area, and building age were identified as strong predictors of probability of presence of space cooling equipment. The model can serve as a basis for

applications such as cost-effective analysis of cooling technology implementation and design of policy measures. While the model was applied to Swiss building stock in this study, it can also be used for national building stocks of other countries with comparable social and economic conditions, in case of paucity of required data.

2.2 GIS-based analysis of space cooling demand in the Swiss service sector

2.2.1 Scope

Space cooling is not traditionally used in Switzerland and therefore understudied. In contrast to the space heating and domestic hot water, data on the energy utilization of space cooling is scarce. In recent years, however, trends in rising ambient air temperature [47] have led to an increasing interest in modelling space cooling demand, as it is essential to model the future energy systems and design policies [52].

Previous published studies [50,64] on estimating the energy demand for space cooling in the Swiss service sector depend heavily on rough estimates of cooling related parameters at national level (e.g. saturation rate, cooling intensity) and do not come to a consensus. Other studies focus on building or district level case studies and are not applicable for the national level [60,61].

A data-driven Monte Carlo model of the building stock has been developed in the publication [125] and is used to estimate the current and future space cooling demand in the Swiss service sector under climate change. In this work, we apply the same method to investigate the spatial distribution of space cooling demand and its growth in Switzerland.

2.2.2 Methods

2.2.2.1 Input data

The model is applied to the building stock of the Swiss service sector based on data from Swiss building registry (RegBL) [99], Geneva cooling system permits [79], current regional cooling degree days (CDD) [79], future climate scenarios [100], and projected change in GDP [101]. Three representative concentration pathways (RCPs) [47] are used to estimate the future space cooling demand: RCP 2.6, RCP 4.5 and RCP 8.5.

RegBL contains basic data on all buildings in Switzerland. In this work, buildings in the categories offices, trade, hotels, and health-related services are studied. Building variables used includes EGID (unique building identifier), location, canton, construction year, building category, ground area, number of floors, total area, and service area (floor area used for activities in the service sector). Geneva cooling systems permits contains records of all air conditioners installed in the canton of Geneva. This dataset provides information on the following cooling variables: EGID, yearly cooling energy, cooled floor area, coefficient of performance (COP), and

number of operating hours. Data in Geneva cooling systems permits is then assumed to be representative for the whole Switzerland.

2.2.2.2 Overview of the data-driven Monte Carlo model of the building stock

The model is proposed by Li et al. in [125], with a through description including equations and underlying assumptions. The key steps of the model are summarized in Figure **2.10** to facilitate the understanding of the analysis introduced in this work.

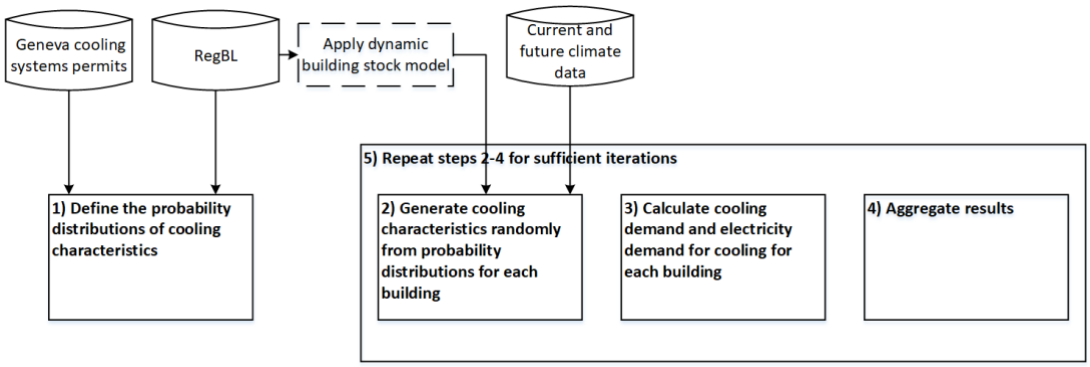

Figure 2.10 - Overview of the Monte Carlo model of the building stock

To estimate the space cooling demand of each service sector building, the following variables are necessary: presence of space cooling equipment, cooled floor area, cooling power intensity, operating hours (equivalent full-load hours), and COP. The empirical cooling data in Geneva cooling system permits is available for a small part of the Swiss building stock. Thus, a Monte Carlo simulation is employed to randomly assign cooling variables from approximated probability distributions.

The Monte Carlo simulation comprises the following key steps. Firstly, probability distribution of each cooling variable is defined by analysing the empirical data in Geneve cooling systems permits. The dependence of a cooling variable on building variable is also investigated by conducting a through statistical analysis. In the case such a dependence exists, it is applied in the probability distribution. Secondly, for each building, cooling variables are randomly sampled from the corresponding probability distributions. Thirdly, building specific annual cooling demand is calculated based on the cooling variables assigned. Then, the space cooling demand is aggregated according to the objective of the analysis. For example, in this work, space cooling demand is aggregated at cantonal and national levels. In the last step, steps 2-4 are repeated for adequate runs in accordance with the principle of Monte Carlo simulation to acquire a stable distribution of the aggregated results.

In contrast to current space cooling demand, additional assumptions are made to forecast future space cooling demand. The demolition of existing building and construction of potential new buildings are simulated by a dynamic building stock model [87,88]. Two major impacts of climate change on space cooling demand are considered: diffusion of space cooling device and cooling intensity. Diffusion of space cooling device is modelled by the linear relation between probability of presence of space cooling device and historical maximum CDD [97]. Cooling intensity is assume to be proportional to CDD [92].

2.2.3 Results

2.2.3.1 Current space cooling demand

The total space cooling demand of the Swiss service sector is estimated to be 900 ± 200 GWh/y. The breakdown of space cooling demand by canton is presented in Figure **2.11**. Cantons estimated to have insignificant space cooling due to low CDD are presented in white. Geneva (320 ± 60 GWh/y) has the highest space cooling demand among all cantons, followed by Basel (180 ± 60 GWh/y), and Zurich (140 ± 30 GWh/y). Figure **2.12** visualizes the three components of space cooling demand: service area, saturation rate, and cooling intensity of cooled floor.

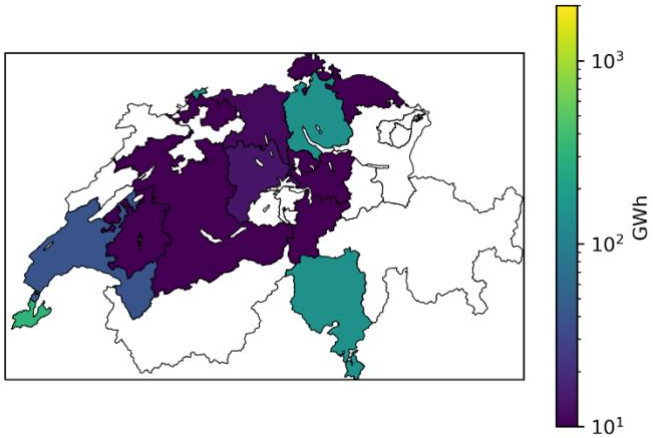

Figure 2.11 - Distribution of space cooling demand in Swiss service sector in 2015 by canton.

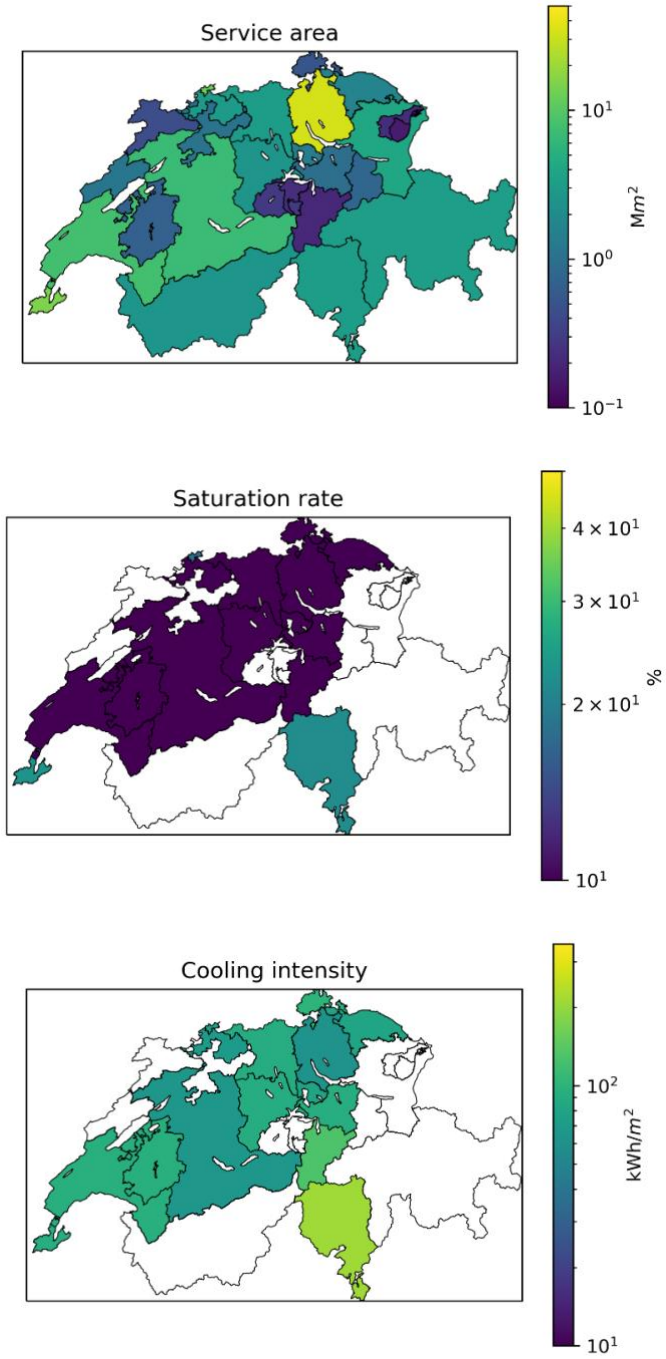

Figure 2.12 - Distribution of service area, saturation rate, and cooling intensity in Swiss service sector in 2015 by canton.

2.2.3.2 Future space cooling demand

Space cooling demand is expected to grow 400% - 600% between 2015 and 2050 in three climate scenarios. The breakdown of space cooling demand in 2050 in three climate scenarios by canton

is presented in Figure **2.13**. The three components of space cooling demand: service area, saturation rate, and cooling intensity of cooled floor in 2050 in RCP 4.5 is shown in Figure **2.14**.

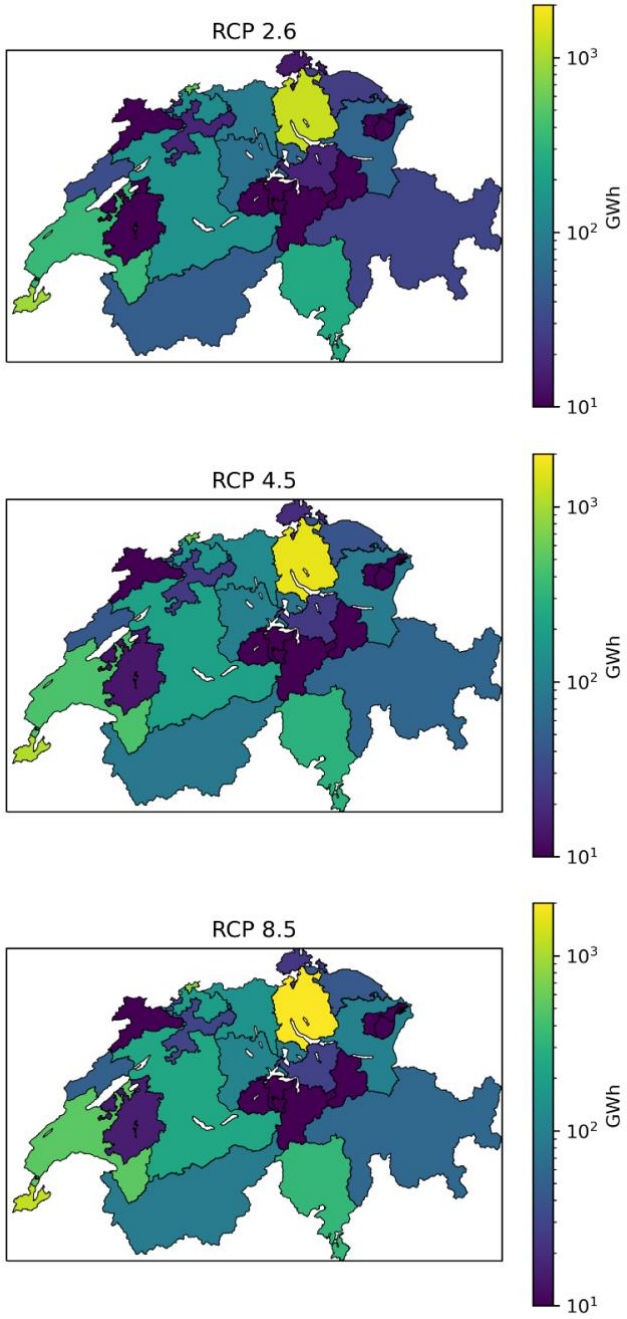

Figure 2.13 - Distribution of space cooling demand in Swiss service sector in 2050 in RCP 2.6, RCP 4.5, RCP 8.5 by canton

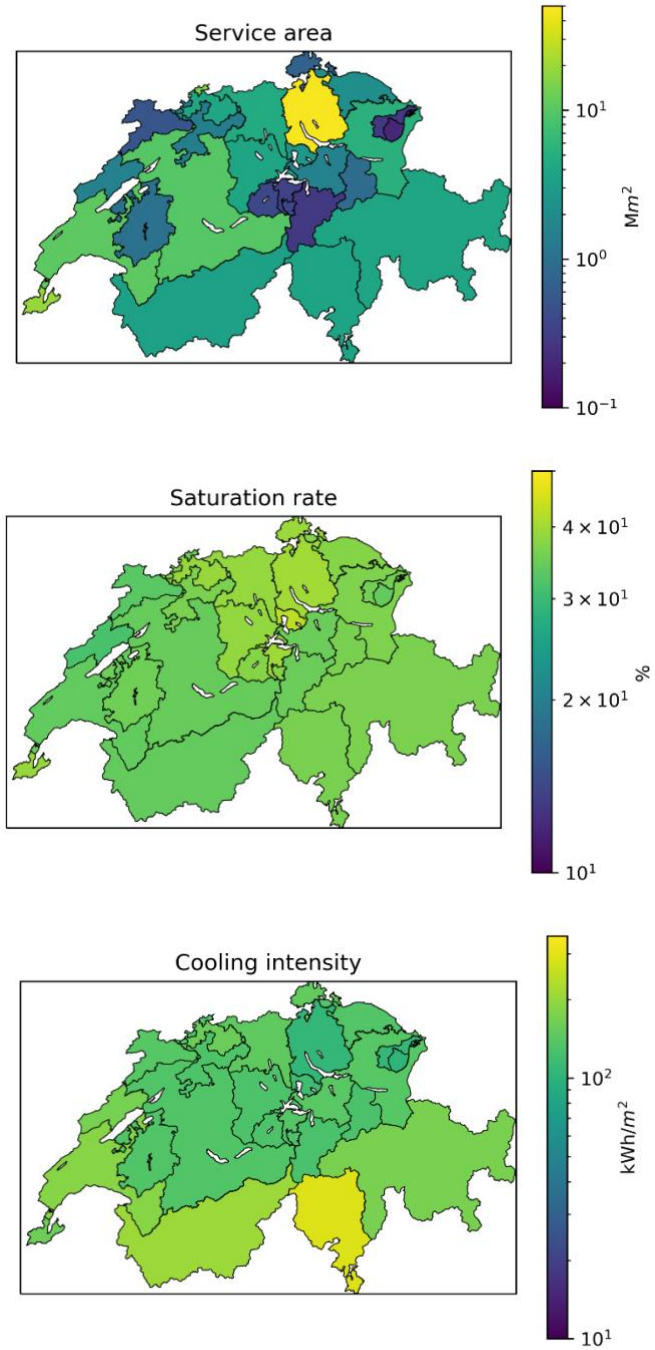

Figure 2.14 - Distribution of service area, saturation rate, and cooling intensity in Swiss service sector in 2050 in RCP 4.5 by canton.

2.2.4 Discussion

Spatial analysis reveals an uneven distribution of space cooling demand among cantons in 2015. Most cooling demand is attributed to cantons with warmer climates, such as Geneva and Ticino. These cantons are characterized with higher saturation rate and higher cooling intensity. For

example, Geneva has a saturation rate of 23% and a cooling intensity of 90 kWh/m².y. In contrast, Zurich has a much lower saturation rate of 7% and a cooling intensity of 60 kWh/m².y

However, cantons with colder climate in 2015 provides the greatest growth potential of space cooling demand by 2050. In all three climate scenarios, Zurich is predicted to become the canton with highest space cooling demand in 2050. The main driver of the growth in space cooling demand is the growth in saturation rate. In the case of RCP 4.5, saturation rates of all cantons fall in the range 32% - 42%, experiencing a substantial growth from 2015. For example, saturation rate of Zurich reaches 40% by 2050, on the same level as Geneva (39%). The growth in cooling intensity is relatively moderate in RCP 4.5. The cooling intensity of Zurich increase from 60 kWh/m².y in 2015 to 110 kWh/m².y in 2050, while that of Geneva increase from 90 kWh/m².y to 160 kWh/m².y. Based on the assumption that the growth rate of service building stock is balanced within Switzerland, the growth in service area is the same among cantons.

2.2.5 Perspectives

The results highlight a rapid growth of space cooling demand in Swiss service sector in the coming decades, especially in cantons with insignificant space cooling demand today. Therefore, it is essential to analyse promising solutions for the substantial increase in energy demand for space cooling in the future, to help decarbonising heating and cooling of buildings based on renewable energy sources and free cooling, and to exploit synergy effects of district heating and cooling network. Another important practical implication is that policy makers needs to regulate the use of air conditioners in advance and promote energy efficient cooling solutions.

3 Availability of shallow geothermal energy and waste energy sources for DHC

Research question 2: What are the technical potentials of shallow geothermal energy usable by DHC?

This chapter responds to the critical need for assessing the availability of renewable and waste energy sources for DHC considering the spatial proximity constraint associated with transporting thermal energy. To fulfil this need, I developed a framework for the optimal allocation of resources under spatial constraints. The framework facilitates large-scale analysis of a broad range of geospatially constrained resources, particularly in the context of mapping renewable energy sources for DHC. The framework's applicability and effectiveness are demonstrated through two case studies. The first case study delves into the technical potential of shallow geothermal energy for direct heat use and for DHC in Cantons Vaud and Geneva, Switzerland. This analysis extends to the exploration of potential synergies between heating and cooling, specifically by considering the use of excess heat generated from cooling processes to regenerate the ground. The second case study quantifies the technical potential of industrial excess heat to supply district heating in Switzerland.

I have prepared three publications based on the work presented in this chapter: two journal papers published in *Computers & Industrial Engineering* and *Energy*, respectively, and one conference paper presented at CISBAT 2021, Carbon Neutral Cities - Energy Efficiency & Renewables in the Digital Era, Lausanne, 8-10 September 2021.

Journal paper 2:

Xiang Li, Alina Walch, Selin Yilmaz, Martin Patel, and Jonathan Chambers. "Optimal Spatial Resource Allocation in Networks: Application to District Heating and Cooling." *Computers & Industrial Engineering* 171 (2022): 108448.

Journal paper 3:

Alina Walch*, Xiang Li*, Jonathan Chambers, Nahid Mohajeri, Selin Yilmaz, Martin Patel, and Jean-Louis Scartezzini. "Shallow Geothermal Energy Potential for Heating and Cooling of Buildings with Regeneration under Climate Change Scenarios." *Energy* 244 (April 2022): 123086. (shared first authorship)

Conference paper 2:

Xiang Li, Jonathan Chambers, Selin Yilmaz, and Martin K. Patel. "An Optimisation Approach for Spatial Allocation of Energy Sources to District Heating Networks." *Journal of Physics: Conference Series* 2042, no. 1 (2021).

.

3.1 Optimal spatial resource allocation in networks: Application to district heating and cooling

3.1.1 Introduction

3.1.1.1 Background

Climate change has become a global concern in the last decades. Many countries have pledged to achieve net-zero emissions in order to mitigate climate change [126]. For instance, the European union (EU) plans to achieve a clean and carbon neutral economy by 2050 through increased deployment of renewable energy, significant energy efficiency improvement, etc [2,127,128]. Heating and cooling play a key role in fulfilling climate commitments, as they account for 49% of global final energy consumption [129]. Furthermore, the demand for cooling is expected to keep growing, caused by expanding demand for air conditioning due to increased frequency and intensity of heat waves under climate change, higher expected thermal comfort, higher wealth and other factors [6,125].

Provision of heating and cooling in buildings using renewable energy sources has a high decarbonisation potential but faces a range of barriers [10]. These include the higher variability of renewable energy sources, the need to connect resources with the demands, and the large range in heat supply temperature (which is higher for less efficient buildings) [130]. District heating and cooling (DHC) has been receiving increasing attention as it enables the wide use of renewables and low-temperature energy sources including solar, geothermal, waste heat, thermal energy from water bodies, etc. [131]. DHC connects multiple buildings in a district by a pipe network, allowing to supply thermal energy from central plants or distributed energy conversion units [11]. Water is typically used as the thermal energy carrier. Advantages of DHC are firstly that it enables the integration of locally available renewable and waste energy, secondly it offers thermal energy storage which ensures flexible and reliable supply of energy, and thirdly it provides the potential to improve system energy efficiency [9]. In particular, 4^{th} and 5^{th} generation district heating and cooling works with a low distribution temperature of 50°C and in the range of 0°C to 30°C respectively thereby allowing better integration of low-temperature renewable and waste heat sources .

However, unlike fossil fuels that can be readily and very efficiently transported by freight, distributing thermal energy via water is subject to considerable thermal and pressure losses, making transporting distance a major factor that influence the system efficiency [132]. Thermal energy, therefore, needs to be consumed within short distance from the generation site.

Consequently, spatial analysis is generally conducted to map potential energy sources for DHC under the constraint of spatial proximity.

3.1.1.2 Previous studies

Many studies have focused on the national scale mapping of prospective DHC areas and low-carbon thermal energy sources [23,133,134]. In many cases where adjacent DHCs are involved, a problem arises about how to efficiently allocate identified energy sources when they are shared by several DHCs. Most studies have not treated the allocation of potential resources to DHC demands in much detail. As DHC is gaining popularity, especially in areas with dense buildings [135], having an appropriate and accurate method to optimally allocate thermal energy for DHC should be of key importance to urban and energy system planners and engineers.

A recent study [133] points out the issue of efficient allocation when investigating allocable energy potential of industrial excess heat, defined as the maximum amount of heat that can be allocated to district heating area under spatial constraints. This study might underestimate the allocable energy potential, since it arbitrarily assigns the excess heat sources to the nearest district heating area, which often is not the optimal assignment for full utilization of the available resource. In another study on the potential of supplying district heating networks using industrial excess heat, Chambers et al. [136] developed a spatial clustering method that enables decomposing a national scale problem into smaller scale clusters of adjacent supplies and demands. This approach further estimates the allocable resources in clusters using a net balance method. If the total supply is lower than the total demand, then all supply is allocable. If the total supply surpasses total demand, the excess supply is curtailed, which means the allocable resources equals the total demand. It assumes that heat energy can be allocated freely within the same cluster, thus possibly overestimating the maximum usable potential.

Overall, there is a lack of studies on how to optimally allocate potential thermal energy sources to DHCs on a large scale. Inability to solve this issue will cause an inefficient use of resources. Further research is therefore needed to develop effective and accurate methods to analyse the optimal spatial allocation of resources.

3.1.1.3 Research aims and objectives

To address this research gap, we aim to develop and evaluate a method to enable optimal spatial allocation of resources applicable to DHC. The method should be scalable to handle large-scale analysis, and estimate maximum allocable resources with improved accuracy.

We propose a spatial allocation with optimisation (SAO) method that integrates geospatial data pre-processing, a graph theory-based cluster partition technique, and an optimal allocation algorithm adapted from transportation theory. We perform a case study of the shallow

geothermal potential for DHC in which we demonstrate the advantage of using the SAO method when allocating thermal resources compared to a reference method without optimisation of the allocation under spatial constraints.

The strength of the SAO method lies in 1) matching between supplies and demands at high spatial resolution, 2) improving the applicability by disaggregating a large-scale problem into smaller units through graph theory, and 3) optimising the allocation of resources in a network of supplies and demands.

The scope of this work is to analyse spatial constraints in resource allocation, while the temporal aspect is not the focus. In the case study, we compute the allocation of geothermal potential for annual values. Nevertheless, when applied to resources subject to temporal constraints, for example, diurnal and seasonal variation of solar energy, the SAO method can be performed in parallel in time steps of appropriate resolution (e.g. month, day, hour).

3.1.2 Theoretical background

The investigated problem is interdisciplinary, combining existing theories from geography, engineering, mathematics, etc. Before outlining our proposed method, we first introduce two theories that provide its basis.

3.1.2.1 Graph theory

In the analysis of resource allocation, graph theory naturally arises, as it studies the pairwise relation between objects [137]. Graph theory is commonly applied in real-world allocation problems like inpatient bed management [138], facility location problem [139], etc. A graph is made up of nodes which are connected by links. In this context, potential thermal energy sources and DHC demands can be treated as nodes, while links between them (graph edges) describes connectivity.

Connected component

One problem of a large-scale analysis of resource allocation is the great number of objects and the following heavy computational burden. Utilizing graph partition techniques, we break down a complex large-scale problem into independent small-scale units and thus reduce the solving time of the allocation optimisation problem. A graph can be separated into connected components. Nodes within the same connected components are connected to each other via a sequence of links (called paths), and are not connected to any other node in the rest of the graph. Two efficient algorithms exist for computing connected components of a graph which have the same running time [140]: breadth-first search [141] and depth-first search [142].

Bipartite graph

Bipartite graphs are mathematical models of interactions between two disjoint sets of objects, such as agencies and clients, jobs and workers. A bipartite graph is a graph which has two disjoint sets of nodes. Each link connects one node from one set and one node from the other set. Bipartite graphs are widely used for problems of optimal matching, including maximum cardinality matching, assignment problems, etc. Specifically, the assignment problem [143] shares some similarity with the resource allocation problem. It aims to find the optimal pairwise matching of nodes in a bipartite graph that minimizes the sum of weights (usually representing cost) assigned to links [144]. It is solvable by integer programming. However, since the number of nodes in an assignment problem is given by an integer value and since the nodes are not dividable, the assignment problem of bipartite graphs is not directly applicable to a resources allocation problem in which supply and demand nodes have various size and are allowed to be divided. Once we drop the integrity constraints on nodes in the assignment problem, it is generalized to a transportation problem, which we illustrate in the next subsection.

3.1.2.2 Transportation theory

In mathematics and economics, the study of optimal transportation and allocation of resources is called transportation theory. The range of applications include, but are not limited to, allocation of medical resources [145] and humanitarian logistic [146]. The Hitchcock–Koopmans transportation problem [147,148] describes a fundamental type of problem in this field. Several sources are supplying a product to numerous localities. The unit transportation costs vary with the routes between supplies and demands. It is required to find the least cost resource allocation plan that satisfies the demands from the supplies.

The original transportation problem deals with transportation cost as a linear function of delivery volume. Linear programming [149] is typically used to solve this general linear model, which is proven to be solvable in polynomial time [150]. The problem is further extended to nonlinear convex problems [151] in which transportation cost is nonlinear to delivery volume, in an effort to widen the range of applications.

3.1.3 Materials and methods

3.1.3.1 Problem description

The problem introduced in Section 3.1.1.1 is to find an optimal allocation of resources to DHCs under spatial constraints. Both supplies and demands are distributed in the study area with limited connectivity. The transportation of resources is only possible via feasible connections between them. In the case of DHC, the constraint of spatial proximity applies. Transporting resources incurs losses resulting in varying transportation efficiencies of each feasible

connection. The problem is then to find the optimal allocation plan between supplies and demands that maximize allocable resources.

The method to address this problem comprises the following steps :1) transformation into a graph: (convert data on supplies and demands into a bipartite graph, 2) partition: split the original graph into subsets of connected components through graph theory, and 3) optimal allocation: calculate the maximum allocable resources within each subset using linear programming. The method is also applicable to the optimal allocation of a range of geographically bounded resources, e.g., irrigation water and medical service.

3.1.3.2 Mathematical model

Transformation into a graph

We solve this problem by modelling it mathematically as a graph. When expressed as a graph, supplies and demands are treated as two independent sets of nodes of a bipartite graph. Feasible connections are identified and defined as links between supply nodes and demand nodes. The following paragraphs detail how to transform data of supplies and demands of resources into a graph.

The input data needed are the locations, geometries, and capacities of supplies and demands. Geospatial analysis is employed to identify feasible connections subject to certain criteria, for instance spatial proximity. This constraint is implemented using a cut-off distance. For each demand, all supplies for which the closest (Euclidean) distance to the demand is below the cut-off distance are connected with the demand. Once all feasible connections are identified, supplies and demands that are not connected to other objects are omitted from the analysis.

It is important to note that this method is flexible, allowing for the integration of other constraints on connecting supply and demand. Although only the constraint of spatial proximity is considered above, other constraints related to the physical properties of the network connection and transportation cost, such as flow density, pipe capacity, etc., could also be considered.

Finally, supplies are formulated as a set of nodes S. Demands are formulated as a set of nodes D. Feasible connections are formulated as a set of links L which connects a node in S to a node in D. Information on the capacity of supplies and demands is kept for further analysis. Links representing feasible connections are characterized by their length and transportation efficiency. However, information on the location and geometry are disregarded in this step. The focus is then on the pairwise connections between supplies and demands. The resulting bipartite graph $BG = (S, D, L)$ covers the whole study area.

Partition

Prior to performing the optimal resource allocation, the original bipartite graph BG is split into connected components based on the existence of links (connectivity of nodes) mentioned in previously. In the graph partition process, supply nodes S and demand nodes D are handled in the same way. Using breadth-first search, we obtain in total p connected components (so-called subgraphs), namely $BG_1, \dots\ BG_p$.

Each connected component is a subset of nodes that are connected to each other by a sequence of links implying spatial proximity, but not to additional nodes outside the subset. There is no link between connected components, which implies that transporting resources between subgraphs is not possible. Therefore, we can analyse the optimal resource allocation of each subgraph separately, without introducing any error.

This has the advantage of reducing the computational cost and increasing the scalability of the method in terms of the amount of data that can be processed. This constraint on the size of the data is caused by the running time of the subsequent analysis on graphs, which tends to grow polynomially with the number of nodes. The partition into connected components limits the maximum number of nodes in each subgraph and allows each subgraph to be processed in parallel. In the case with as many parallel processes as nodes, the computation time is a function of the size of the largest single node.

Optimal allocation

Let an arbitrary subgraph $BG_k = (S_k, D_k, L_k)$ have m supply nodes $S_k = (S_1, \dots, S_m)$, n demand nodes $D_k = (D_1, \dots, D_n)$, and a set of links L_k. Specifically, the i^{th} supply node has capacity of s_i, while the j^{th} demand node has capacity of d_j. S_i and D_j are connected if and only if L_{ij} (connecting S_i and D_j) $\in L_k$. Transporting resources via link L_{ij} is subject to the transporting efficiency of η_{ij}, which depends on the application. It is assumed that η_{ij} is not a function of the resource transported via the link.

The connectivity of the bipartite graph BG_k can be represented by a biadjacency matrix B (the adjacency matrix of a bipartite graph). Where $b_{ij} = \eta_{ij}$ if and only if $L_{ij} \in L$, and $b_{ij} = 0$ when $L_{ij} \notin L$.

An optimal allocation algorithm is introduced to accurately find the maximum allocable resources within each subgraph. The optimisation problem is formulated as a variation of the Hitchcock–Koopmans transportation problem. The total supply capacity and total demand capacity in each subgraph in our study are generally unbalanced, resulting in solving a transportation problem with surplus and deficit. Moreover, the objective of our optimisation problem is maximizing the allocation of resources, instead of minimizing the transportation

cost. The mathematical formulation of the Hitchcock–Koopmans transportation problem is therefore adapted as follows:

The objective is to find an optimal allocation plan represented by matrix X in which the allocated resources z_k are maximized:

$$maximize\ z_k = \sum_i \sum_j b_{ij} x_{ij} \tag{3.1}$$

Where x_{ij} is an element of X that denotes the amount of resource allocated from S_i to D_j.

The resources transported via each link must be larger than zero:

$$(i = 1, 2, \dots, m, \quad j = 1, 2, \dots, n) \quad x_{ij} \geq 0 \tag{3.2}$$

The allocation plan represented by matrix X is subject to the additional constraints, i.e. i) that the total resource transported from a supply must not exceed the supply capacity and ii) that the total energy transported to a demand must not exceed the demand size.

For supplies this constraint may be expressed as:

$$(i = 1, 2, \dots, m) \quad \sum_j x_{ij} \leq s_i \tag{3.3}$$

For demands this constraint may be expressed as:

$$(j = 1, 2, \dots, n) \quad \sum_i b_{ij} x_{ij} \leq d_j \tag{3.4}$$

Since the optimisation problem introduced above is linear, it can be solved using linear programming [149] and is guaranteed to find the global optimal.

The total allocable resource is the sum of the maximized allocable resource of all subgraphs:

$$z_{total} = \sum_k z_k \tag{3.5}$$

3.1.3.3 Method implementation

The proposed method is implemented in Python 3.7. The Python library Geopandas [152] is used for spatial operations on geospatial data. The library NetworkX [153] is used for the creation, partition, and investigation of graphs. The linear programming library PuLP [154] is utilized to obtain the maximum allocable resources in a graph, as well as the optimal allocation plan. Other Python libraries used in this method to manipulate data include Xarray [155], Rasterio [156], Numpy [157], and Pandas [158]. Table **3.1** summaries the functions used to implement the method.

Table 3.1 - Python functions used in method implementation.

Step	Function	Description
Transformation into a graph	Code written by the authors using Pandas, Geopandas, Xarray, Numpy, and Rasterio	Data preparation.
	Geopandas.GeoSeries.distance	Calculate the closest distance between geospatial objects.
Partition	NetworksX.Graph	Create a graph.
	NetworkX. connected_components	Implement the breadth-first search to calculate connected components.
Optimal allocation	PuLP	Implement linear programming to solve the transportation problem. Linear programming is done via the Revised Simplex Method.

3.1.4 Case study

In this case study, the potential of geothermal energy from shallow ground-source heat pumps (GSHPs) to supply DHC is quantified in the Cantons of Vaud and Geneva (Switzerland). In the case study, potential shallow geothermal sources are spatially distributed and are required to be allocated as energy suppliers to local DHCs. The need for spatial allocation arises when there is an excess geothermal supply or a demand deficit within a DHC. Specifically, an optimal spatial allocation is required when a geothermal source is reachable by more than one DHC and the energy resource must be divided among them. We demonstrate the advantage of the SAO method by comparing it with a simpler reference method [136], which performs spatial clustering but does not apply optimal allocation.

The input data of the case study include potential shallow geothermal supplies and potential DHC regions in the format of geographic information system (GIS) polygons. Each polygon is associated with its excess annual heating supply (for geothermal supplies) or demand deficit (for DHCs). Table **3.2** summarises the input data set, which is visualised in Figure **3.1**. It is assumed that the geothermal supplies within a cut-off distance of 1km from DHC areas are potential heat sources. The transportation losses are ignored (transportation efficiency is set to 100%).

Table 3.2 - Summary of the input data set of the case study.

	Data	Description	Source
Supplies	Potential shallow geothermal supplies	Geothermal sources represent the maximum energy that can be extracted from the shallow subsurface (< 200 m) using closed-loop GSHP technology, without over-exploiting the heat capacity of the ground [159]. This data include 4241 polygons, with in total 4187 GWh/year of excess shallow geothermal heating potential.	[160]
Demands	Potential DHC areas	Geographical areas for potential low-temperature district heating. This data include 291 polygons, with in total 1688 GWh/y heating demand deficit.	[161]

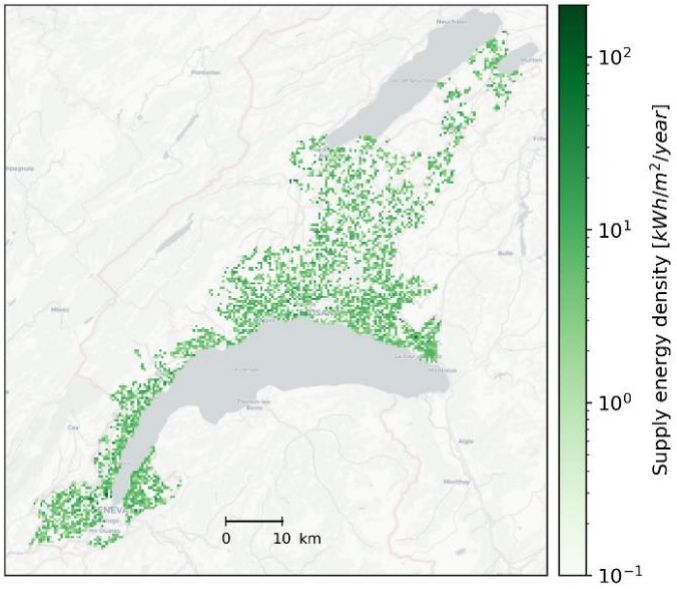

(a)

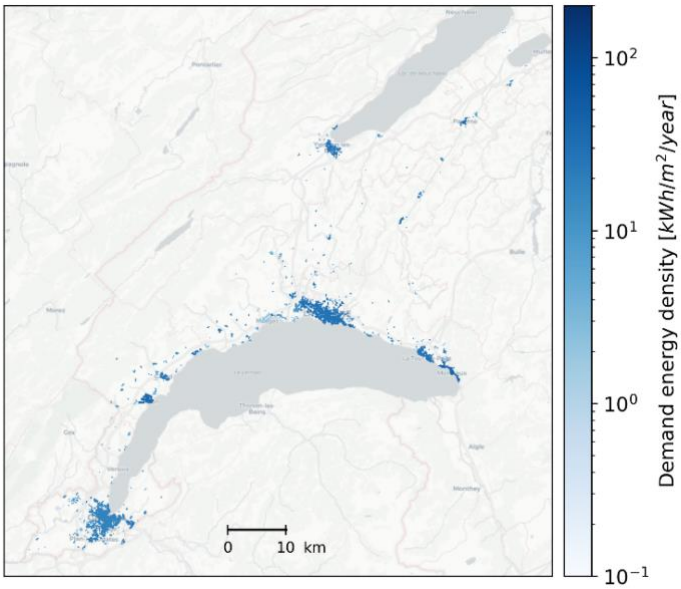

(b)

Figure 3.1 - Input data. (a) Potential shallow geothermal supplies and (b) district heating and cooling (DHC) areas.

3.1.5 Results

In this section, we investigate the advantages of the SAO method by applying it to the case study. Section 3.1.5.1 presents the demonstration on large data set. Section 3.1.5.2 presents the estimated allocable geothermal energy of the SAO method in comparison with the reference method

without optimisation. Section 3.1.5.3 investigates the impact of adding an optimal allocation algorithm on estimated allocable resources in an illustrative subgraph.

3.1.5.1 Demonstration on large-scale spatial allocation problem

The case study demonstrates that the SAO method can solve the spatial resource allocation problem for a large data set. Table **3.3** provides the change in size of the spatial resource allocation problem while applying SAO to the case study. We found that both step one (Transformation into a graph) and step two (Partition) contribute to reduce the computational burden. In step one, more than half (54%) of supply and demand nodes are omitted before creating the bipartite graph as they cannot be feasibly connected to any other node. This largely reduces the complexity of the allocation problem. In step two, the bipartite graph covering the whole study area is decomposed into 82 subgraphs, as shown in Figure **3.2**. It is apparent from Figure **3.2** that the scale of the subgraphs is significantly smaller than the original bipartite graph (decreasing from a total of 2077 nodes to at most 341 nodes). The computing time required to solve the optimal allocation algorithm increases polynomially with the number of nodes. Therefore, it is almost impossible to solve the original large-scale spatial allocation problem in a reasonable time. By breaking down the complex allocation problem into smaller pieces, it becomes computationally feasible to solve the allocation for the collection of subgraphs (run time for the case study of approximately 2 minutes on 1 CPU).

These results indicate that the SAO method can solve large-scale spatial allocation problems. In particular, the graph partition technique used in step two contributes substantially to reducing the computational complexity while preserving a high spatial resolution.

Table 3.3 - Change in size of allocation problem.

Stage	Size of allocation problem
Input data	4241 supply nodes, 291 demands demand.
After step one - Transformation into a graph	A bipartite graph with 2077 nodes (1799 supply nodes, 278 demand nodes) and 2916 links.
After step two - Partition	In total 82 subgraphs. The biggest subgraph (in terms of number of elements) has 341 nodes (296 supply nodes, 45 demand nodes) and 578 links.

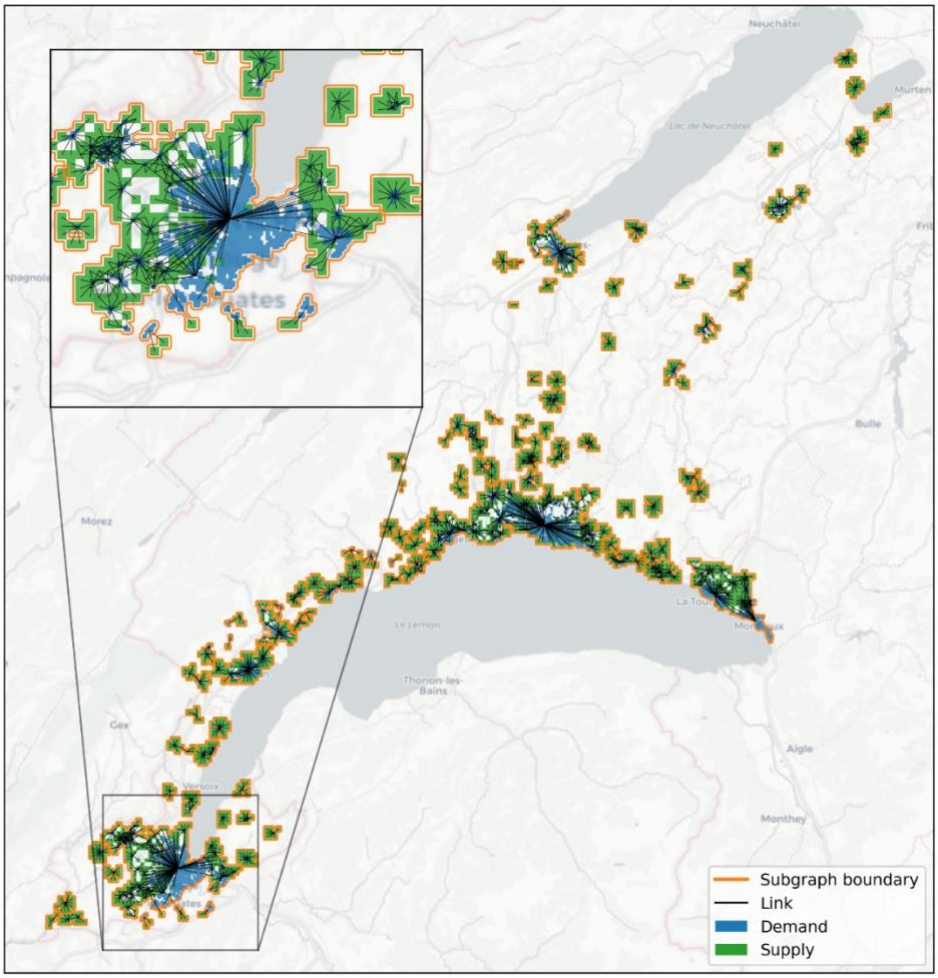

Figure 3.2 - Results of partition into independent subgraphs, with a zoom into the region of Geneva.

3.1.5.2 Estimation of the allocable resources

To evaluate the performance of the SAO method in optimising the resource allocation, the results of the estimated allocable geothermal energy to DHCs in the case study, as obtained by the proposed method, is presented in comparison with a reference method without optimisation [136]. Figure **3.3** compares the total allocable resources (sum of all subgraphs) of the case study estimated by the two methods, while Figure **3.4** shows the subgraphs in which the two methods report different results.

The SAO method estimates that the total allocable geothermal energy is 783 GWh/y, while the reference method without optimisation estimates the total allocable geothermal to be 1105 GWh/y (Figure **3.3**). Hence, adding optimal allocation results in a significantly lower (29.1%) estimate of the total allocable geothermal potential. This is because, at the subgraph level, the SAO method always gives estimations less than or equal to the estimation obtained by the reference method. This is expected since the SAO method introduces additional constraints on

the resource allocation with the subgraphs, in comparison to the reference method. There is a large range in the differences compared to the reference method (15%-45%) in 9 out of 82 subgraphs (marked in Figure **3.4**). In general, the differences are larger in the larger subgraphs, however this is not exclusively the case. In the remaining subgraphs, the two methods report the identical results.

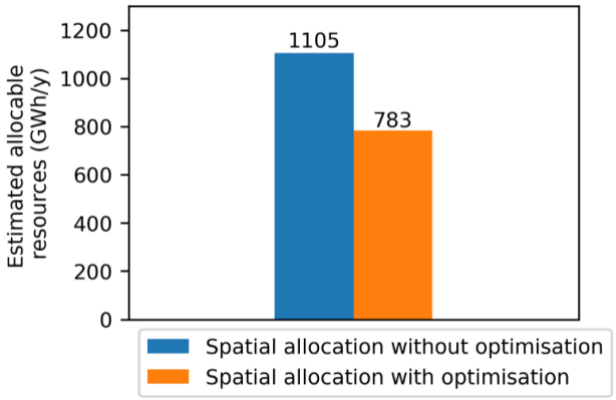

Figure 3.3 - Comparison of the estimated allocable resources by the spatial allocation with optimisation method and the reference method without optimisation.

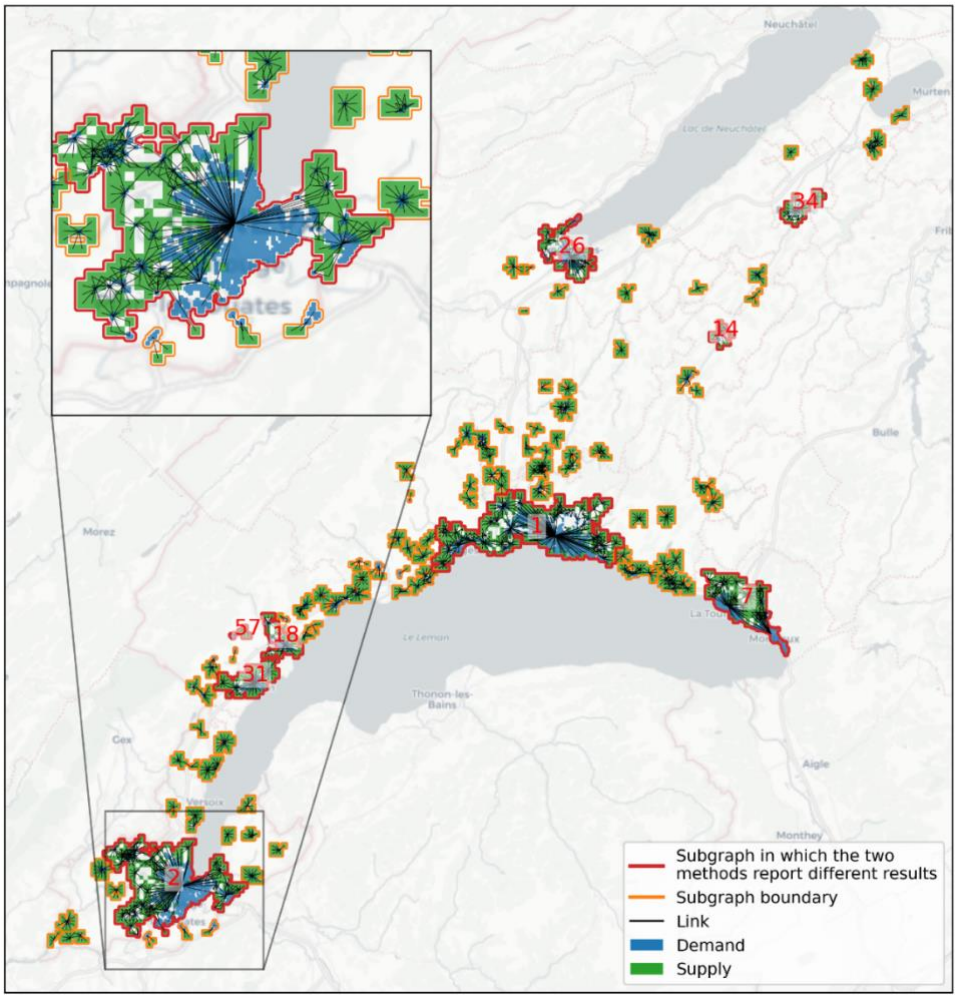

Figure 3.4 - Graphical representation of the difference in results between the spatial allocation optimisation methods and the reference method without optimisation, with a zoom into the region of Geneva. The numbers in red are subgraph labels.

3.1.5.3 Investigation of impact of SAO in illustrative subgraph

To visualise the impact of adding optimisation on the result of resource allocation, we select a single subgraph (subgraph 57, Figure **3.4**) as an example since there is too much data in the whole case study. Subgraph 57 has five supply nodes, two demand nodes, and six links. It covers in total 3.7 GWh/y geothermal potential supply and 4.0 GWh/y heating demand within the DHC area (Figure **3.5**a). The allocable geothermal energy is 3.7 GWh/y without optimisation and 2.1 GWh/y with optimisation, representing a decrease by 43%.

Without optimisation, estimating the resource allocation would possibly lead to invalid transportation of resources. Figure **3.5**b shows the detailed optimal allocation plan generated by the SAO method that maximise the allocable resources. In this example, although the nodes S4

and D2 could be related by a long sequence of links (S4-D1-S3-D2), the SAO method does not transport the resources along this pathway (only direct links are allowed). When such long sequences of links exist, optimising the spatial allocation is necessary to avoid an overestimation of the allocable resource.

The overestimation of allocable resources by ignoring optimal allocation also applies to other subgraphs. We found overestimation in 9 subgraphs which have at least one long sequence of links in the case study. These situations occur especially when there are relatively dense regions of supplies and demands, e.g., in the extended suburban areas around cities. Without optimisation, the allocation of resources within these extended clusters could erroneously assume that resources can be used where in reality they cannot. These results highlight the importance of intra-subgraph spatial constraints in the resource allocation problem, and demonstrate the necessary significant correction compared to the assumption that resources can be distributed freely within each subgraph.

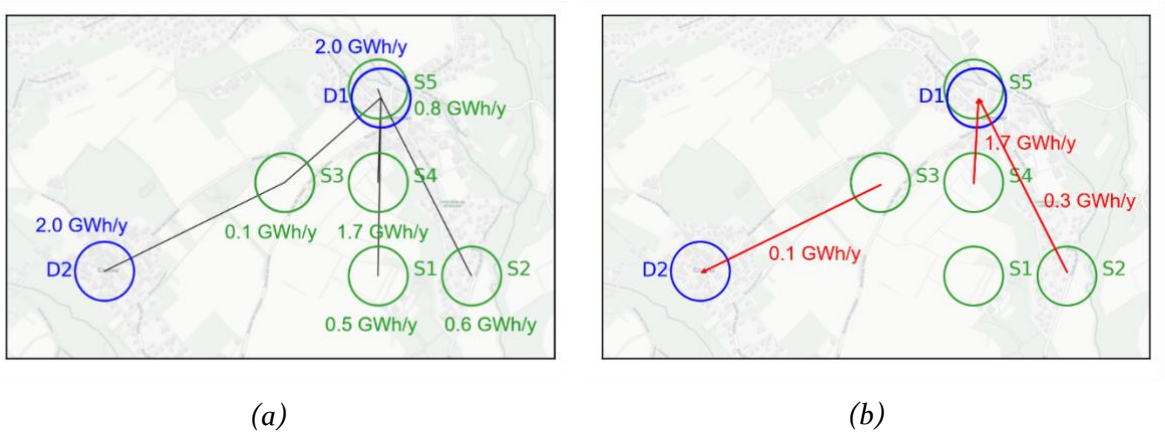

Figure 3.5 - Subgraph 57 (see Figure **3.4**) as an illustrative example of supply, demand, and links. (a) Nodes and links. The supply potential (green) and demand potential (blue) of the nodes are marked. (b) Solution of optimal allocation plan (red).

3.1.6 Discussion

This paper proposes a method combining geospatial analysis, graph theory, and transportation theory to model large-scale spatial allocation problems. The main findings and implications for policy makers, urban infrastructure designers and planners can be summarised as follows:

The SAO method significantly improves the accuracy in computing allocable resources in comparison to the reference model without optimisation. We showed that the reference method without optimisation overestimates the allocable resources under spatial constraints, especially in larger subgraphs (in terms of the number of nodes) that generally account for a greater proportion of the resources to be allocated. In particular, it is common that numerous supplies

and demands in close proximity form a large subgraph in dense areas such as cities. These findings suggest that it is crucial to use optimisation for spatial allocation of resources under constraints (e.g., geothermal, waste water). This allows to avoid planning errors in systems design for districts and cities.

The SAO method generates an optimal resource allocation plan in addition to computing allocable resources, which is a clear advantage compared to the reference method present in literature (without optimization). Such detailed plans could be used by urban planners and engineers as a basis for planning the exploitation of resources.

The computational efficiency of the SAO method allows for it to be broadly applied, due to the lower computational power needed and the potential of automated analysis.

This work is subject to several limitations. The SAO method allows to flexibly consider weights of links between supplies and demands. While fixed transportation efficiency is assigned as weights of all links in the case study, the method accepts any weights that are a linear function of transportation quantity. However, if non-linearity is included in the objective function, which is common in the real world, linear programming is not sufficient to solve the problem. In this case, nonlinear programming is necessary to extend the range of applications of the method. This is an important issue for future research. Another limitation of the method is that in the partition step, it is still possible to create subgraphs with a large quantity of nodes and links, requiring massive computing power. Further work is needed to address these computational difficulties.

3.1.7 Conclusion

This paper presents a method to estimate the maximum allocable resources in networks of supplies and demands under spatial constraints. This method for spatial allocation with optimisation (SAO) combines multidisciplinary approaches, including geospatial analysis for data processing, graph theory formulation to partition the problem into smaller scale, and an adapted Hitchcock–Koopmans transportation problem that addresses the efficient allocation of resources. We investigated the advantages of the SAO method in a regional case study of shallow geothermal potential supplying building thermal demands in the Cantons of Vaud and Geneva, Switzerland, by comparing the SAO results to a reference model without optimisation. The advantages of the SAO method include improving the accuracy in computing allocable resources compared with the reference method, and additionally providing the optimal allocation plan that maximise the resource allocation. Furthermore, we found that the method can address the spatial allocation of resources on a large scale.

The developed SAO method could be applied to the allocation of diverse geospatially bounded resources, especially in the field of mapping sources for district heating and cooling, such as industrial excess heat, geothermal energy as well as lakes and rivers as thermal reservoirs.

3.2 Shallow geothermal energy potential for heating and cooling of buildings with regeneration under climate change scenarios

3.2.1 Introduction

Shallow geothermal energy is a promising low-carbon source to meet heating and cooling demands of buildings. The most commonly used type of shallow geothermal system in many European countries, including Switzerland, are vertical ground-source heat pumps (GSHPs) [162]. These systems exchange heat with the ground through one or multiple borehole heat exchangers (BHEs) installed at depths of up to 400m [163]. As temperatures are rising and extreme heat events are becoming more frequent due to climate change, space cooling demands may increase worldwide by up to 750% in residential buildings and 275% in commercial buildings by 2050 [45]. In heating-dominated climates such as central Europe, growing cooling demand could motivate a combined use of shallow geothermal energy for heating and cooling of buildings, using the ground as seasonal heat storage [164]. The re-injection of excess heat from space cooling to the ground hereby permits its seasonal regeneration, which reduces negative impacts of geothermal installations on the surrounding shallow subsurface [165,166]. This has two-fold benefits for the technical geothermal potential, defined as the maximum thermal energy that can be exchanged with the ground using GSHP technology. Firstly, it allows a renewable supply of cooling demand, and secondly, it increases the potential for heating.

Evaluating the potential of GSHPs with seasonal regeneration requires (i) determining the amount of excess heat available during the regeneration period, and (ii) linking the potential GSHP systems to buildings. While individual GSHPs are directly connected to a nearby building, district heating and cooling (DHC) systems allow to transport heat between areas with high geothermal potential and areas with high energy demand [11]. In particular, 4th generation DHC, also known as low-temperature district heating (LTDH), has become attractive in Europe due to improved system efficiency, ability to integrate renewable and low-temperature sources and low carbon emissions [25,167]. DHC is thus a promising technology to increase the useful geothermal potential, defined as the useful energy for supplying building energy demands.

To date, many studies of the technical geothermal potential quantify the energy that may be extracted from a single installation at a given location, for example in Italy [168,169], Spain [170], Chile [171] and southern Switzerland [172]. These studies focus on the quantification of ground parameters but neglect the impact of the built environment or other GSHP systems. The built environment and its impact on the available area for installing BHEs has so far been primarily considered in studies at district scale [173,174]. However, these studies rarely account for thermal

interference [175], referring to increased ground temperature changes around densely installed BHEs, which increases the environmental impact of GSHPs and reduces their technical potential [176]. Thermal interference is addressed in studies of hypothetical borehole fields [177,178] or by studying thermal plumes around existing installations [179,180]. The regional-scale effects of thermal interference and the available area for BHE installation on the technical GSHP potential have been considered in a previous study by the authors [159], which however did not consider seasonal regeneration.

Seasonal regeneration, defined as the re-injection of heat to the ground during summer, has been mentioned in city-scale studies as a possibility to increase the geothermal potential [181]. Different heat sources for seasonal regeneration of GSHPs, notably space cooling needs and solar thermal generation, are discussed and compared in [182]. Case studies of individual buildings with seasonally regenerated GSHPs, referred to as "hybrid GSHP" (HGSHP) in [164], can be found for buildings of the residential [183], service [184] or transport sector [185]. While these studies provide an indication of the potential of seasonal regeneration, the results are specific to each case study. A large-scale view of the regeneration potential is provided in some studies by comparing fictive HGSHP systems in across a number of locations, for example for 19 cities in the EU [186], 40 cities in Greece [187] or three locations in Australia [188]. A sensitivity analysis of five types of HGSHPs across several building types in North America is provided in [189]. None of these studies, however, quantify the impact of seasonal regeneration on the geothermal potential for an entire region.

Accounting for seasonal regeneration of GSHP systems requires matching the technical geothermal potential with building energy demands. Such matching has been done at building level [190], district level [175], and at city/large scale [191,192]. However, these studies have only dealt with the mapping of potential installations to nearby buildings, thus not considering the potential of DHC. To date, the potential of shallow geothermal energy to supply DHC has mostly been assessed for case studies of individual DHC, often focusing on the techno-economic analysis of the DHC design [193,194]. Some case studies also address the potential of combining geothermal energy with other renewables such as wind [195] and/or solar thermal energy [196,197] in DHC. The design of DHC with geothermal heat sources has also been assessed at city scale, focusing on network design rather than technical limitations of geothermal systems [198]. At regional or national scale, a spatial mapping of potential heat sources for DHC has been provided for Denmark [134], but excludes geothermal resources. Stegnar et al. [199] have assessed the techno-economic potential of shallow geothermal energy for DHC in Slovenia, accounting for thermal interference and local ground characteristics. Of these studies, only Formhals et al. [197] consider seasonal regeneration, and no study beyond building scale quantifies the potential for supplying heating and cooling demands from GSHP systems.

To fill the above-mentioned gaps, this paper presents a novel framework to estimate the technical and useful shallow geothermal potential from GSHPs for space heating and cooling at regional scale. The proposed framework combines, for the first time, (i) the spatial mapping between building energy demands and potential GSHPs at regional scale, (ii) the analytical modelling of seasonal regeneration for GSHPs, and (iii) the optimization of heat supply for district heating and cooling (DHC). To this aim, we expand the analytical model for quantifying technical geothermal potential at regional scale, proposed by Walch et al. [159], to account for bi-directional GSHP operation (heat injection and heat extraction). In this work, excess heat from space cooling is considered for heat injection, but the proposed approach can also be used for other heat sources. We further apply a graph-theory based optimization for maximising the supply of technical geothermal potential to buildings using DHC. The method is applied to a case study in the cantons of Vaud and Geneva in Switzerland, the country with the world's highest density of direct geothermal energy use per land surface [162], mostly from GSHPs [200]. Following a scenario-based approach, we obtain the technical and useful shallow geothermal potential with and without DHC, for two market penetration levels of building cooling systems and for three climate change scenarios. To the best of our knowledge, the results present the first regional-scale estimate of shallow GSHP potential that combines space heating and cooling.

3.2.2 Methods

The proposed framework for assessing the technical and useful potential of GSHPs to cover building heating and cooling demands consists of three stages, as shown in Figure **3.6**: First, geospatial processing is performed to match potential GSHP systems to building energy demands (Section 3.2.2.1, green boxes in Figure **3.6**). Second, analytical modelling is used to quantify the technical heat exchange potential for GSHP systems (Section 3.2.2.2, blue boxes in Figure **3.6**). The considered GSHP systems consist of vertical closed-loop BHEs, from which heat is extracted during the winter months for space heating and re-injected using excess heat from space cooling during the summer months, leading to seasonal regeneration. Third, spatial analysis is applied to optimally allocate the technical potential between individual GSHPs and DHC, yielding the useful geothermal potential (Section 3.2.2.3, orange box in Figure **3.6**). All modelling steps described below were implemented using the *python* programming language.

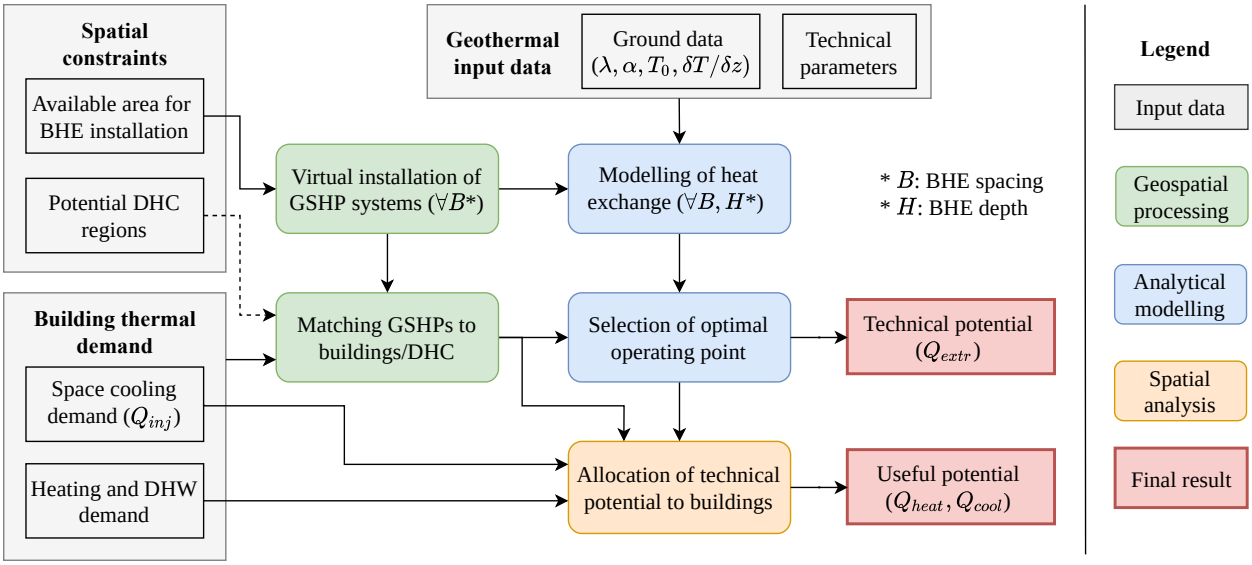

Figure 3.6 - Workflow for modelling the technical potential of GSHP ($\boldsymbol{Q_{extr}}$) and the useful potential for supplying heat ($\boldsymbol{Q_{heat}}$) and cooling ($\boldsymbol{Q_{cool}}$), consisting of three stages: (1) Geospatial processing (green boxes), (2) Analytical modelling (blue boxes), and (3) Spatial analysis (orange box), corresponding to the following sub-sections. Dashed lines are used only if DHC is considered.

3.2.2.1 Geospatial processing

To assess the potential for ground-source heat pumps at regional scale, we use a spatial mapping approach to (i) assign the location and arrangement (i.e., spacing) of potential BHE installations and (ii) match the resulting virtual borehole fields with the building energy demand.

Virtual installation of GSHP systems

To assign the location and arrangement of potential BHEs, we use the estimated available areas for BHE installation provided in [159], which have been derived from parcel data. These parcels represent individual property units, from which building footprints, other built-up areas (roads, railways, traffic-related areas and leisure zones) and natural habitat that is likely unsuitable for the installation of BHEs (water bodies, forests and wetlands, protected areas) have been removed. To obtain the available areas, a buffer of 3m has further been subtracted from parcel boundaries and building footprints, as specified in the technical norm for geothermal installations of the Swiss association of engineers and architects (SIA) [201].

On these available areas, we virtually install BHEs as rectangular grids with spacings (B) ranging from 5m to 100m, assuming that all available area is covered by these BHE grids. The lower boundary for B (5m) equals the minimum distance between BHEs in a field as defined in the SIA norm [201], while the upper boundary (100m) equals half of the maximum considered borehole depth (see Section 3.2.3.2). As the thermal interference between boreholes decreases logarithmically with borehole spacing [159], the simulated B follow this pattern ($B \in \{5, 7, 10,$

15, 20, 25, 30, 40, 50, 70, 100} m). The intersection of the BHE grids with the available area yields the individual GSHP systems, one for each parcel and for each selected spacing B.

Matching of GSHPs to building energy demand

To match the potential GSHP systems to building energy demands, spatial constraints for the transportation of heat must be considered. In this step, we virtually connect GSHPs to buildings, for individual GSHP systems and for DHC. Generally, individual GSHPs are only connected to buildings in the same parcel, subject to land ownership. To ensure the scalability of the approach to regional scale, the matching is done for pixels of 400×400m² resolution. If DHC does not exist, we hence assume that GSHPs and buildings inside the same pixel are connected. By contrast, DHC enables the connection of buildings and GSHPs with a distribution network, such that all buildings are reachable by thermal energy from GSHPs. Consequently, in areas where DHC exists, we match all GSHPs and buildings inside the same DHC and treat them as an interconnected system.

As heating demands exceed cooling demands in heating-dominated climates, the analytical model described in the following is designed to estimate the maximum heat extraction for a given amount of injected heat. Thus, the level of heat injection, here given by the space cooling demand, must be assigned to each parcel. For this, we rank all parcels within a given pixel or DHC based on their area. As the benefits of seasonal regeneration increase with the level of cooling re-injection, we re-inject the maximum possible amount of heat to the largest borehole field. If the cooling demand exceeds the maximum capacity of the largest field, cooling energy is re-injected into the second largest field and to the following parcels until all cooling demand is satisfied. This approach reduces the number of BHE fields that are used bi-directionally for heating and cooling, which is more realistic than a small heat re-injection in all fields.

3.2.2.2 Analytical modelling of heat exchange potential for bi-directional GSHPs

The proposed analytical model of bi-directional GSHPs expands upon previous work [159] to account for seasonal regeneration through the re-injection of heat to the BHEs. To this aim, a heat injection load (Q_{inj}) is added during the summer season, which reduces the long-term temperature drop in the ground. Consequently, the thermal interference between BHEs is reduced and the heat extraction potential (Q_{extr}) is increased. We further add technical limitations for heat injection and consider a higher operating time, which is typical for GSHPs with seasonal regeneration [185,202]. We focus on space cooling as heat source, but the methodology can be equally used for other sources of heat injection, such as solar thermal or industrial waste heat.

The proposed method follows a two-step approach: First, we simulate the annual extractable energy of a borehole field (Q_{field}), the maximum heat extraction power (q_{max}), and the number

of full-load heating hours ($t_{op,h}$) for a range of borehole spacings B and depths H, as well as for two operating modes (nominal $t_{op,h}$ and nominal q_{max}), such as to comply with the installation standards defined in the SIA norm [201]. Second, the borehole arrangement of each GSHP system is optimised by choosing the B, H and operating mode that maximise the technical potential ($Q_{extr} + Q_{inj}$) while sustaining a feasible q_{max} and $t_{op,h}$. As the methodology is aimed at regional-scale potential analyses, it is assumed that the heat pumps of each GSHP system are well-sized to supply the estimated Q_{extr}, Q_{inj} and q_{max}. For simplification, we further assume that all systems start their operation simultaneously at time $t = 0$.

Modelling of heat exchange potential

The annual extractable energy of a borehole field (Q_{field}), which is simulated for each borehole arrangement (B, H), is defined as [159]:

$$Q_{field} = q_{max} \times t_{op,h} \times H \times N_B \tag{3.6}$$

where q_{max} is the maximum heat extraction power (in W/m) and N_B is the number of BHEs in the field. While H and N_B are assumed to be fixed for a given simulation, q_{max} and $t_{op,h}$ are free parameters that need to be selected. To assure feasible operating conditions of the GSHPs, we constrain q_{max} to at least 80% of the nominal operating power [159] and $t_{op,h}$ between the nominal operating time t_{nom} (residential heating only) [201] and the maximum operating time, which assumes that the GSHP is operated 100% of the time in the month with maximum heating load:

$$q_{max} \geq 80\%\ q_{nom} \tag{3.7}$$

$$t_{nom} \leq t_{op,h} \leq \frac{t_m}{w_{hdd,max}} \tag{3.8}$$

where t_m is the number of hours in the month of maximum heating operation.

The choices of q_{max} and $t_{op,h}$ are further constrained by the mean temperature of the heat carrier fluid inside the BHE (T_{mf}). The T_{mf} must never drop below a minimum value $T_{mf,min}$ in heating mode and must not exceed a maximum value $T_{mf,max}$ during cooling operation. Both constraints must be fulfilled at all times, from the first year to the last year of the planning horizon (t_{dim}). To simulate the heat transfer between BHE fields and the ground, we use Eskilson's analytical model [203], which represents each BHE as a finite line source. Following the principles of spatial and temporal superposition, we model the BHE operation by superimposing a long-term and a seasonal heat extraction component, as well as the thermal interference of all surrounding boreholes. The T_{mf} then equals the undisturbed ground temperature (T_g) at half the borehole depth minus the sum of the temperature drops due to each

superimposed component. To not violate any temperature constraint, the chosen q_{max} and $t_{op,h}$ must hence fulfil the following equations for peak heat extraction (heating mode) and heat injection (cooling mode) in the first ($t = 0$) and last year ($t = t_{dim}$) of operation (cf. [202,204]):

$$T_{mf,min} \leq T_{mf,h}(t) = T_g - q_{max,h}\left(R'_{LT,h}(t) + R'_{seas,h} + R^*_b\right) + \frac{Q_{inj}}{N_B t_{op,c} H} R'_{LT,c} \quad (3.9)$$

$$T_{mf,max} \geq T_{mf,c}(t) = T_g + \frac{Q_{inj}}{N_B t_{op,c} H}\left(R'_{LT,c}(t) + R'_{seas,c} + R^*_b\right) - q_{max,h} R'_{LT,h} \quad (3.10)$$

where $T_{mf,h}$ and $T_{mf,c}$ are the T_{mf} in peak heating (h) and cooling (c) modes; Q_{inj} is the injected heat (in Wh); $t_{op,c}$ (in h) is the operating time in cooling mode; R^*_b is the borehole thermal resistance (in mK/W); R'_{LT} and R'_{seas} denote the long-term and seasonal ground thermal resistance, weighted for heating or cooling operation. At $t = 0$, we assume that $R'_{LT} = 0$. At $t = t_{dim}$, the R'_{LT} is weighted for annual mean operation, given by the fraction of operating time, and is composed of the long-term resistance of the borehole itself (R_{LT}) and the mean thermal resistance of all other BHEs within and around a field (R_{field}), which depends on B and H:

$$R'_{LT,h/c}(t) = \begin{cases} 0 & t = 0 \\ \frac{t_{op,h/c}}{t_a}\left(R_{LT}(H) + R_{field}(B,H) - R_{seas}\right) & t = t_{dim} \end{cases} \quad (3.11)$$

where $t_a = 8760h$ and R_{seas} is the seasonal maximum thermal resistance, which is subtracted for mathematical consistency of the model. Following [159], we model R_{LT} and R_{field} from a heat extraction pulse of duration t_{dim}, and R_{seas} from the peak of a sinusoidal heat extraction with periodicity of 1 year. The thermal resistances are functions of the ground parameters, which vary regionally (see Section 3.2.3.2), and the borehole geometry. R_{field} further depends on the borehole arrangement within the field, decreasing logarithmically as B increases. The mathematical formulations for R_{field}, R_{LT} and R_{seas} are provided in [159].

The R'_{seas} is the maximum monthly thermal resistance, given by multiplying R_{seas} with the fraction of the maximum monthly operating time:

$$R'_{seas,h/c} = \frac{w_{hdd/cdd,max}\, t_{op,h/c}}{t_m} R_{seas} \quad (3.12)$$

where t_m is the number of hours in the month of maximum heating/cooling operation, and $w_{hdd/cdd,max}$ is the weight attributed to maximum monthly operation. The weight is obtained from the heating degree days (HDD) for heating mode and from the cooling degree days (CDD) in cooling mode and allows to account for the monthly variation of the heating and cooling

demand (see Appendix A). Due to the lack of a norm for cooling operation, we set $t_{op,c}$ to the maximum operating time, such that $t_{op,c} = t_m / w_{cdd,max}$ in analogy to Equation 3.8.

Selection of optimal operating point

To select the optimal operating point of a GSHP system with a given B and H for any level of Q_{inj}, we aim to find the highest q_{max} and $t_{op,h}$ that fulfil Eqs. (2)-(5) at any time. To reduce the complexity of the selection, we consider two operating modes. The first represents a heating-only use, where $t_{op,h}$ equals the nominal value (t_{nom}, 1800-2000h in Switzerland) [201]. We thus compute the highest q_{max} that fulfils all constraints by fixing $t_{op,h} = t_{nom}$. The second operating mode represents large installations used for both heating and cooling. These systems typically have higher operating times, around 2500-3000h [202], while being operated at nominal power (q_{nom}). We hence fix $q_{max} = q_{nom}$ and maximise $t_{op,h}$. This second configuration is often infeasible for heating-only cases, but it is suitable for seasonal regeneration because the long-term temperature drops around BHEs decreases as more heat is injected.

Using Equation 3.6, Q_{field} is then computed for each B, H and operating mode. Out of these, the heat extraction potential of the borehole field (Q_{extr}) and the optimised borehole arrangement are obtained as the feasible solution that maximises the heat exchange potential:

$$Q_{extr} = \max_{B,H,op.mode} Q_{field} + Q_{inj} \qquad subject\ to\ Eqs.\ (2)-(5)\ \forall t, H \leq H_{max} \tag{3.13}$$

where H_{max} represents the maximum allowed drilling depth (see Section 3.2.3.2).

To obtain the heating (Q_{heat}) and cooling (Q_{cool}) energy exchanged with the buildings from Q_{extr} and Q_{inj}, the coefficient of performance (COP) of the heat pumps (HP) must be taken into account. We model the GSHPs as water-to-water heat pumps, which are prevalent in DHC [205]. Expecting a small increase in future HP performance compared to current COPs [39,206], we choose a constant COP for heating (COP_{heat}) as 4.5 and for cooling (COP_{cool}) as 5.5, such that (cf. [39]):

$$Q_{heat} = Q_{extr} \frac{COP_{heat}}{(COP_{heat} - 1)} \tag{3.14}$$

$$Q_{cool} = Q_{inj} \frac{COP_{cool}}{(COP_{cool} + 1)} \tag{3.15}$$

3.2.2.3 Spatial analysis of useful geothermal potential

Once the technical potential is modelled, we map it with building heating demand on-site, based on matching results derived in Section 3.2.2.1. The useful potential for heating and cooling is defined as the portion of technical potential that is smaller than or equal to the heat demand

of matched buildings. The portion of technical potential that exceeds the heat demand of matched buildings is considered as surplus potential. The surplus potential is only obtained for heating, as the analytical model described in Section 3.2.2.2 always attempts to inject the maximum possible amount of cooling demand. There are also areas where technical potential is insufficient to supply building heating or cooling, which is considered as deficit.

If DHC is considered for heat distribution, we further allocate surplus potential to nearby DHC areas with a deficit, following the on-site mapping. This allows an increase in the useful potential, as DHC is usually located in dense areas with a high demand. These areas likely have insufficient technical potential to supply the demand. The allocation process is adapted from the method of Chambers et al. [136]. This allows to analyse the supply of DHC with geothermal energy in neighbouring areas, accounting for the spatial constraint that the potential energy sources need to be within a limited range of DHC. The key strength of this method is that it uses spatial analysis and graph theory to disaggregate a large-scale case into sub-clusters of supply and demand, thus expanding the applicable spatial scale. However, this method allocated energy using the simple net-balance across each sub-cluster, which assumes that energy can be allocated from supplies to demands that are not directly connected. This limitation is addressed in the present study by introducing an optimisation algorithm which finds the maximum allocation of supply to demand within each sub-cluster. A detailed description of the new method is presented in a methods paper accompanying this research article [207]. Figure **3.7** shows an overview of the method to link surplus geothermal potential and DHC demand. It consists of the following key steps:

Step 1. Each area with surplus geothermal potential and each DHC area with a deficit are treated as the vertices of a bipartite graph. These vertices are characterized by their geometries and heating capacities (either supply surplus or deficit). We call vertices representing areas with surplus geothermal potential 'sources', and vertices representing DHC areas with deficit 'demand'.

Step 2. For each demand, all sources for which the closest distance to the demand is below a certain threshold are connected to the demand by an edge. To account for the variation in DHC sizes, the threshold is chosen as 20% of the length of the oriented minimum bounding box of the DHC area.

Step 3. The source/demand vertices and linking edges is converted into a large bipartite graph covering the whole study area, which is split into subgraphs of connected components (defined as a subset of vertices that are connected to each other, but not to any vertices outside the set).

Step 4. The maximum possible allocation of technical potential from sources to demands within each subgraph is formulated as a Hitchcock transportation problem [147] and then solved using linear programming [149].

Step 5. Finally, the maximum possible allocation of all subgraphs is summed and added to the usable potential estimated.

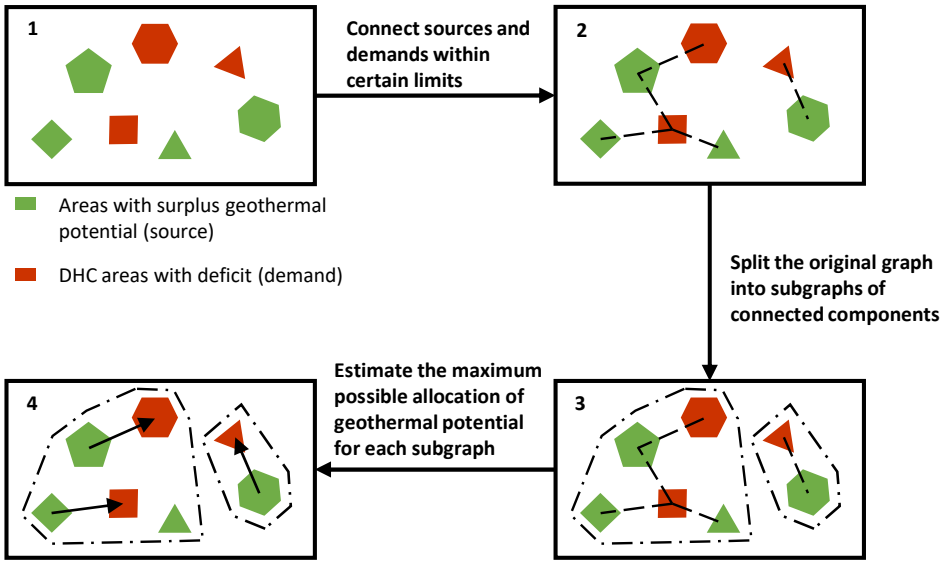

Figure 3.7 - Overview of the method to allocate surplus geothermal potential to district heating and cooling areas.

3.2.3 Case Study

The proposed method is applied to a case study in the cantons of Vaud and Geneva in Switzerland. The case study area covers a surface of around 1,600 km² in western Switzerland, containing two of Switzerland's largest cities (Geneva and Lausanne). The presence of high-resolution geothermal cadastres and landscape data, as well as a rapid projected growth in cooling demand [61,208], make this area particularly suitable for a regional-scale study of the shallow geothermal potential.

To match the technical geothermal potential with the building energy demand, we use simulated annual heating and service-sector cooling demands for the year 2050. This modelling horizon is chosen as (i) the adoption of space cooling technology is expected to increase in the coming years, and (ii) the installation of a large amount of GSHP systems would take several years. Furthermore, considering different climate change scenarios for 2050 allows to assess the robustness of the technical geothermal potential with seasonal regeneration in relation to climate change.

3.2.3.1 Scenarios considered

This work uses a scenario-based approach to assess the impact of seasonal regeneration from space cooling and the existence of DHC on the useful geothermal potential. Table **3.4** presents

the different scenario components, namely three levels of space cooling demand, three climate change models and the possibility to use DHC. The levels of space cooling demand correspond to different penetration levels of cooling equipment in the building stock. These levels are (i) a reference case without cooling ('no cooling'), (ii) the projected penetration of cooling equipment under current tight regulation ('partial cooling'), and (iii) an extreme case saturating nearly all cooling demand ('full cooling'). The climate change models describe three representative concentration pathways (RCPs) adopted by the IPCC [47]. These are linked to the space cooling demand by modelling the diffusion of space cooling devices and the cooling intensity corresponding to each RCP. To assess the robustness of the potential estimate to climate change, we choose a stringent emission reduction scenario (RCP 2.6), an intermediate scenario (RCP 4.5), and a worst-case scenario (RCP 8.5). The method presented in Section 3.2.2 is applied to each combination. All scenario combinations and their naming convention used throughout the paper are shown in Table 3.5.

Table 3.4 - Description of scenario components.

Scenario components	Levels	Description
Space cooling demand	No Cooling	No space cooling demand met by GSHP (no seasonal regeneration).
	Partial Cooling	Only a portion of buildings are actively cooled. The diffusion of space cooling equipment and the growing space cooling demand is predicted based on the past trend.
	Full cooling	Extreme scenario where space cooling demand is mature and nearly saturated.
IPCC climate change models	RCP 2.6	Stringent emission reduction scenario where emissions peak around 2020 [47].
	RCP 4.5	Intermediate scenario where emissions peak around 2040 [47].
	RCP 8.5	Worst-case scenario where emissions increase throughout the 21st century [47].
DHC utilization	Without DHC	No DHC is installed (GSHPs are only connected to on-site building thermal demands).
	With DHC	In each DHC potential area, the distribution network connects all GSHPs and buildings. This allows integrating surplus geothermal potential within a limited range.

Table 3.5. Summary of scenario combinations

	Climate model	**Without DHC (ND)**	**With DHC (D)**
No Cooling (NC)		Base scenario (NC-ND)	NC-D
Partial Cooling (PC)	*RCP 2.6*	PC-ND-2.6	PC-D-2.6
	RCP 4.5	PC-ND-4.5	PC-D-4.5
	RCP 8.5	PC-ND-8.5	PC-D-8.5
Full Cooling (FC)	*RCP 2.6*	FC-ND-2.6	FC-D-2.6
	RCP 4.5	FC-ND-4.5	FC-D-4.5
	RCP 8.5	FC-ND-8.5	FC-D-8.5

3.2.3.2 Regional datasets

Conducting a regional-scale study of geothermal potential requires the availability of high-quality data on the ground thermal properties, the building energy demand and the spatial constraints for the installation of GSHPs and the coverage of the energy demand (see Figure **3.6**). Table **3.6** provides an overview of all regional datasets and their sources.

Table 3.6 - Overview of regional datasets.

	Dataset	Description	Resolution	Sources
Spatial constraints	Parcel boundaries	Boundaries of public & private property units	Polygons	ASIT-VD [209], SITG [210]
	Topographic Landscape Model	Incl. building footprints, other built-up areas, natural habitat	Polygons	SwissTopo [211]
	DHC zones	Potential areas for DHC	Polygons	Chambers et al. [136]
	GSHP restrictions	Permitted, limited and prohibited zones for GSHPs	Polygons	ASIT-VD [212], SITG [213]
Geothermal input data	Thermal ground properties	Thermal conductivity & diffusivity	50x50x50m3 (50-300m depth)	ASIT-VD [212], SITG [213]
	Surface temperature	Average ground surface temperature at 1m depth	200x200m2	Assouline et al. [214]
	Air temperature	Daily mean air temperature at 2m above ground	1x1km2, daily (1991-2010)	MeteoSwiss [215]
	Digital Elevation Model	Elevation map	2x2m2	SwissTopo [216]
Building energy demands	Building heating demand	Space heating and domestic hot water demand	Buildings, annual	Chambers et al. [161], Schneider et al. [81]
	Building cooling demand	Building space cooling demand in the service sector	Buildings (service sector), annual	Li et al. [125]

Spatial constraints

Spatial constraints for the mapping of shallow GSHP potential include (i) the parcels, buildings and landscape features, required to estimate the available area for borehole installation (Section 3.2.2.1), (ii) potential areas for DHC (Section 3.2.2.3), and (iii) restrictions for GSHP installation (see below). The parcel boundaries are based on the official mensuration data for roughly 100,000 property units. The topographic landscape model (TLM) contains a 3D representation of various landscape objects, some of which are unsuitable for installing BHEs. A 1m buffer is added around all unsuitable objects to account for inaccuracies of the TLM. Potential areas for low temperature district heating networks, shown in Figure **3.8**a, are obtained from an existing model [136]. Restrictions on the installation of GSHPs are divided into permitted, limited and prohibited zones (Figure **3.8**b). In permitted zones we assume a maximum drilling depth (H_{max})

of 200 m, in limited zones of 150 m, while no GSHP systems are installed in prohibited zones. These values are obtained based on typical drilling depths of existing installations in each zone, as shown in [159].

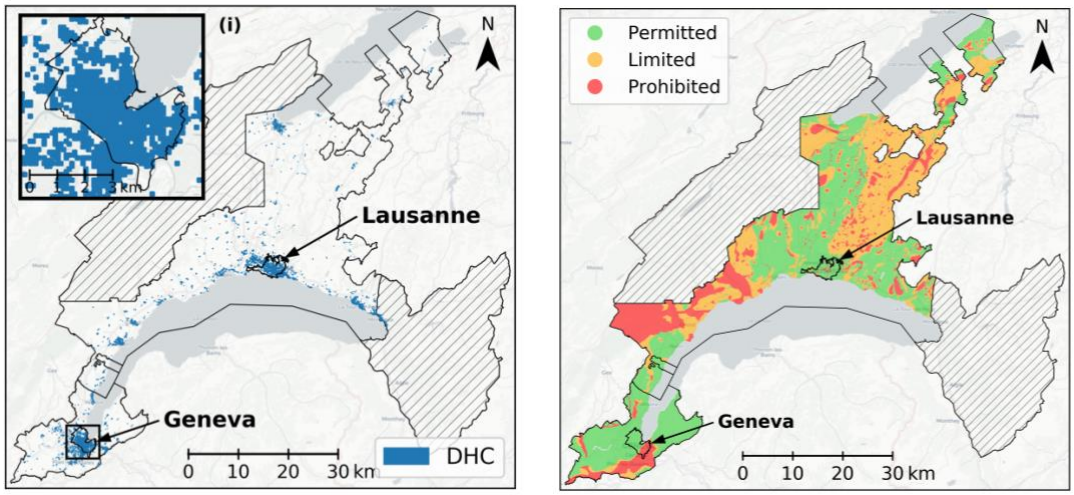

(a) *(b)*

Figure 3.8 - Spatial constraints, a) for the potential DHC areas, and b) for the permitted areas of BHE installation. Hatched areas are not included in the case study due to a lack of available ground data.

Geothermal input data

Estimating the technical geothermal potential (Section 3.2.2.2) requires an estimate of the long-term and seasonal thermal resistance (R_{LT}, R_{seas}), the nominal operating time ($t_{op,h}$), the seasonal load ($w_{hdd/cdd,max}$) and the nominal heat extraction rate (q_{nom}) for each borehole configuration. The borehole configurations are discretised for each parcel into 11 borehole spacings (see Section 3.2.2.1) and four depths, ranging from $50m$ to $H_{max} = 200m$ following the spatial resolution of the ground data (Table **3.6**). The thermal resistance for a dimensioning horizon of $t_{dim} = 50$ years is obtained from previous work [159], where it was derived from regional-scale data of the ground thermal conductivity (λ), diffusivity (α), the surface temperature (T_0) and the temperature gradient in the ground ($\delta T/\delta z$), which may be approximated as 0.03 K/m in the case study region [201]. The ground data is equally used to compute q_{nom} and T_g for each H based on the guidelines in the SIA norm [201]. The t_{nom} is mapped from the altitude following [201] based on a digital elevation model, assuming that it corresponds to the minimum operating time for all building types (residential and service sector). The degree days used to estimate $w_{hdd/cdd,max}$ are derived from gridded data of daily mean ambient temperature, averaged across 20 years [217]. As the data has a coarse resolution of 1×1km2, we spatially interpolate it to a grid of 200×200m2 pixels. Further technical parameters are the minimum and maximum fluid temperatures, which are set to $T_{mf,min} = -1.5°C$ and $T_{mf,max} = 50°C$. These temperatures limits are chosen based on the SIA norm [201] (for $T_{mf,min}$)

and existing installation examples in Switzerland [202] (for $T_{mf,max}$) such as to avoid damage of the heat exchanger tubes due to freezing or overheating.

Building thermal demands

An existing model was used to estimate total demand per building for heating and hot water on a yearly basis [81,161]. This is a regression-based model where typical measured heat demand intensities were linked to different building types based on the extensive metadata included in the Swiss Building Registry. A 50% reduction of demand is then applied uniformly to all building, based on the target of the Swiss Energy Strategy 2050 [218]. This 50% reduction heat demand scenario is used consistently across all scenarios, yielding the energy demand shown in Figure **3.9**a. In total of all buildings in the studied area, the heating demand is 6.11 TWh/y.

Building cooling demand for the partial cooling (PC) and the full cooling (FC) scenarios are generated using the Monte Carlo model introduced in the work [125]. The Monte Carlo model forecasts future building cooling demand in the service sector (e.g., offices, trade, hotels, etc.) by applying a probability distribution for the adoption of space cooling equipment in buildings, to thereby estimate the magnitude and uncertainty in the cooling demand as a function of current and future building characteristics and climate. The results are reported in Table **3.7** for 2000 iterations of the model. An example for a single scenario and Monte Carlo run is shown in Figure **3.9**b.

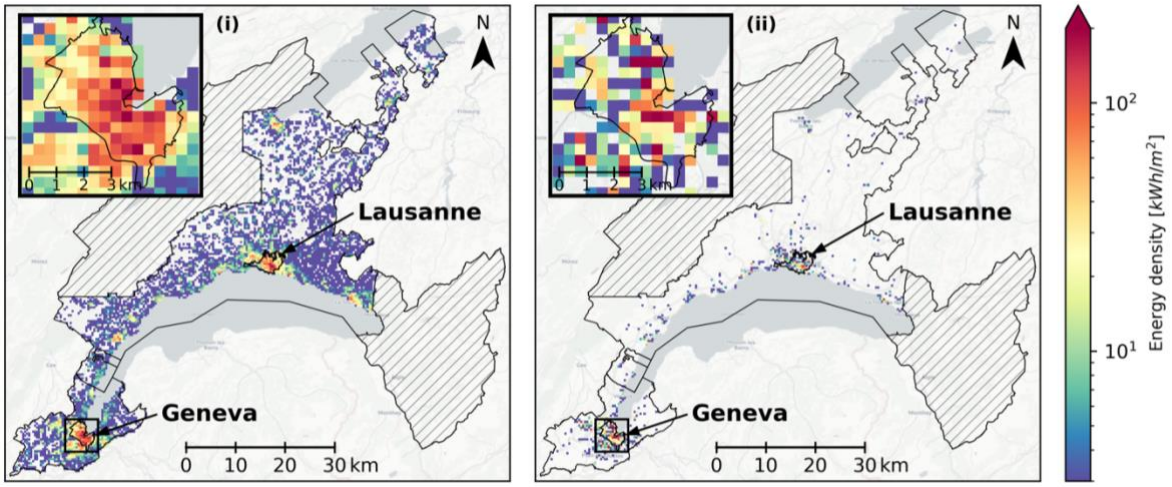

(a) *(b)*

Figure 3.9 - Building energy demand density, a) for space heating and domestic hot water and b) for space cooling for one Monte-Carlo simulation (climate change model RCP 4.5, partial cooling). The insets (i), (ii) show the city of Geneva.

Table 3.7 - Mean and 95% confidence interval of total building cooling demand in all scenarios.

	Climate model	Total building cooling demand (TWh/y)
No Cooling (NC)		0
Partial Cooling (PC)	RCP 2.6	1.33±0.18
	RCP 4.5	1.57±0.21
	RCP 8.5	1.82±0.24
Full Cooling (FC)	RCP 2.6	2.70±0.18
	RCP 4.5	3.17±0.21
	RCP 8.5	3.63±0.24

3.2.4 Results

3.2.4.1 Impact of cooling injection on technical geothermal potential

The case study in western Switzerland shows that seasonal regeneration from the re-injection of space cooling demands increases the technical heat extraction potential (Q_{extr}) significantly. While the scenario without regeneration (NC-ND) shows a maximum annual energy density of around 15 kWh/m² per pixel of 400×400m² (Figure **3.10**a), the maximum heat extraction density exceeds 300 kWh/m² in pixels with high levels of heat injection (> 330 kWh/m²), as shown in Figure **3.10**b and c. This 20-fold increase is explained by the strongly reduced thermal interference between boreholes, which has two-fold effects on the technical potential. Firstly, the number of boreholes increases quadratically as the average BHE spacing is reduced from $B_{opt} = 20–25m$ to $B_{opt} = 5–7m$ (Figure **3.11**a). Secondly, reduced thermal interference allows for higher operating power and time (Figure **3.11**b and c), which increases the heat extraction per borehole. These high energy densities are found primarily in dense urban areas, such as the city centre of Geneva (see insets in Figure **3.10** and Figure **3.11**).

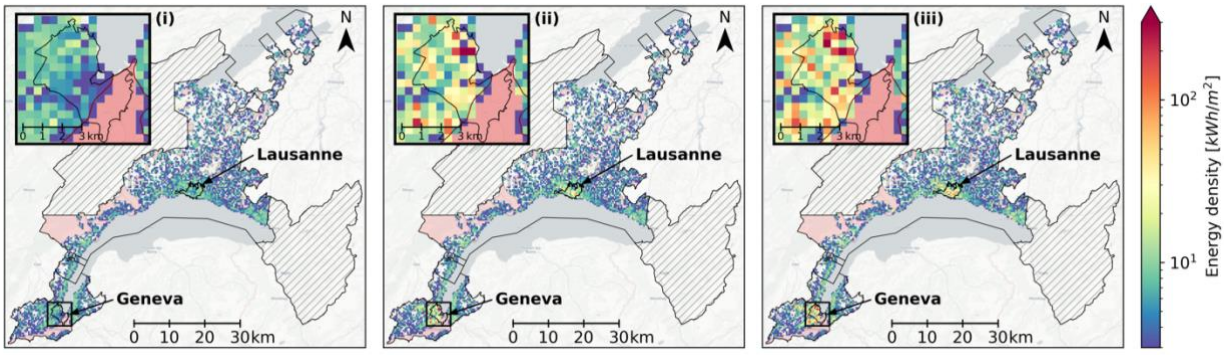

(a) *(b)* *(c)*

Figure 3.10 - Heat extraction potential ($\boldsymbol{Q_{opt}}$) of individual GSHPs, aggregated to pixels of 400×400m2, for (a) baseline scenario (NC-ND), (b) partial cooling (PC-ND-4.5) and (c) full cooling scenario (FC-ND-4.5). In pink zones, GSHPs installation is prohibited.

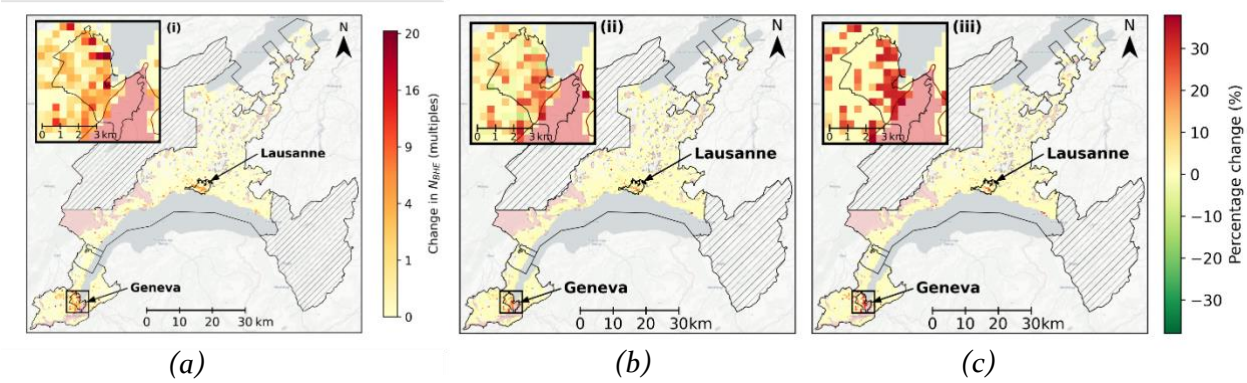

(a) *(b)* *(c)*

Figure 3.11 - Change in number of boreholes $\boldsymbol{N_{BHE}}$ (a), heat extraction rate $\boldsymbol{q_{max}}$ (b) and heating operating time $\boldsymbol{t_{op,h}}$ (c) of the partial cooling scenario (PC-ND-4.5) compared to the baseline (NC-ND), computed as the difference between the two scenarios divided by the baseline. The change in $\boldsymbol{N_{BHE}}$ is shown as multiples on a quadratic scale.

In absolute terms, the technical potential can be increased by around 1 TWh if no DHC is considered (PC-ND), by 1.5 TWh with DHC (PC-D) for partial cooling, and by 2-3 TWh for full cooling (FC) (see Q_{extr} in Table **3.8**). The results are relatively robust to different climate change scenarios, varying by ±5% with respect to the RCP 4.5 climate model. The confidence intervals of the Monte Carlo runs vary by 5-10% for heat injection and <5% for extraction, suggesting that the total heat exchange is equally robust to the spatial distribution of cooling demand within the studied area. The scenarios further provide insights into the relation between the injected and extracted heat. As the linear fit of all scenarios (Figure **3.12**) shows, roughly 90% of the injected heat during summer can be extracted in winter in addition to the baseline potential of 4.6 TWh. This high conversion rate of 90% is due to the strong effect of seasonal regeneration on reducing thermal interference between boreholes. These results show that seasonal regeneration is essential for a sustainable large-scale deployment of GSHPs.

Table 3.8 - Mean and 95% confidence intervals of the technical heat exchange potential (heat injection and heat extraction) summed over the case study area for all scenarios, based on Monte Carlo simulation.

Scenario	Heat injection $\boldsymbol{Q_{inj}}$ (TWh/y)			Heat extraction $\boldsymbol{Q_{extr}}$ (TWh/y)		
Base scenario	0			4.64		
PC-ND	0.99 ± 0.10	1.15 ± 0.12	1.30 ± 0.13	5.56 ± 0.09	5.70 ± 0.10	5.84 ± 0.12
FC-ND	1.93 ± 0.15	2.21 ± 0.17	2.46 ± 0.34	6.42 ± 0.13	6.67 ± 0.15	6.89 ± 0.38
PC-D	1.35 ± 0.14	1.60 ± 0.17	1.85 ± 0.19	5.90 ± 0.13	6.12 ± 0.15	6.34 ± 0.17
FC-D	2.78 ± 0.23	3.24 ± 0.27	3.69 ± 0.30	7.18 ± 0.20	7.59 ± 0.23	7.98 ± 0.26
Climate model	*RCP 2.6*	*RCP 4.5*	*RCP 8.5*	*RCP 2.6*	*RCP 4.5*	*RCP 8.5*

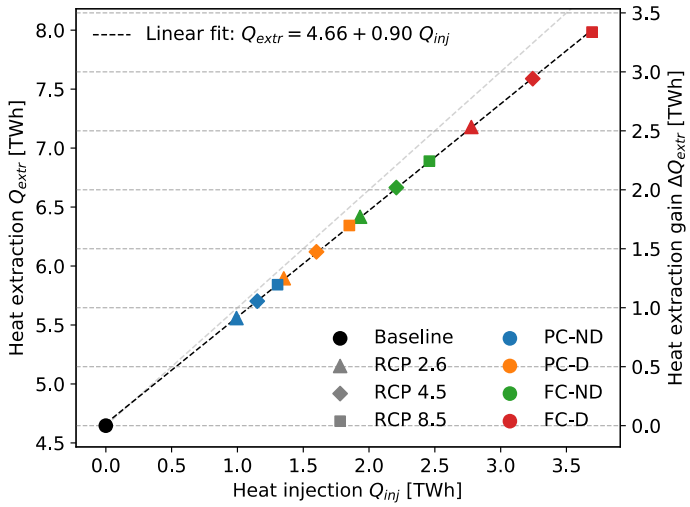

Figure 3.12 - Geothermal potential ($\boldsymbol{Q_{extr}}$) as a function of injected excess heat ($\boldsymbol{Q_{inj}}$), for all scenarios (see Table 3.5). The black dashed line shows the linear fit, the grey dashed line represents a slope of 1.

3.2.4.2 Supply of building heating and cooling demands with geothermal potential

The useful potential to supply heat and cooling demand in seven scenarios of cooling penetration and climate change without DHC is presented in Table **3.9** and Figure **3.13**. Due to the spatial constraint that geothermal energy can only supply demand in a limited range from the GSHP, only a fraction of the technical potential is useful. In the base scenario (NC-ND), only 2.2 TWh of the 6.0 TWh of Q_{heat} (from 4.6 TWh of Q_{extr} provided to HPs) is useful, which would cover 35% of building heating demand. When considering seasonal regeneration from space cooling in the PC-ND scenario, 1.1-1.4 TWh of space cooling demand could be supplied by GSHPs while increasing the useful potential for supplying heat demand by 0.5-0.6 TWh. Similarly, in the FC-ND scenario, GSHPs could meet 1.9-2.5 TWh building cooling demand, as

well as supply additional 1.1-1.2 TWh to building heating demand. The fraction of demand covered (values in brackets) is nearly constant across the three climate models for all scenarios, which suggests a high robustness of the results to climate change.

Figure **3.14** shows maps of the heat and cooling supply in percentage for the PC-ND-4.5 scenario as an example. In the case of supplying cooling (Figure **3.14**a), we found that building cooling demand could be sufficiently supplied where GSHP installation is allowed, due to the high capacity of BHEs to inject excess heat from space cooling. By contrast, no cooling demand can be supplied in areas where GSHP installation is prohibited (see insets in Figure **3.14**a). In the case of supplying heat (Figure **3.14**b), despite an increased potential due to seasonal regeneration, heat demand is not sufficiently supplied in dense urban areas with an excessive demand density. Although the technical potential is abundant in low-density areas, it is not available to other areas with a deficit, due to spatial constraints. In addition, constraints on GSHP installation further limit the heat supply (see Figure **3.8**b).

Table 3.9 - Useful potential to supply building heating and cooling demands in scenarios without DHC.

Scenario	Useful cooling potential $\boldsymbol{Q_{cool}}$ (TWh/y)			Useful heating potential $\boldsymbol{Q_{heat}}$ (TWh/y)		
Base scenario	0			2.19 (35%)		
PC-ND	0.84 (63%)	0.97 (62%)	1.10 (60%)	2.90 (47%)	2.96 (48%)	3.02 (49%)
FC-ND	1.63 (60%)	1.87 (59%)	2.08 (57%)	3.26(53%)	3.32 (54%)	3.37 (55%)
Climate model	*RCP 2.6*	*RCP 4.5*	*RCP 8.5*	*RCP 2.6*	*RCP 4.5*	*RCP 8.5*

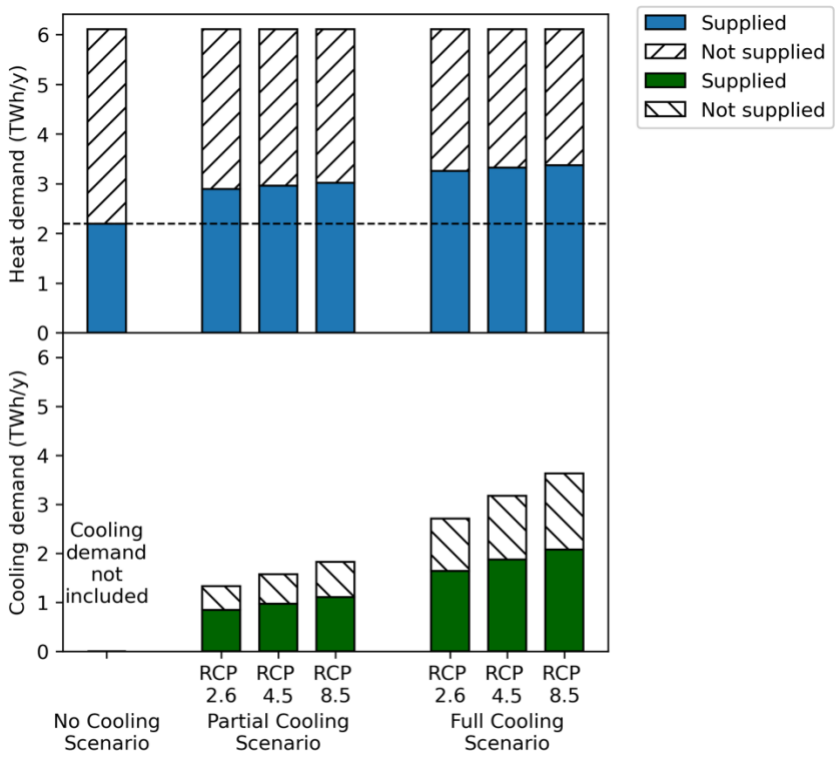

Figure 3.13 - Supply of building heating and cooling demands in scenarios without DHC.

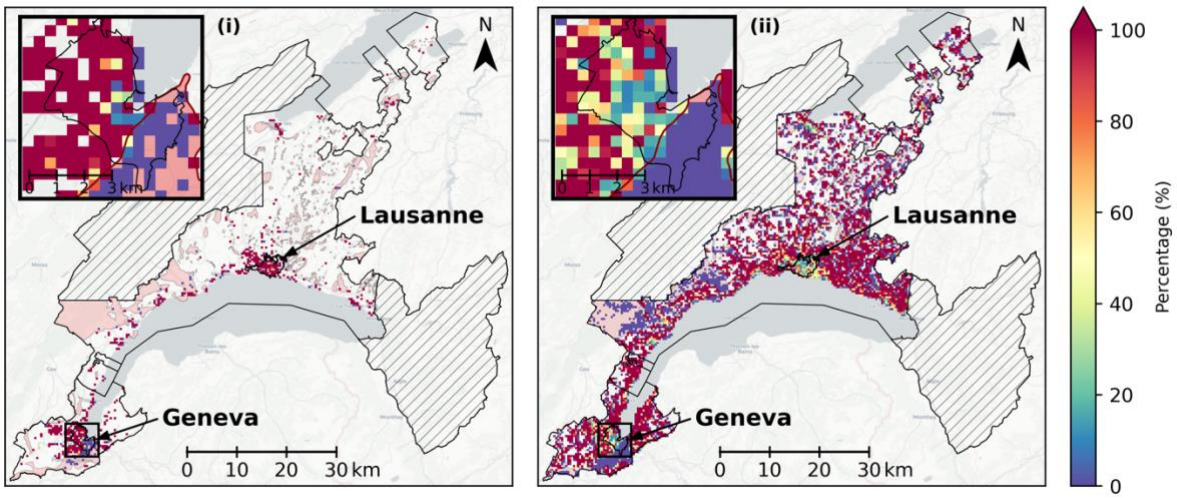

(*a*) (*b*)

Figure 3.14 - Distribution of demand coverage per pixel in the PC-ND-4.5 scenario: (a) percentage of cooling demand supplied; (b) percentage of heat demand supplied.

3.2.4.3 Impact of district heating and cooling

The integration of GSHPs in DHC increases the useful potential to supply cooling demand by at least 12%, and by at least 22% for heat demand compared to the results presented in Section 3.2.4.2. As shown in Table **3.10**, the utilization of DHC significantly improves the useful potential in all seven scenarios with DHC, which are again robust to the climate models. The amount of energy supplied within DHC increases as more heat is re-injected to the ground, due to the high demand in dense areas (see Figure **3.15**). These results demonstrate the two-fold benefit of DHC: First, more injection of space cooling demand results in an increased technical potential. Second, DHC eases the spatial constraints for the useful potential for heating and allows integrating more surplus geothermal energy in neighbouring areas as potential supply sources of the DHC.

To illustrate the impact of DHC at regional scale, Figure **3.16** shows maps of the change in heating and cooling supply between PC-ND-4.5 and PC-D-4.5 scenarios as an example. In the case of cooling (Figure **3.16**a), the utilization of DHC allows the distribution of cooling energy from GSHPs to buildings located in areas where GSHP installation is prohibited (see inset (i) in Figure **3.16**a). In the case of heat supply (Figure **3.16**b), DHC could largely improve the insufficient supply in dense urban areas.

Table 3.10 - Useful potential to supply building heating and cooling demands in scenarios with DHC.

Scenarios	Useful cooling potential $\boldsymbol{Q_{cool}}$ (TWh/y)			Useful heat potential $\boldsymbol{Q_{heat}}$ (TWh/y)		
NC-D	0			3.86 (63%)		
PC-D	1.14 (86%)	1.35 (86%)	1.57 (86%)	4.20 (69%)	4.44 (73%)	4.60 (75%)
FC-D	2.35 (87%)	2.74 (86%)	3.13 (86%)	5.07 (83%)	5.15 (84%)	5.20 (85%)
Climate model	*RCP 2.6*	*RCP 4.5*	*RCP 8.5*	*RCP 2.6*	*RCP 4.5*	*RCP 8.5*

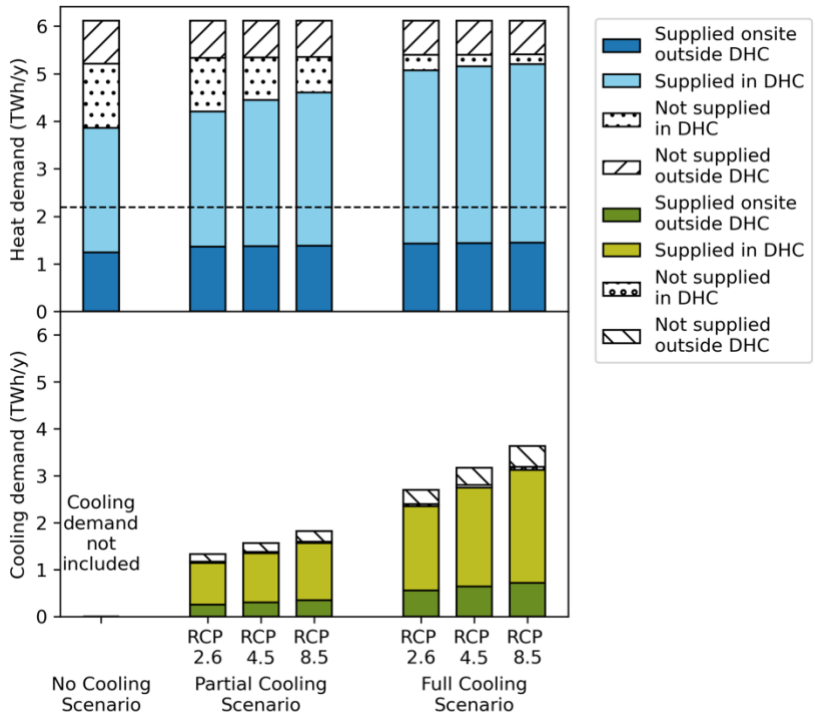

Figure 3.15 - Supply of building heating and cooling demands in scenarios with DHC.

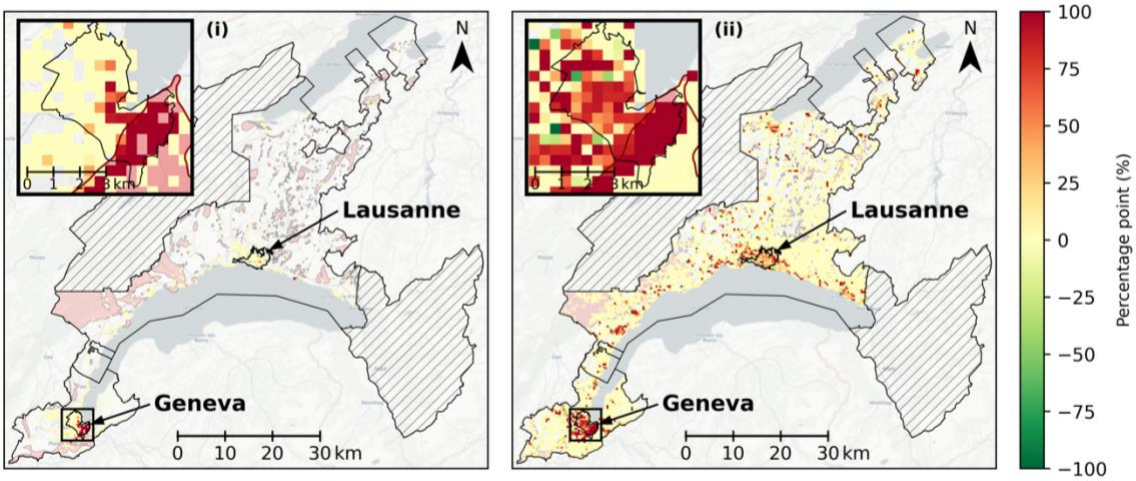

(a) (b)

Figure 3.16 - The difference between PC-ND-4.5 and PC-D-4.5 scenarios: a) percentage of cooling demand supplied; b) percentage of heat demand supplied.

3.2.5 Discussion

3.2.5.1 Methodological contribution

This paper proposes a novel framework to estimate the technical and useful potential of shallow GSHPs for building heating *and* cooling in individual GSHP systems and in DHC, which scalable to entire regions. For the first time, this framework combines (i) the spatial mapping between heat demands and virtually installed BHEs, (ii) the analytical modelling of the technical heat exchange potential from bi-directional GSHPs, considering seasonal regeneration through the re-injection of space cooling demands, and (iii) the optimal allocation of potential heat sources within DHC. The analytical model, which is built upon previous work on the heat extraction potential from GSHPs [159], to account for (i) technical constraints due to the combined heat injection and extraction, and (ii) different operating strategies of GSHP systems. The advantages of the proposed method are that it (i) accounts for thermal interactions between densely installed GSHPs and the seasonal variation of the energy demand, (ii) proposes a trade-off between operating power and heat exchange potential, and (iii) is scalable to thousands of borehole fields.

We further expanded previous work on the identification of potential DHC areas [136] by introducing a graph-theory based optimization to match building thermal energy demand to technical geothermal potential. This approach permits to quantify the impact of DHC on the useful geothermal potential. The proposed method is transferable to other heat sources for seasonal regeneration, such as solar thermal generation, waste heat or air-source heat pumps [219]. The framework may also be replicated in other regions within or outside of Switzerland. Many of the required regional input data are available at European scale or beyond, or can be mapped from the literature using existing methods. An overview of these datasets and mapping approaches, which assure the replicability beyond the case study, are provided in Appendix B.

3.2.5.2 Practical implications and application

The results of the case study in the Swiss cantons of Vaud and Geneva imply that seasonal regeneration of GSHP systems may significantly increase the potential heat extraction. We found that the re-injection of space cooling demands into the ground allows for maximum annual heat extraction densities above 300 kWh/m² at heat injection densities above 330 kWh/m², especially in centres of large urban areas. The comparison of shallow geothermal potential studies by Bayer et al. [176] indicates that the maximum energy densities correspond to the yields of boreholes with little or no thermal interference [191,220]. We also found that the maximum technical potential is consistent with a previous Swiss case study for a commercial GSHP installation [202], which suggests a heat extraction density of 440 kWh/m² at 610kWh/m² of heat injection. Across the case study region, the heat extraction potential increases with the

amount of cooling injection from 4.6 TWh without regeneration up to 6.9 TWh. The spatial resolution of pixels of 400x400m² highlights regional differences of the shallow geothermal potential between rural, suburban and urban areas.

We further estimate that the conversion rate of injected to additional extracted heat is 90%, showing the high impact of seasonal regeneration on reducing thermal interference. Integrating GSHPs within DHC increases the fraction of the building thermal demand supplied through geothermal energy by up to 25% for cooling by up to 30% for heating. The fractions are nearly independent of different climate change scenarios for 2050, which implies robustness towards uncertainties in future climate. Low confidence intervals across 2000 Monte Carlo runs also suggest that the spatial distribution of the cooling demand has a low impact on the total potential.

The results may be applied to identify strategic areas for installing GSHPs in individual and district heating systems. This work can further be used as a basis for economic studies to compare the cost-effectiveness of renewable energy sources, therefore helping to design future energy systems. Finally, the findings presented above may provide useful input for policy makers to discuss the regional and national renewable energy strategies.

3.2.5.3 Limitations and future work

Quantifying the impact of seasonal regeneration of GSHPs is subject to assumptions and limitations related to the data and the modelling approach. The main assumptions and limitations related to data are that (i) all potential GSHP systems and energy demands within each pixel of 400 x 400 m² are connected. This assumption is necessary to assure the scalability of the approach; (ii) for each potential DHC area, all GSHP systems and buildings are connected to the same DHC. Any GSHP system adjacent to DHC areas is a potential further heat source; (iii) the mapping of geothermal potential to building energy demands is done by calculating heat balances. DHC network topologies, operating temperatures and thermal losses are not addressed; and (iv) we consider only the space cooling demand in the service sector. Space cooling in the residential sector is not modelled, as the proportion of expected residential space cooling demand for 2050 is small (5%-35%) according to forecasts for neighbouring countries [24].

The key assumptions of the analytical model, which are described in detail in [159], are that (i) the impact of groundwater flow on the technical geothermal potential is neglected, due to a lack of available data. Groundwater flow may impact both the magnitude of the GSHP potential and the direction of thermal interferences, which we assumed to be isotropic in all directions; (ii) the GSHP systems use the full available area and are designed such as to provide the estimated heat extraction rate and annual energy; and (iii) all systems start the heat extraction simultaneously, neglecting any previously existing systems.

Future work is needed to assess the technical barriers for using shallow geothermal energy in future DHC and to account for the impact of groundwater flow on the technical potential. Furthermore, environmental consequences of long-term warming or cooling trends of the ground related to the net injection or extraction of heat may be investigated. To adapt the method to country scale, statistical methods such as Machine Learning may be used. The method proposed here may also be used to model other systems for seasonal regeneration at large scale, such as the re-injection of excess solar thermal generation. This study can be used as the basis for further work to explore the economic and emission reduction potential of shallow geothermal combined with district heating and cooling. Such further work may also address the potential of hybrid GSHPs with other heat sources such as industrial waste heat or solar thermal generation, as well as complementarities with renewable electricity generation from wind turbines or solar photovoltaics.

3.2.6 Conclusion

This work presents a novel framework to estimate the technical and useful potential of shallow ground-source heat pumps (GSHPs) to supply building heating and cooling demands at regional scale. The framework accounts for the geospatial matching of heat demands and potential GSHP systems, the modelling of technical potential with seasonal regeneration of GSHPs through re-injection of excess heat from space cooling, and for the optimal allocation of heat supply in district heating and cooling (DHC). The useful potential is obtained for the direct heat exchange between buildings and geothermal fields and by considering DHC. A scenario-based approach is used to assess the technical and useful geothermal potential under different climate change scenarios, market penetration levels of cooling systems, and the possible use of DHC.

The case study in western Switzerland suggests that seasonal regeneration may significantly reduce thermal interference between boreholes. This increases the maximum technical geothermal potential density from 15 kWh/m² without heat injection to above 300 kWh/m² in pixels with heat injection densities above 330 kWh/m². These values are consistent with results reported in related scientific literature and case studies of existing installations. Results further suggest that the useful geothermal potential may cover up to 71% of service-sector cooling demand and up to 55% of heat demand in 2050 (assumed at 50% of current heat demand) for individual GSHP systems, which increases to 87% and 85% if DHC is used. The results are robust to uncertainties in future climate. The outcomes of the study may be used to conduct techno-economic analyses of future energy systems with a high share of renewable heat generation and to inform decision-making aimed at achieving Switzerland's renewable energy targets for 2050.

3.3 An optimisation approach for spatial allocation of industrial excess heat to district heating networks

3.3.1 Introduction

Decarbonising heating of buildings is highlighted by European Union (EU) as a requirement to deliver its greenhouse gas emission reduction goal [4]. District heating networks (DHN) combined with low-carbon energy generation has proved to help emission reduction, improve system efficiency and energy security [17]. Although many studies have been published on mapping renewable and waste energy potential to supply DHN [193,221,222], few works have addressed the problem of allocating heat supplies to DHN heat demands considering the spatial proximity constraint of transporting heat energy.

Furthermore, in situations where energy supplies are shared by several DHN energy demands, it is necessary to consider an allocation method that maximise the total useable potential. Chambers et al. [136] developed a spatiotemporal analysis method to evaluate the potential for supplying DHN by industrial excess heat (IEH). They use a spatial clustering method to link and cluster heat supplies and demands. However, a key limitation of this work is that there is no attempt to determine the allocation of supplies to demands within each cluster of nearby sources and demands. Instead, it simply calculated the net energy balance per cluster. This results in the overestimation of the allocable heat energy. This work applies a new method to estimate the maximum allocable heat potentials in networks of supplies and demands and compares the result with that of the previous work. A method is developed that adapts a transport optimization algorithm to the case of district heat network energy distribution.

3.3.2 Methods and input data

3.3.2.1 Case study and input data

To demonstrate the performance of the new optimal allocation method, we conducted a comparison between the results of it and the original net heat balance method on the same case study – potential of IEH supply for DHN in Switzerland [136]. The input data for the case study includes datasets on IEH supply, DHN potential areas with predicted heat demand in the study area, as described in Table **3.11**. For simplicity, only the reduced heat demand scenario 'SwissRes' (the energy saving scenario based on 'SwissRes' residential building retrofit model) and low temperature district heating networks (LTDH) are considered in this study.

Table 3.11 - Summary of input data.

Datasets	Description	Sources
IEH supply	IEH supply from industrial processes and waste incineration	[223]
Heat demand scenario 'SwissRes'	Total demand per building for heating and hot water on a yearly basis in energy saving scenario based on 'SwissRes'	[81,224]
District network potential regions	GIS polygons of areas for potential low temperature district heating for heat demand scenario 'SwissRes'	[161]

The total IEH supply in Switzerland is estimated to be 11.8 TWh/year. It is assumed to be constant over the year. The total heating demand of the 'SwissRes' scenarios is 54 TWh/year, of which 12.2 TWh/year could potentially be supplied by DHN. Figure **3.17** shows the monthly variation in total DHN demand, as well as total IEH supplies. IEH supplies and DHN areas are spread spatially, as shown in the example in Figure **3.18**. Viable connections need to be identified when utilizing IEH for DHN, subject to spatial proximity constraints.

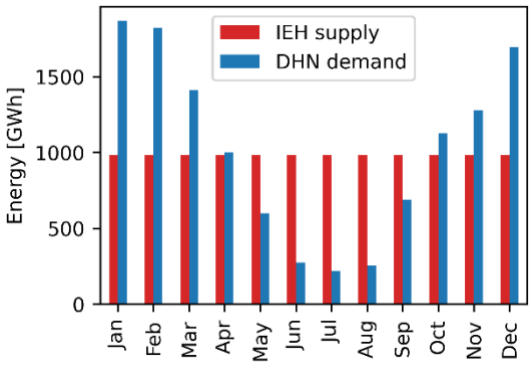

Figure 3.17 - Monthly profiles of industrial excess heat supply and district heating demand in Switzerland.

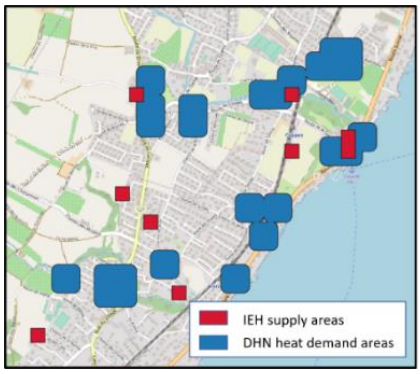

Figure 3.18 - An example area with industrial excess heat supplies and district heating networks

3.3.2.2 Data preparation

The data pre-processing is adapted from an existing spatial clustering method, and is described in detail in the corresponding work [136]. All possible connections between IEH supplies and DHN demands are firstly filter by spatial constraint of 5km distance using geographic information system (GIS) tools. Then these connections are further filtered by threshold heat transporting density of 1.8 MWh.y/m. Finally, the set of IEH supplies and DHN demands are clustered into distinct intra-connected components according to viable connections using graph theory.

3.3.2.3 Optimal allocation methods

The optimal allocation method applied in this work solves the problem of maximizing allocable heating energy within each cluster subject to connectivity constraints. The problem is framed as a variant of Hitchcock transportation problem [147]. The adaptation is made by enabling unbalanced total supplies and demands, as well as modifying the objective function to maximise

the allocation of heat energy. Finally, the optimization problem is solved using linear programming.

The objective function is maximizing the total allocable energy:

$$maximize \sum_i \sum_j \eta_{ij} e_{ij} \tag{3.16}$$

Where i indicates the index of IEH supply. j indicates the index of DHN demand. η_{ij} is the distributing efficiency of the connection between IEH supply i and DHN demand j, which equals 0.9 (accounting for 10% heat loss) when the connection is viable and equals 0 otherwise. e_{ij} is the decision variable which indicates the allocable heat demand in this connection.

The decision variable e_{ij} are constrained by the capacity of supplies and demands:

$$\sum_j e_{ij} \leq s_i \tag{3.17}$$

Where s_i is the capacity of IEH supply i.

$$\sum_i \eta_{ij} e_{ij} \leq d_j \tag{3.18}$$

Where s_i is the capacity of DHN demand j.

3.3.2.4 Storage system

Without seasonal storage system, the use of IEH to supply DHN is subject to temporal balance of supply and demand. The matching of supply and demand is therefore done on a monthly basis. The yearly total useable IEH is the sum of twelve months.

When seasonal storage is considered, surplus IEH supply in the months when heat demand is low could be stored and used in other months when IEH supply is insufficient. In this study, heat losses of the storage system are ignored. Usable IEH potential is assessed by solving the allocation problem on a yearly basis. The extra usable IEH potential compared with sum of monthly useable potential without storage is achieve by seasonal storage, and thus termed as storable IEH supply. Following the original method, the utilization of storable IEH is assumed to be distributed proportional to monthly energy deficit.

3.3.3 Results

A comparison between the results of usable IEH supply of the new method and the original one is carried out by applying them on the same Swiss case study. The results are summarized in Table **3.12**.

Table 3.12 - Comparison of results of the new optimal allocation method and the old method.

	IEH supply (TWh/y)	DHN demand (TWh/y)	Useable IEH supply without seasonal storage (TWh/y)	Useable IEH supply with seasonal storage (TWh/y)
Original net heat balance method	11.8	12.2	7.1	8.7
New optimal allocation method			5.2	6.0

Figure **3.19** presents the estimated useable IEH supply without considering seasonal storage. The original method estimated in total 7.1 TWh/year useable IEH supply, corresponds to 58% of total DHN heat demands. The new method instead estimated in total 5.2 TWh/year useable IEH supply, decreased 27% compared with the original method.

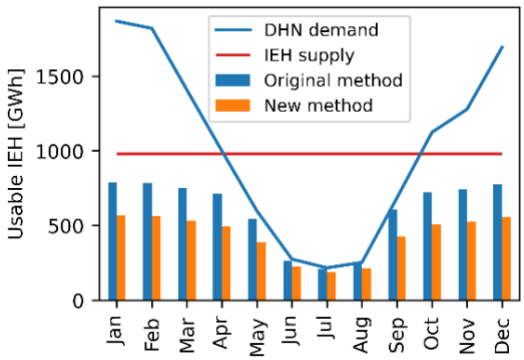

Figure 3.19 - The results of useable IEH without seasonal storage estimated by the original and new methods, as well as IEH supply and DHN demand.

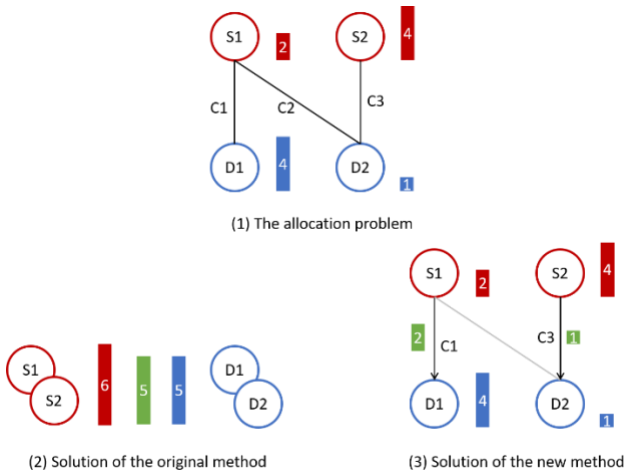

Figure 3.20 - A virtual example of one cluster. The circle indicates supply and demand nodes. The bar indicates their capacity.

The original net heat balance method does not solve the problem of optimal allocation with each cluster and therefore cause overestimated useable IEH supply. The implicit assumption of the original net heat balance method is that heat energy can move freely within the cluster. In reality, heat can only be transported through direct connection, but not sequence of connections, since it would result in heat transmission lines that are longer than the transmission limit threshold used in the original filtering. This is illustrated in the virtual cluster presented in Figure **3.20**. S1 (Source #1) is connected to D1 (Demand #1) and D2, S2 is connected to D1. Although S2 and D1 are in the same cluster, heat energy is not able to distribute from S2 to D1. Ignoring the spatial constraint within the cluster, the original method overestimates the useable supply to be 5 units, while the new method gives accurate estimate of 3 unit.

In the Swiss case study, we found large clusters that contain numerous supply nodes and demand nodes (up to 4059 nodes) and spread in huge areas. It is essential to use the optimal allocation method to solve the allocation problem within each cluster, in order to fully assess the impact of spatial constraint.

In the case when seasonal storage is considered, the surplus IEH in summer when the heat demand is low could be saved and used in winter when supply is in shortage. The original method finds 1.6 TWh/year storable IEH, contributing extra 22% of useable IEH. With the optimal allocation method, the storable IEH is 0.8 TWh/year, 15% of useable IEH without seasonal storage.

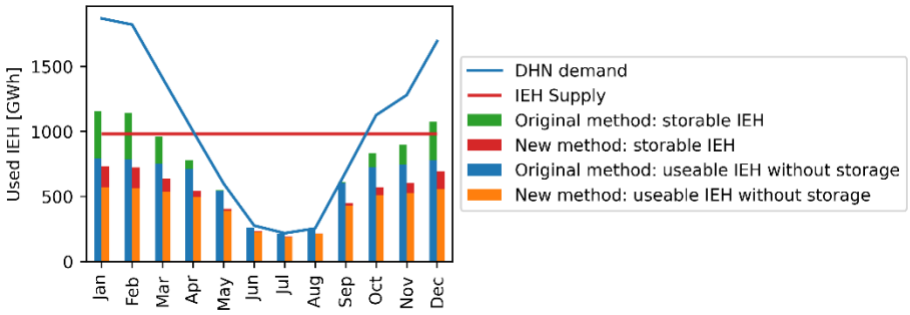

Figure 3.21 - The results of storable IEH estimated by the original and new methods, as well as useable IEH, IEH supply and DHN demand.

3.3.4 Discussion

We found that the new allocation method improves the accuracy in estimating the maximum allocable energy in clusters with long sequences of links. It is essential to implement the new optimal allocation method which properly models spatial constraints. This method can be generalised to allocate other types of resources in networks of suppliers and users. In the field of energy, it is specifically suitable to evaluate the potential of spatially bounded energy sources, such as IEH, geothermal, free thermal energy from waterbodies, etc.

If there is no spatial constraint, 8.9 TWh/year IEH could be utilised after considering monthly balancing of IEH supply and DHN demands. The spatial constraint is a major limiting factor of using IEH, making large amount of IEH supply not accessible by DHN. It reduces the useable potential to 5.2 TWh/year. Season storage only offers extra 0.6 TWh/year of storable potential. By improving the efficiency and decreasing the cost of DHN, we could further ease the spatial constraint in utilising renewable and waste energies, and in the end support the transition to a decarbonized energy system.

3.3.5 Conclusion

This paper presents a method to calculate the maximum allocable resource within network of supplies and demands. The method improves an existing spatiotemporal analysis method by introducing an adapted form of Hitchcock transportation problem and linear programming to solve the optimal allocation problem. The effectiveness of the new method is demonstrated by applying both the new and the original method on a case study of IEH potential to supply DHN in Switzerland. The new method is found to improve the accuracy of estimating IEH potential. The method could be applied to diverse thermal sources, such as industrial excess heat, geothermal, lakes and rivers, etc.

Under spatial and temporal constraints, 5.2 TWh/year out of 11.8 TWh/year IEH supply is found to be useable to supply DHNs. Seasonal storage could contribute another 0.8 TWh/year storable IEH by lifting the temporal constraint.

4 Techno-economic performance of 5GDHC

Research question 3: What is the technical and economic performance of a 5GDHC integrated with shallow geothermal energy?

This chapter contributes to an enhanced understanding of the potential of 5GDHC to address heating and cooling demands, particularly when it is integrated with shallow geothermal energy. While most of existing research primarily focused on assessing the performance of 5GDHC concerning the realization of synergies between simultaneous heating and cooling demands, this chapter delve into evaluating the performance of 5GDHC integrated with BTES, emphasising the unlocked synergies in scenarios with poor simultaneity between heating and cooling demands. The evaluation of 5GDHC's performance includes five aspects: levelized cost of energy, upfront cost, greenhouse gas emission, exergy efficiency, and electricity peak load. Moreover, a comprehensive examination of the components of cost structure that could potentially be addressed by policy incentives, such as subsidies, is conducted to provide insights for supporting the adoption of these systems.

The outcomes of this work have been prepared as a journal paper published in *Energy*.

Journal paper 4:

Xiang Li, Selin Yilmaz, Martin K. Patel, and Jonathan Chambers. 'Techno-Economic Analysis of Fifth-Generation District Heating and Cooling Combined with Seasonal Borehole Thermal Energy Storage'. *Energy* 285 (December 2023): 129382.

4.1 Techno-economic analysis of fifth-generation district heating and cooling combined with seasonal borehole thermal energy storage

4.1.1 Introduction

4.1.1.1 Background

Decarbonising the heating and cooling sector has been highlighted as a priority to reach a carbon-neutral economy in the coming decades [127]. District heating and cooling (DHC) is a promising technology to meet building thermal demands as it facilitates the use of renewable energy sources, increases energy efficiency, and improves security of supply [8]. District heating (DH) systems have been widely built to supply heat directly to buildings in heating-dominated climates like Northern Europe [225]. The latest major development of DH is to shift from third generation district heating (3GDH) to fourth generation district heating (4GDH), decreasing the supply temperature from around 100°C down to 50-70°C, in order to adapt to future renewable energy sources (e.g. solar and geothermal heat) and to reduce energy losses [26]. In contrast, district cooling (DC) systems are rarely used in Europe as space cooling is not widely provided in the heating-dominated climate [54]. In recent years, however, space cooling demand has shown a strong growth trend under climate change [6]. This has motivated a novel concept of combined district heating and cooling to emerge in countries including France [226], Switzerland [227], and Italy [33].

In the literature, different names have been given to the same concept but with different foci. 'Fifth-generation district heating and cooling (5GDHC)' is the mostly used, defining it as the successor of 4GDH [29,228,229] that further reduce the operating temperature to below 30°C. The name 'Combined heating and cooling network' highlights its integrated heating and cooling supply [230,231]. In Germany and Switzerland, they are called 'cold district heating' ('Kalte Fernwärme' in German) [31] and 'anergy network' ('Anergienetz' in German) [90]. The name 'reservoir network' is also used [227] and it indicates that the network is used as a thermal reservoir by decentralised heat pumps. More recently, researchers have adopted the term 'neutral temperature district heating and cooling' [232] to stress the combined heating and cooling enabled by an operating temperature (<30°C) that is neutral relative to ground temperature. Since the low operating temperature is not sufficient to supply building heating demands directly, 5GDHC relies on booster heat pumps (BHP) to reach the temperature level required by individual buildings [228].

The concept of 5GDHC technology can be traced back to ground-source heat pumps (GSHP), but it extends to a broader and more extensive scope [29]. While GSHP typically functions as an individual system designed for a single building, 5GDHC focus on providing heating and cooling

to multiple buildings on district level through pipe networks. This innovative approach brings multiple benefits [29,33]. 5GDHC enables simultaneous heating and cooling to buildings with mixed purposes via the same network. It also minimises the barrier to integrate low-grade heat sources, especially waste heat. It is beneficial to recover the waste heat from cooling use in 5GDHC, taking advantage of the synergy between heating and cooling. In addition, the thermal energy loss at the neutral temperature is negligible, which allows to use uninsulated pipes at reduced cost. Considering the differences between 5GDHC and 4GDH, Lund et al. [35] argue that 5GDHC should not be seen as the next generation of 4GDH, but rather as a complementary option. 5GDHC is particularly suitable for areas with combined heating and cooling needs.

4.1.1.2 Previous studies on the potential of district networks

To-date, most studies on the potential of district networks are limited to address heating demand. They have failed to address space cooling demand, although it will play a vital role in future thermal energy systems in central Europe [6,125]. A large number of published studies focus on identifying appropriate district areas for implementing DH. The feasibility of DH depends on multiple factors, including size of demand, distribution cost, available energy sources, etc. [134,198,233,234]. Overall, linear thermal demand density, which measures energy demand per unit length of thermal network, is commonly used as the major filtering parameter [161,235]. It is assumed that below a given linear demand density threshold, the investment and thermal losses of the network outweigh the benefit of increasing efficiency in meeting the supplied demands, making it not profitable to building DH.

The feasibility of using BHPs in the DH has been evaluated by some researchers. Østergaard and Andersen [236] show that BHPs reduce energy use and cost. Averfalk and Werner [237] find that lower operating temperature facilitates the use of low temperature sources such as geothermal heat and industrial excess heat. However, according to Lund et al. [238], the economic feasibility of using BHPs is very questionable. This view is supported by Meesenburg et al. [239] who note that the additional cost of BHPs outweighs the lower operational cost, although it could become economically feasible if cheap heat sources are available.

A few case studies have attempted to evaluate the capability of 5GDHC to integrate the fast-growing cooling demand in the district networks. It has been shown that 5GDHC may become a more energy-efficient alternative when there is sufficient simultaneity of heating and cooling demands [240]. Wirtz et al. have developed an optimization model for designing and evaluating 5GDHC [241]. They further define a metric called 'Demand overlap coefficient (DOC)' to quantify the overlapping heating and cooling demands in and between buildings [46]. Their work shows that a DOC larger than 0.45 leads to lower annualized cost and higher exergy efficiencies in 5GDHC. Miller et al. [242] show that when there is low simultaneity of heating

and cooling demands, the utilisation of thermal storage largely promotes the financial benefit of 5GDHC.

However, these studies are mostly restricted to short-term thermal storage. Research on the effect of adding seasonal thermal energy storage (STES) in 5GDHC is limited, although several studies have highlighted the advantages of adopting the ground as thermal energy storage of 5GDHC. For example, Walch et al. [160] demonstrate that DHC combined with borehole heat exchanger (BHE) provides substantial potential to supply building thermal demands. Another study that designed a 5GDHC system of a small district (50 buildings) modelled using 3 representative building archetypes using TRNSYS [44] suggests that the integration of GSHP in 5GDHC significantly enhances the system efficiency. To-date however there are few works that present methods allowing characterisation of the potential of 5GDHC with BTES in more general cases. Notably, it is demonstrated in our previous work [160], the optimal density of borehole fields and their heat extraction potential (and therefore cost-effectiveness) depends on the potential for regeneration; therefore to understand the potential requires methods that allow co-simulation and optimisation of the thermal network and thermal storage. In addition, few works to-date perform direct comparisons between different thermal energy decarbonisation scenarios, notably between current (business as usual), individual electrification (each building with their own heat pumps/chillers), and community (district energy) cases. Finally, studies on DHC potentials today have focused on existing locations that are heating dominated [239] or combined heating and cooling [44]; but did not consider the future impact of climate change. We have previously demonstrated [125] that in hot summer/cold winter locations (such as Switzerland, the subject of our case study) cooling demand is likely to increase by 400-600% over the coming 30 years (i.e. the lifetime of 5GDHC systems built today) with significant consequences on their performance and cost effectiveness potentials.

4.1.1.3 Objectives

This paper aims to evaluate the potential of 5GDHC combined with BTES in unlocking the potential synergy of heating and cooling to achieve decarbonised future energy systems. We develop a methodology for designing and evaluating 5GDHC integrated with BTES. The proposed model combines the optimal designing of building substations, BHE fields, thermal network layout and pipe capacity, as well as simulation of the interaction between building substations, thermal network, and BHE fields during operation. The system is evaluated according to several Key Performance Indicators (KPI): levelized cost of energy, upfront cost, greenhouse gas emissions, exergy efficiency, and the electricity peak power. The performance indicators are presented in comparison to stand-alone HP system and traditional gas-driven system. The impact of heating and cooling demand structure will be assessed, to understand under which circumstances 5GDHC becomes more favourable than its alternatives.

This work presents the following novel contributions. Increasing cooling loads have been rarely addressed in the context of historically heating dominated climates; we assess the benefit of 5GDHC with BTES in the context of balanced heating and cooling loads and assess future prospects with regards to increasing cooling load relative to heating, which is likely to occur due to climate change (in particular increased adoption of active cooling in response to more frequent heatwaves and hot spells). We compare the KPIs for such a system with alternative decarbonisation scenarios and determine what components of the cost structure might be addressed by policy incentives (subsidies) in order to support adoption. We furthermore evaluate the benefits of seasonal energy storage in the context of mixed, non-simultaneous heating and cooling loads.

We develop a novel method that integrates our multiple previous works on projections of energy demand for heating and cooling, thermal network modelling and routing, BTES simulation into a single model that optimises the 5GDHC with BTES system design for a given area. This work presents the application of the model to a test area but is applicable much more broadly wherever the base geospatial data is available.

The remainder of this paper is structured as follows: Section 4.1.2 introduces the proposed model developed for designing and evaluating 5GDHC integrated with BTES. Section 4.1.3 presents the chosen case study for demonstration. Section 4.1.4 presents the results of 5GDHC performance on the case study. This is followed by a discussion of implications, and limitations of this study. Finally, Section 4.1.6 concludes the paper.

4.1.2 Methods

A model for the design and operation of 5GDHC supplied by BTES is presented in this section. The model sizes the three major components and simulates their operation: building substations equipped with BHPs, a 2-pipe thermal network, and BHEs. The model considers a time horizon of one year, with time step Δt of one hour. The workflow of the model is shown in Figure **4.1**. and described in detail in Section 4.1.2.1 – 4.1.2.3. Following the design of the 5GDHC, it is compared with reference systems by evaluating their economic, technical, and environmental performance.

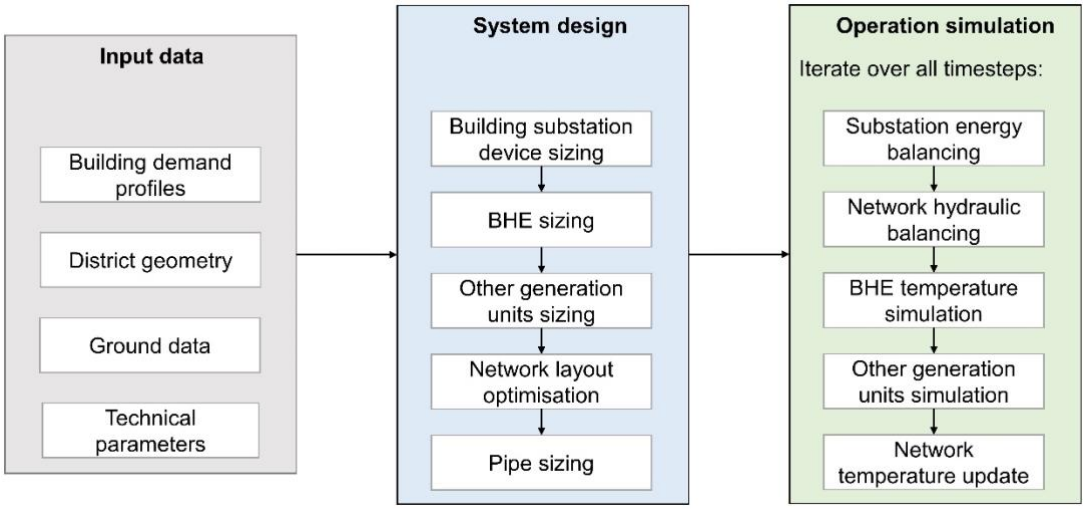

Figure 4.1 - The workflow of the model of 5GDHC.

4.1.2.1 Input data

Input data required for the model of 5GDHC is presented in Table **4.1**.

Table 4.1 - Input data of the model of 5GDHC.

Type	Data	Description
Building demand profiles	$\dot{Q}_h$	Building heating demand profile (useful energy), including space heating (SH) and domestic hot water (DHW) demands.
	T_h	Temperature requirement for heating demand. It can vary depending on the building or the usage (SH/DHW).
	$\dot{Q}_c$	Building cooling demand profile, including space cooling (SC) demand.
	T_c	Temperature requirement for cooling demand.
District geometry	Building locations	Latitude and longitude.
	Road network	Existing road network for potential thermal network routing.
	A_{avail}	Available area for borehole drilling.
Ground data	λ	Ground thermal conductivity.
	α	Ground thermal diffusivity.
	T_g	Undisturbed ground temperature.
Technical parameters	Efficiencies	Efficiencies of energy conversion devices, such as heat pumps, chillers.
	H_{BHE}	Borehole length.
	B_{BHE}	Spacing between adjacent boreholes.
	r_{BHE}	Borehole radius.
	R_{BHE}	Effective borehole thermal resistance.
	$T_{mf,min}$	Minimum allowed heat carrier fluid temperature. This value is chosen to avoid freezing.
	$T_{mf,max}$	Maximum allowed heat carrier fluid temperature. This value is chosen to ensure that direct cooling is possible.

4.1.2.2 System design

Building substations

A building substation connects the building's energy system with the thermal network, as illustrated in Figure **4.2**. It is equipped with BHP to supply $\dot{Q}_h$, and heat exchangers (HX) to supply $\dot{Q}_c$. Water circulation pumps (WCP) are used to control the mass flow rate passing through the substation.

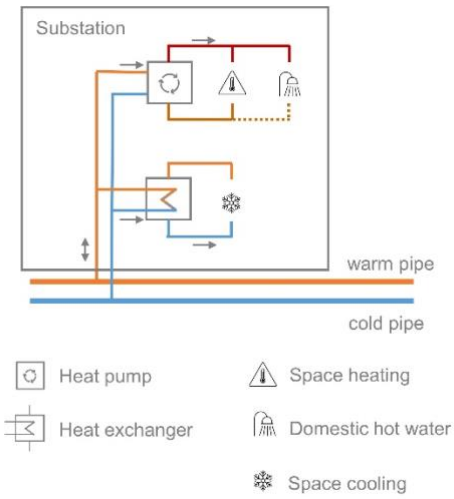

Figure 4.2 - Functional diagram of the building substation.

Since the large thermal mass of building envelopes and equipped water tanks provide moderate flexibility in substation operation, we shave peak loads by averaging building load profiles in four hour intervals. Substation devices are sized to fulfill peak load conditions after peak shaving.

The substation load to the thermal network can be evaluated by considering the energy balance at the substation as follows:

$$\dot{Q}_{SUB,b,t} + \dot{E}_{BHP,b,t} = \dot{Q}_{h,b,t} + \dot{Q}_{c,b,t} \quad (4.1)$$

Where b denotes the building, t denotes the time step. $\dot{Q}_{SUB,b,t}$ is the substation demand, defined as the required energy exchange between the substation and the network. $\dot{E}_{BHP,b,t}$ is the electricity consumption of BHP. The coefficient of performance (COP) of BHP depends on the temperature of warm pipe (which is assumed to be the inlet temperature of BHP). However, it remains unknow in the design stage. Therefore, we take T_g as an approximation of BHP inlet temperature for design purpose. The electricity consumption of WCP $\dot{E}_{WCP,b,t}$ is estimated as 3% of the sum of $\dot{Q}_{h,b,t}$, and $\dot{Q}_{c,b,t}$.

Generation units

In the proposed 5GDHC model, the residual demand of thermal network is supplied by a BTES made up of BHE fields when total substation loads do not counterbalance each other. It serves as a seasonal storage, enabling balancing of heating and cooling demands that occur in different periods over the year. If the local available area to install BHE is insufficient to meet all demands, supplementary generation units are added. In this model, the default choice is a central biogas boiler and a central chiller as they are widely available. Other energy conversion technologies could also be considered when required. Figure **4.3** shows the diagram of the generation units.

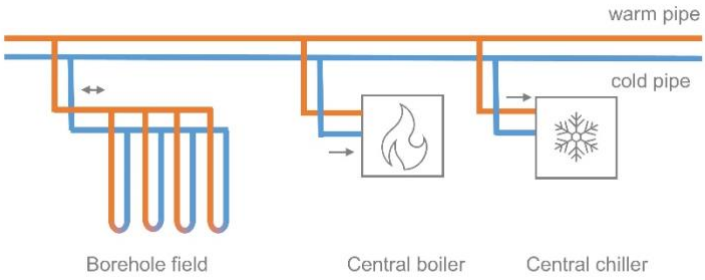

Figure 4.3 - Functional diagram of the generation units.

Unlike sizing substation devices that only considers the peak loads, designing BHEs requires to consider borehole loads over time. Since the temperature of fluid is close to the ground temperature, thermal losses are negligible. We estimate the borehole load as the sum of substation loads:

$$\dot{Q}_{BHE,t} = \sum_b \dot{Q}_{SUB,b,t} \tag{4.2}$$

Note that Equation 4.2 estimates borehole load only for design purpose. The accurate operation profiles of BHEs is re-evaluated in the operation simulation stage. The total length of BHEs L_{BHE}, is selected considering the constraint on mean fluid temperature T_{mf} inside the BHEs. T_{mf} must remain within the temperature limits, $T_{mf,min}$ and $T_{mf,max}$, in the planned service life t_{dim}. In Switzerland, t_{dim} equals 50 years. $T_{mf,min}$ and $T_{mf,max}$ are determined by the temperature requirement of building loads and the technical requirement of substation devices. T_{mf} depends on many factors: borehole load, borehole configuration, ground properties, etc. Following the principle of temporal superposition, the extreme values of T_{mf} are modelled by superposing three load components: 1) a long-term component represents annual average borehole load, 2) a periodic component represents seasonal variation, and 3) a short-term pulse component represents peak borehole load [160,202,204]. The equations to calculate extreme temperatures are given below considering the three load components and the respective ground thermal resistances, plus the borehole thermal resistance:

$$\begin{aligned}(T_g - T_{mf,min}) \times L_{BHE} \leq max(\dot{Q}_{mean}, 0) \times R_{long-term} + (\dot{Q}_{month,h} - max(\dot{Q}_{mean}, 0)) \times R_{peri} \\ +(\dot{Q}_{peak,h} - \dot{Q}_{month,h}) \times R_{pulse} + \dot{Q}_{peak,h} \times R_{BHE}\end{aligned} \tag{4.3}$$

$$\begin{aligned}(T_g - T_{mf,max}) \times L_{BHE} \leq min(\dot{Q}_{mean}, 0) \times R_{long-term} + (\dot{Q}_{month,c} - min(\dot{Q}_{mean}, 0)) \times R_{peri} \\ +(\dot{Q}_{peak,c} - \dot{Q}_{month,c}) \times R_{pulse} + \dot{Q}_{peak,c} \times R_{BHE}\end{aligned} \tag{4.4}$$

Where $\dot{Q}_{mean}$ is the yearly average borehole load, $\dot{Q}_{month,h/c}$ is the maximum monthly average borehole heating/cooling load, and $\dot{Q}_{peak,h/c}$ is the peak borehole heating/cooling load. Note

that heating load has a positive value, while cooling load has a negative value. Regarding the thermal resistances, $R_{long-term}$ is the long-term ground thermal resistance of BHE fields [243]. It accounts for the average long-term influence of a constant borehole load over t_{dim} on the ground temperature, considering the thermal interference of neighbouring BHEs. R_{peri} is the periodic ground thermal resistance, accounting for the influence of a periodic borehole load with one year period on the ground temperature [244]. R_{pulse}, the pulse ground thermal resistance, accounts for the influence of a short-term pulse that lasts four hours on the ground temperature [244]. Lastly, R_{BHE} is the effective borehole thermal resistance. It accounts for the temperature difference between the heat carrier fluid (water) and the borehole wall [177].

To calculate these thermal resistances, parameters of borehole dimensions, and configuration are required, such as length of each borehole H_{BHE}, and borehole spacing B_{BHE}, borehole radius r_{BHE}. Since L_{BHE} influences borehole configuration and hence the ground thermal resistances, it should be evaluated in an iterative process until convergence. In addition, L_{BHE} is constrained by the available area for BHE installation. Hence, we propose the following process to find the proper L_{BHE}, as shown in Figure **4.4**.

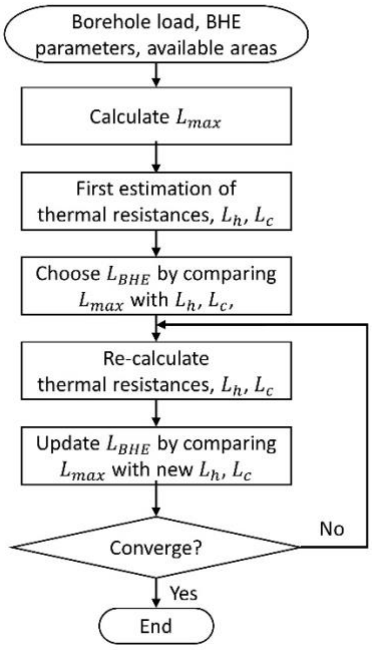

Figure 4.4 - Process to size borehole fields.

The maximum allowed total length of BHE L_{BHE}^{max} that could be installed in the available area with the assumed borehole spacing is firstly calculated. To have a first estimation of $R_{long-term}$, we assume each BHE field is arranged as borehole fields in 20 * 20 rectangular grids. The thermal interference between two BHE fields is negligible as the distances between them are large enough. Subsequently, the required length for the heating operations L_h and cooling operation

L_c are calculated using Equation 4.3 and 4.4, respectively. L_h and L_c are then compared with L_{BHE}^{max}. If L_{BHE}^{max} is larger than both L_h and L_c, L_{BHE} equals the larger one of L_h and L_c. Otherwise, L_{BHE} is limited to L_{BHE}^{max}. This means supplementary generation units are needed to cover peak loads that cannot be met by limited number of BHEs. As explained before, L_{BHE} is evaluated over 50 years in an iterative process until the last two estimates converge (Difference less than 1%). To re-calculate the ground thermal resistances considering thermal interference, we need to determine BHEs configuration. BHEs is firstly assigned to the largest parcel of available area, then the second largest, etc., until the total length reaches L_{BHE}.

After L_{BHE} is finally sized, in the case where L_{BHE} is limited by L_{BHE}^{max}, the capacity of BHEs for heating $\dot{Q}_{BHE}^{max}$ and cooling $\dot{Q}_{BHE}^{min}$ is adjusted based on L_{BHE}. The part of total substation demand that exceeds $\dot{Q}_{BHE}^{max}$ or $\dot{Q}_{BHE}^{min}$ will be supplied by a central biogas boiler or a central chiller.

Thermal network

In this section, we determine the routing of the thermal network and the diameter of pipes. It consists of a warm pipe, with temperature T_{wp}, and a cold pipe, with temperature T_{cp}. T_{wp} and T_{cp} are designed to be within the range of 4°C - 21°C. The temperature difference between warm pipe and cold pipe is assumed to be kept at ΔT of 4°C.

Firstly, locations of thermal network nodes, namely building substations and generation units, is necessary information for network layout design. The location of building substations is given as input data to the model. Locations where a BHE field connects to the thermal network is assumed to be the nearest building. The layout of the network is designed by the geospatial network routing method developed by Chambers [245]. This method facilitates finding the shortest path of pipes through the existing road network.

Secondly, the diameters of pipes are selected based on the mass flow rate $\dot{m}_{p,t}$ in pipes. The mass flow rates passing through BHP, HX, central gas boiler, and central chiller (when supplemental generation units are installed) are controlled to maintain a temperature difference ΔT of 4°C between the supply and return flows. Consequently, the mass flow rate of substations is:

$$\dot{m}_{SUB,b,t} = \frac{\dot{Q}_{SUB,b,t}}{\Delta T c_w} \tag{4.5}$$

Where c_w is the thermal capacity of the heat carrier fluid. The mass flow rate passing the central gas boiler and central chiller is calculated likewise.

The flow passing through BHEs is therefore the residual flow of all other nodes:

$$\dot{m}_{BHE,t} = \left(\sum_b \dot{Q}_{SUB,b,t} - \dot{Q}_{boiler,t} - \dot{Q}_{central\ chiller\ ,t} \right) \Big/ \Delta T c_w \tag{4.6}$$

Once the mass flow at each node is figured out, the mass flow rate of pipes is obtained by solving Equation 4.7 for each time step:

$$\boldsymbol{N} \times \dot{\boldsymbol{m}}_{\boldsymbol{p,t}} = \dot{\boldsymbol{m}}_{\boldsymbol{node,t}} \tag{4.7}$$

Where $\boldsymbol{N}$ denotes the matrix representing the connection between pipes and nodes. $\dot{\boldsymbol{m}}_{\boldsymbol{p,t}}$ and $\dot{\boldsymbol{m}}_{\boldsymbol{node,t}}$ are the vectors of flow rate of pipes and nodes. Finally, pipe inside diameter d_p is picked based on Equation 4.8:

$$d_p = \sqrt{4\dot{m}_p^{max}/\pi v \rho_w} \tag{4.8}$$

Where $\dot{m}_p^{max}$ is the peak mass flow rate among all time steps, v is the maximum allowed flow velocity, and ρ_w is the density of the heat carrier fluid.

4.1.2.3 Operation simulation of 5GDHC

In this section, the methodology for simulating the operation of the 5GDHC for one year is presented. In the operation simulation process, it is essential to evaluate the energy balance and hydraulic balance in the 5GDHC using COP of BHP calculated based on fluid temperature in the thermal network. Since the fluid temperature, mass flow rate, and heat transfer in boreholes are dependent on each other, an iterative process is required [246,247].

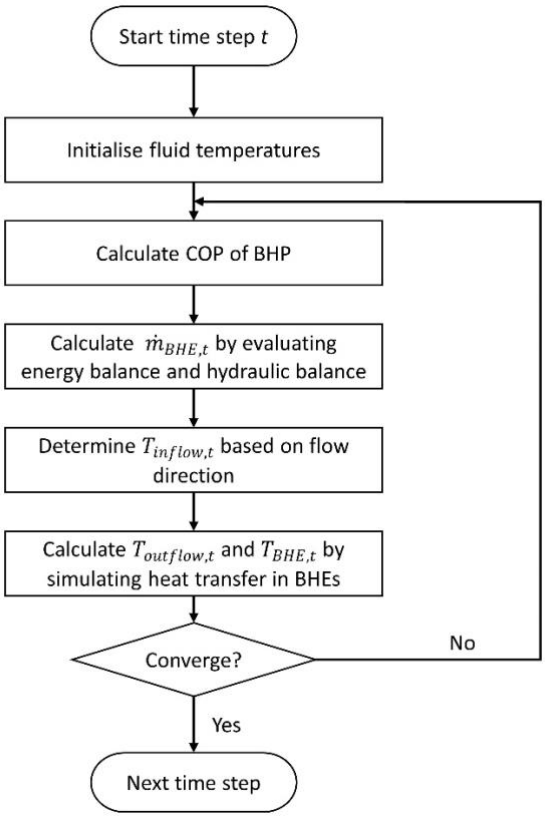

Figure 4.5 - Iterative process to solve system operation variables.

The iterative process is summarised in Figure **4.5**. At each time step t, the temperature of the warm pipe $T_{wp,t}$ and the cold pipe $T_{cp,t}$ is firstly initialised using the values from the previous time step. Then the COP of BHP is calculated depending on $T_{wp,t}$. The energy balance (Equation 4.1) and hydraulic balance (Equation 4.6) are then evaluated to obtain the mass flow rate passing through BHEs $\dot{m}_{BHE,t}$. The inflow temperature of BHEs $T_{inflow,t}$ is determined based on the flow direction in BHEs. When BHEs are operating in heating mode ($\dot{m}_{BHE,t} > 0$), fluid from the cold pipe passes through BHEs before joining the warm pipe, thus $T_{inflow,t}$ equals $T_{cp,t}$. Otherwise, $T_{inflow,t}$ equals $T_{wp,t}$. Subsequently, the outflow temperature $T_{outflow,t}$ and the borehole wall temperature $T_{BHE,t}$ are calculated using Pygfunction [248]. Pygfunction is a Python package for the calculation of thermal response factors, or g-functions [203], to model the heat transfer between boreholes and the ground and then predict fluid and ground temperatures in geothermal borehole fields. It relies on the analytical finite line source solution to evaluate g-functions considering the thermal interference between boreholes [243,244,249]. The updated fluid temperatures are then passed to the next iteration. The iterative loop is finally terminated when $T_{outflow,t}$, $T_{BHE,t}$, and $\dot{m}_{BHE,t}$ of two consecutive iterations converge within a certain tolerance. $T_{outflow,t}$ and $T_{BHE,t}$ are solved at an absolute tolerance of 0.001°C. $\dot{m}_{BHE,t}$ is solved at a relative tolerance of 0.0001%.

4.1.2.4 Reference systems

Reference systems are modelled to be compared with the proposed 5GDHC. The first reference system is called 'Business-As-Usual (BAU)'. It represents present-day thermal energy systems where SH and DHW demands are supplied by individual gas boilers and SC is supplied by individual chillers. The second reference system is named 'Electrification', representing state-of-art electrified thermal systems. In 'Electrification' system, building substations are equipped with air-source heat pumps (ASHP) and individual chillers. In both reference systems, building substations are stand-alone and not connected to a district network.

4.1.2.5 Key performance indicators

In this section, we define the key performance indicators (KPIs) to evaluate the performance of the designed 5GDHC.

The economic performance indicators include the upfront cost C_{inv} and the levelized cost of energy $LCOE$. C_{inv} considers the investment cost of equipment, including BHP, BHE, central gas boiler, central chillers, and thermal network pipes. The levelized cost $LCOE$ measures the average net present cost of the 5GDHC to supply building loads over its lifetime. It consists of the annualized investment cost of equipment, operation and maintenance costs (O&M), and final energy cost.

$$LCOE = \frac{\sum_i C_{inv,i} \times \left(f_{annu,i} + f_{o\&m,i}\right) + C_{FE}}{\sum_{b,t}\left(\dot{Q}_{SH,b,t} + \dot{Q}_{DHW,b,t} + \left|\dot{Q}_{SC,b,t}\right|\right) \times \Delta t} \tag{4.9}$$

Where i indicates the 5GDHC equipment. $f_{annu,i}$ is the annuity factor, which depends on the lifetime of the equipment and the discount rate. The default discount rate is 2%. $f_{o\&m,i}$ is the annual operation and maintenance factor of the equipment. C_{FE}, the cost of final energy, can be calculated using equation:

$$C_{FE} = \sum\left(\dot{E}_{BHP,b,t} + \dot{E}_{WCP,b,t} + \dot{E}_{central\ chiller,t}\right) \times \Delta t \times c_{el} + \sum \dot{Q}_{biogas,t} \times \Delta t \times c_{biogas} \tag{4.10}$$

Where c_{el} and c_{biogas} are the unit cost of electricity and biogas, respectively.

To evaluate the environmental performance of 5GDHC, we calculate the system's average greenhouse gas emissions per year using Equation 4.11. The embodied emission of equipment is not considered.

$$e_{avg} = \frac{\sum\left(\dot{E}_{BHP,b,t} + \dot{E}_{WCP,b,t} + \dot{E}_{central\ chiller,t}\right) \times e_{el} + \sum \dot{Q}_{biogas,t} \times e_{biogas}}{\sum\left(\dot{Q}_{SH,b,t} + \dot{Q}_{DHW,b,t} + \left|\dot{Q}_{SC,b,t}\right|\right)} \tag{4.11}$$

Where e_{el} and e_{biogas} are the emission factor of electricity and biogas, respectively.

To assess the technical performance of 5GDHC, we investigate the exergy efficiency η_{ex} and the electricity peak power $\dot{E}_{max}$. η_{ex} is calculated as the exergy of building load EX_{load} (see Equation 4.12) divided by the exergy of consumed final energy EX_{FE} (see Equation 4.13).

$$EX_{load} = \sum_{b,t}\left(\dot{Q}_{SH,b,t} \times \left(1 - \frac{T_{ref}}{T_{SH}}\right) + \dot{Q}_{DHW,b,t} \times \left(1 - \frac{T_{ref}}{T_{DHW}}\right) + \dot{Q}_{SC,b,t} \times \left(1 - \frac{T_{ref}}{T_{SC}}\right)\right) \times \Delta t \quad (4.12)$$

$$EX_{FE} = \left(\sum\left(\dot{E}_{BHP,b,t} + \dot{E}_{WCP,b,t} + \dot{E}_{central\ chiller,t}\right) \times ex_{el} + \sum \dot{Q}_{biogas,t} \times ex_{biogas}\right) \times \Delta t \quad (4.13)$$

Where the reference temperature T_{ref} is 298.15K (25°C). ex_{el} and ex_{biogas} are the exergy factor of electricity and biogas, respectively.

$\dot{E}_{max}$ is the maximum total electricity load among all time steps:

$$\dot{E}_{max} = max\left(\sum_{b}\left(\dot{E}_{BHP,b,t} + \dot{E}_{WCP,b,t}\right) + \dot{E}_{central\ chiller,t}\right) \quad (4.14)$$

4.1.3 Case study

The proposed model is demonstrated by a case study of a residential area in Canton of Geneva, Switzerland. It consists of 263 multi-family houses, 18 office buildings, 10 buildings for trade, 6 buildings for education, 5 buildings for recreation, 2 buildings for health, and 1 hotel. The total floor area of buildings is 1.05 km². The case study area is suitable for this study as it provides high-resolution datasets on building information, district geometry, etc. The building demand profiles in hourly resolution are obtained from an archetypical energy demand database [250].

The input data of the case study is summarized in Table **4.2**. Figure **4.6** presents the geometry of the case study, including building location and route network [245]. The aggregated building thermal loads are plotted in Figure **4.7**. The data about equipment and final energy are given in Table **4.3** and Table **4.4**, respectively.

Table 4.2 - Input data of the case study.

Type	Data	Description
Building demand profiles [250,251]	$\dot{Q}_h$	Total heating demand that requires 35°C is 5.7 GWh per year (useful energy). Total heating demand that requires 60°C is 47.4 GWh per year (useful energy). The average specific heating demand is 50.5 kWh/(m².y).
	T_h	Depends on the building conditions and the usage, it can be 35°C or 60°C.
	$\dot{Q}_c$	Total cooling demand is 18.2 GWh per year (useful energy). The average specific cooling demand is 17.3 kWh/(m².y).
	T_c	15°C
District geometry [159,245]	Building locations	Plotted in Figure **4.5**
	Road network	Plotted in Figure **4.5**
	A_{avail}	Aggreged into a grid of 200m * 200m
Ground data [214]	λ	2.4 $W/(mK)$
	α	$1.1 \times 10^{-6} m^2/s$
	T_g	13.4 °C
Technical parameters [159,252]	H_{BHE}	200 m
	B_{BHE}	6 m
	r_{BHE}	0.065 m
	R_{BHE}	0.15 mK/W
	$T_{mf,min}$	6°C
	$T_{mf,max}$	19 °C

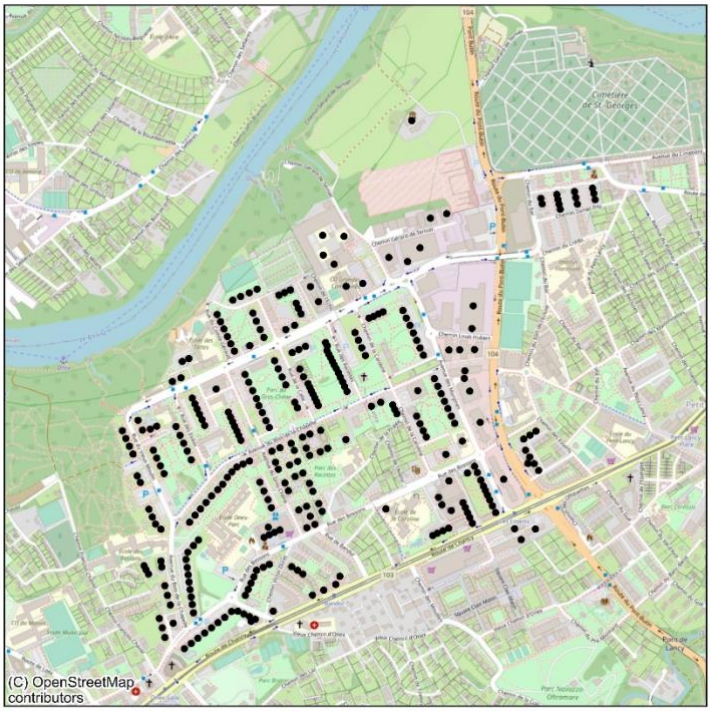

Figure 4.6 - District geometry of the case study. The black dots represent buildings.

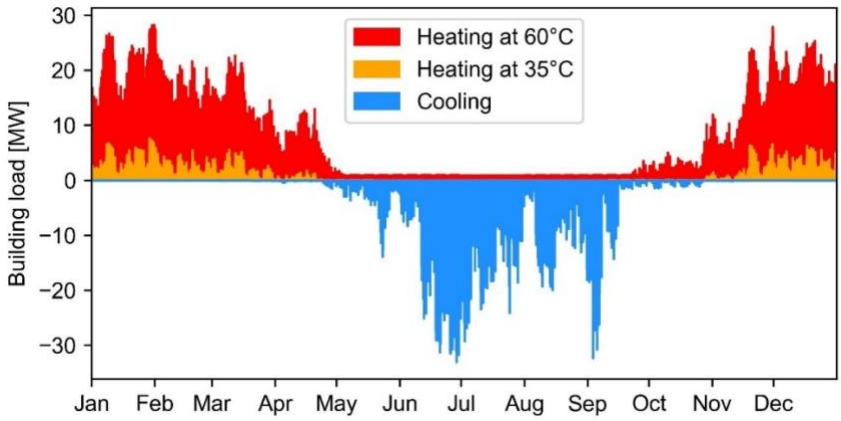

Figure 4.7 - The total thermal loads of buildings in the case study.

Table 4.3 - Information of equipment.
[241,253,254]

Equipment	Unit cost[1]	Service life [year]	Annuity factor	O&M factor [%]	Efficiency
BHP	1200 CHF/kW	20	0.0612	2.5	$0.5\frac{T_{sink}}{T_{sink}-T_{source}}$
BHE	18500 CHF/ borehole	50	0.0318	1	N/A
Central biogas boiler	470 CHF/kW	20	0.0612	3	0.9
Central chiller	2000 CHF/kW	20	0.0612	3.5	$0.4\frac{T_{eva}}{T_{sink}-T_{source}}$
Pipe	See Appendix A	40	0.0366	0.5	N/A
ASHP	2000 CHF/kW	20	0.0612	2.5	$0.4\frac{T_{sink}}{T_{sink}-T_{source}}$
Individual chiller	2000 CHF/kW	20	0.0612	3.5	$0.4\frac{T_{source}}{T_{sink}-T_{source}}$
Gas boiler	470 CHF/kW	20	0.0612	3	0.9

[1]The unit cost includes device and installation cost.

Table 4.4 - Information of final energy.
[241,255,256]

Final energy	Unit cost [CHF/kWh]	Exergy factor	Emission factor [kg CO_2/kWh]
Electricity	0.283	1	0.125
Biogas	0.161	0.913	0.124
Gas	0.12	0.913	0.23

To further explore the potential synergy between building heating (SH and DHW) and cooling (SC) demand and the impact on the economic performance of 5GDHC, we analysed demand scenarios with different heating and cooling demand structure. We define cooling to heating ratio $\varphi_{c:h}$ as total cooling demand (in absolute value) divided by total heating demand. We construct demand scenarios by scaling the cooling demand of the case study from 0% to 400%, in 10% intervals. The heating demands are kept constant. In total, we analysed 41 demand scenarios, where $\varphi_{c:h}$ ranges from 0 to 1.4. In order to closely observe the impact of $\varphi_{c:h}$, we lift the constraint on L_{BHE}^{max} when applying the proposed model to demand scenarios.

4.1.4 Results

4.1.4.1 Design and operation results

In this section, we present the designed capacity of equipment and their operations. For the proposed 5GDHC, the total capacity of BHPs installed in substations is 36.2 MW. Since the low temperature of the cold pipe is sufficient for direct cooling by HX, no chiller is installed in the substations. A thermal network with total length is 15.8 km is designed to connect building substations and BHE fields. In total 13812 BHEs is required as the main energy source. Since there is enough space for borehole drilling in the case study area, no supplemental generation unit is needed. An overview of the 5GDHC design is illustrated in Figure **4.8**.

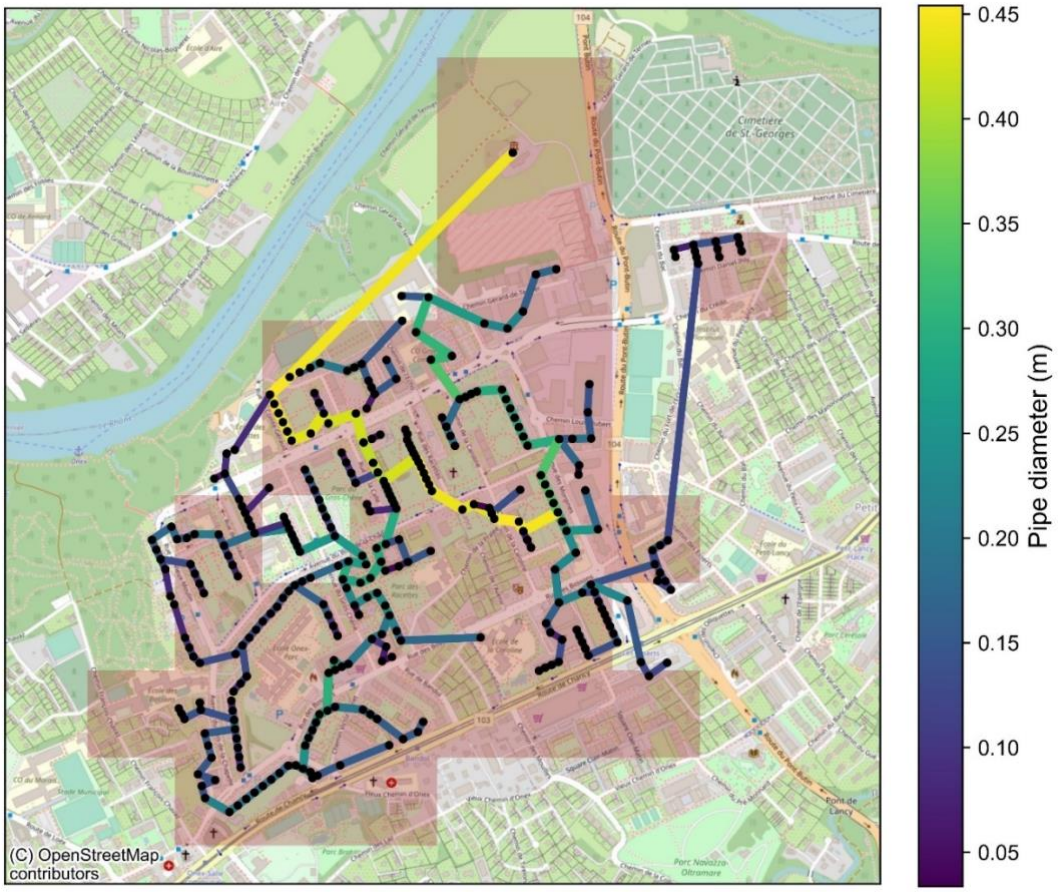

Figure 4.8 - Overview of 5GDHC design. Black dots indicate buildings. Lines indicate thermal network routes, with colour showing pipe diameter. The shaded area indicates pixels where BHEs are installed.

The operation of the installed equipment is modelled. The sources of thermal energy to supply building demands are summarized in Figure **4.9**. BHEs is the largest energy supply. BHEs provides 37.4 GWh of heating and 16.8 GWh of cooling. The direct balancing out of heating and cooling demands is insignificant, which can be explained by the low simultaneity between them.

The direct balancing out happens at building substations and the thermal network, it accounts for 1.9 GWh and 1.0 GWh, respectively. The rest of heating demands is supplied by BHPs, which consumes 14.2 GWh of electricity.

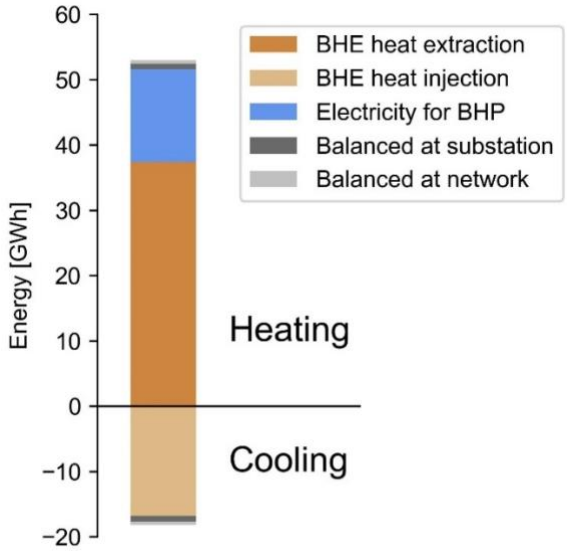

Figure 4.9 - Thermal energy sources of the proposed 5GDHC.

As thermal energy is extracted or injected to the BHE fields, the average temperature of borehole wall fluctuates, as well as T_{wp} and T_{cp}. As plotted in Figure **4.10**, T_{wp} and T_{cp} change between 8-19°C, which is within the designed temperature range.

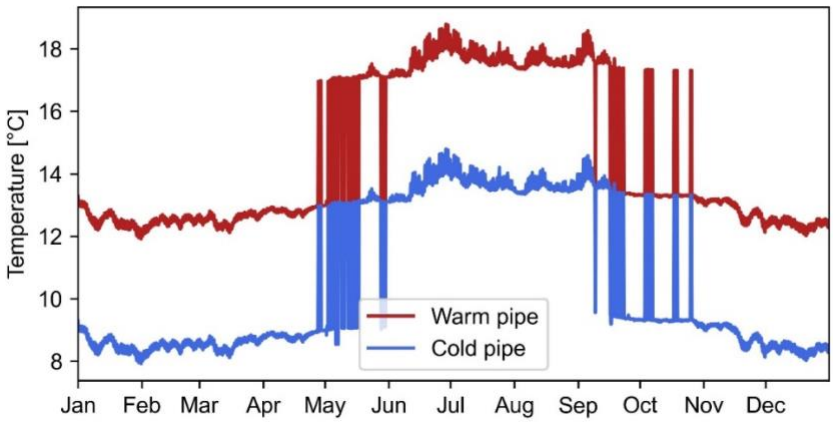

Figure 4.10 - Temperature profile of the thermal network.

The total final energy consumption of 5GDHC and the reference systems are shown in Figure **4.11**. In the proposed 5GDHC, BHPs consume 14.2 GWh of electricity, corresponding to an average seasonal performance factor of 3.7. WCPs consume a minor 1.7 GWh of electricity. In the Electrification option, ASHPs consume 21.3 GWh of electricity and individual chillers consume

3.0 GWh of electricity. The average seasonal performance factor of ASHPs is 2.5. The higher electricity consumption of ASHPs than that of BHPs is due the higher efficiency of BHPs by using BHEs instead of ambient air as the thermal reservoir. In the BAU option, gas boilers consume 59.0 GWh of natural gas. The consumption of individual chillers remains the same as the Electrification option.

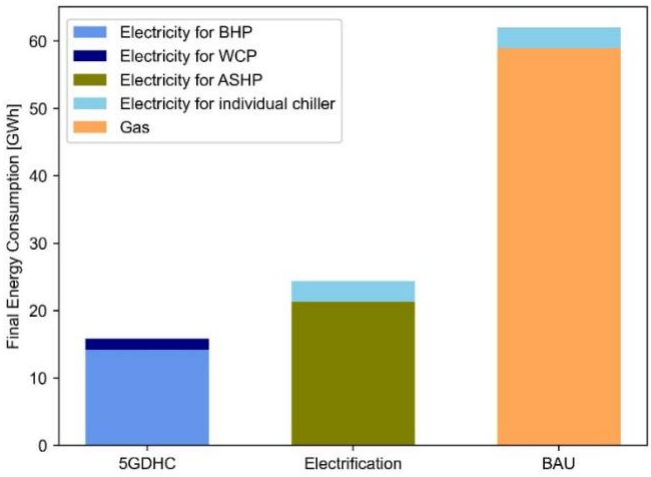

Figure 4.11 - Final energy consumption of 5GDHC compared with the reference systems.

4.1.4.2 Performance evaluation

In this section, we compare the performance of 5GDHC with the reference systems. The evaluated KPIs are summarised in Figure **4.12**. Overall, 5GDHC performs competitively in most aspects, except its considerably higher upfront cost.

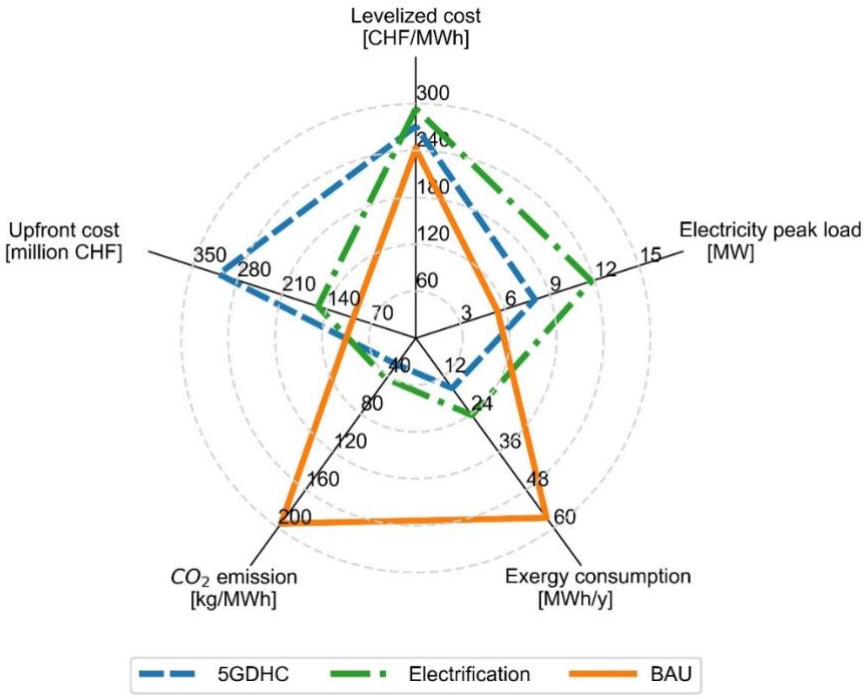

Figure 4.12 - Comparison of KPIs of 5GDHC with reference systems.

In terms of environmental impact, The BAU option shows significantly higher impacts than the 5GDHC and the Electrification option. This is primarily because gas boiler has a low efficiency compared with HPs and that natural gas has a high emission intensity. The greenhouse emission of 5GDHC (28 kg eq. CO_2/MWh) is by one third lower than that of Electrification option (43 kg eq. CO_2/MWh). This can be explained by two factors: 1) BHPs have higher COPs than ASHP, 2) direct cooling only consuming a small amount of electricity to run WCP, much smaller than using individual chillers.

5GDHC performs best from the exergy point of view, since it utilizes the low-temperature thermal energy from BHEs to supply building thermal demands. The BAU option performs poorly due to the substantial exergy waste when high temperature thermal energy from burning natural gas is used.

Electricity peak load relates to the required grid capacity. Since 5GDHC meets building thermal demands with more efficient BHPs and HXs, it has a lower electricity peak load than the Electrification option. The BAU option has even lower electricity peak load, as it does not use electricity to supply building heating demands.

The upfront cost of 5GDHC is substantially higher than that of the reference systems. The breakdown of upfront cost is shown in Figure **4.13**. To build the 5GDHC, 309 million CHF is required. Electrification option costs 153 million CHF, around half of 5GDHC scenario. BAU

option cost only 98 million CHF. It is obvious that BHEs contribute to most, accounting for 83% of total upfront cost. BHPs account for another 14%.

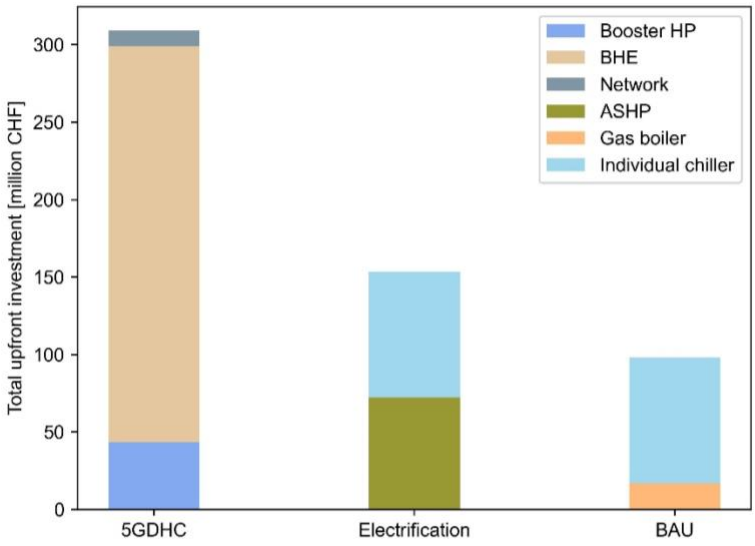

Figure 4.13 - Breakdown of upfront cost.

Although the upfront cost of 5GDHC is high, its levelized cost is comparable to the reference systems. The electrification option has the highest levelized cost of 294 CHF/MWh. 5GDHC has slightly lower levelized cost of 271 CHF/MWh. BAU has the lowest levelized cost of 242 CHF/MWh. The breakdown of levelized cost is shown in Figure **4.14**. The annualized investment cost of 5GDHC is only slightly higher than that of the Electrification option because BHEs have 50 years of service life, much longer than the 20 years of ASHP. Another advantage of 5GDHC is that it has the lowest cost for final energy consumption. Moreover, the low O&M cost of BHEs further adds to the cost competitiveness.

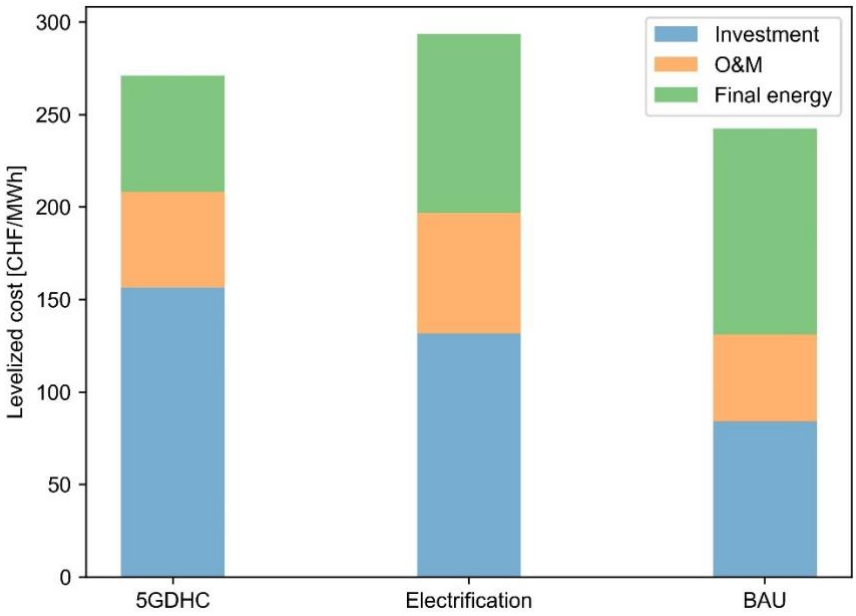

Figure 4.14 - Breakdown of levelized costs.

4.1.4.3 Impact of cooling to heating ratio

In terms of levelized cost, 5GDHC is competitive compared with the reference systems. The main contributing factor is that BHEs unlocks the synergy between heating and cooling demands. In this section, we explore how the cost competitiveness of 5GDHC evolve with changing $\varphi_{c:h}$. The results are presented in Figure **4.15**. The levelized cost of the two reference systems grow unidirectionally as $\varphi_{c:h}$ increase. Interestingly, the levelized cost of 5GDHC show a V shape as $\varphi_{c:h}$ increase. It reaches the lowest value of 221 CHF/MWh at $\varphi_{c:h}$ of 0.48. When $\varphi_{c:h}$ ranges between 0.3 – 1.2, 5GDHC achieves lower levelized cost than the Electrification option. When $\varphi_{c:h}$ falls between 0.4 – 1.0, 5GDHC achieves lower levelized cost than both reference systems.

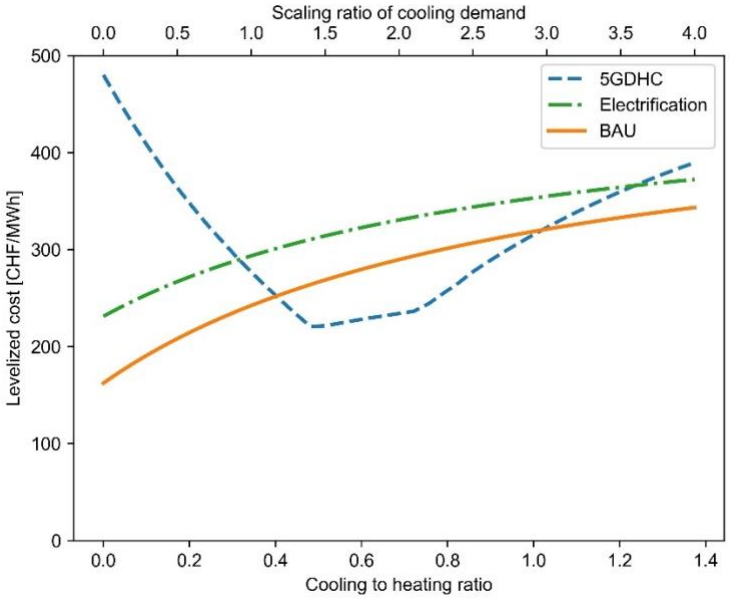

Figure 4.15 - Levelized costs as a function of cooling to heating ratio $\varphi_{c:h}$.

To explain the trend of the levelized cost of 5GDHC, we show the investment cost for BHEs in Figure **4.16**. When $\varphi_{c:h}$ starts from zero, L_h is dominating L_c, meaning the size of BHEs is constrained by long-term ground cooling caused by extraction of heat. As $\varphi_{c:h}$ increases, the waste heat from cooling usage helps to regenerate the ground and thus reduces the required amount of BHEs. L_{BHE} reaches its lowest value when L_c exceeds L_h, corresponding to a $\varphi_{c:h}$ of 0.48. At this turning point, L_c starts to dominate because cooling peak load is larger and there is less room for the ground temperature to increase ($T_{mf,max}$ is closer to T_g than $T_{mf,min}$), although borehole load is still primarily heating demand (extraction of heat). When borehole cooling demand exceeds heating demand, the ground is subject to long-term heating, further pushing up L_c. This explains the faster increasing trend of 5GDHC levelized cost at $\varphi_{c:h}$ of 0.72.

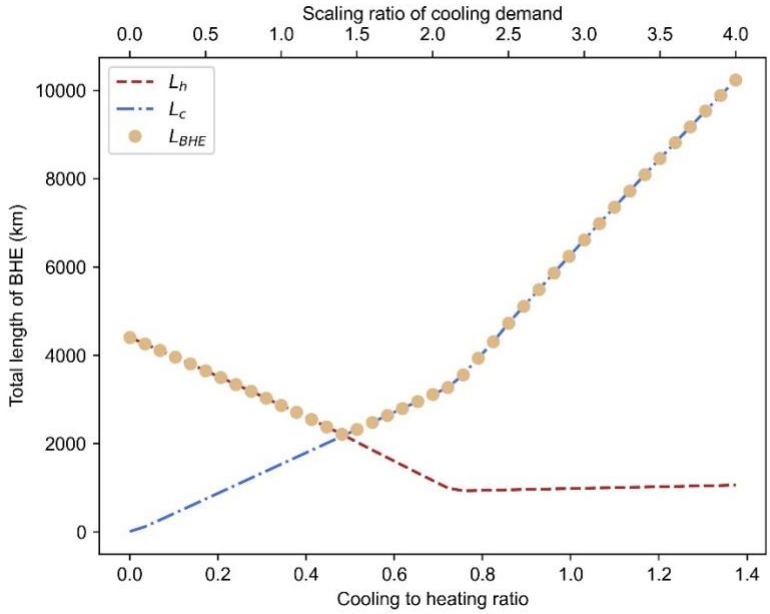

Figure 4.16 - Total length of BHEs as a function of cooling to heating ratio.

4.1.5 Discussion

4.1.5.1 The role of seasonal storage in unlocking synergy between heating and cooling

The results of performance evaluation (see Section 4.1.4.2) demonstrate that BTES is the key promoter of 5GDHC performance. By integrating BHEs as the seasonal thermal energy storage, 5GDHC can reach higher efficiency and lower levelized cost of energy compared with the reference systems. According to [46], when 5GDHC is equipped with no or small storage capacity , the performance of 5GDHC strongly correlates with 'Demand overlap coefficient (DOC)', a measure of overlapping heating and cooling demands in and between buildings: a small value for DOC implies low efficiency and high levelized cost while the opposite is true for high values of DOC. A DOC larger than 0.45 leads to lower cost of energy and higher efficiency in 5GDHC compared to the other two options. In the case study, however, the DOC is only 0.04 since a major part of building heating and cooling demands show a strong seasonality. The low DOC indicates that the saved final energy from direct balancing out of overlapping heating and cooling demands cannot compensate the high investment cost on 5GDHC if no seasonal storage is installed. It is therefore advantageous to add BTES in 5GDHC to realize more synergies between heating and cooling. A large portion of heating demand can be supplied by waste heat from cooling that is stored in summer. Apart from BTES, there are also other types of STES, such as aquifer thermal energy storage and pit storage. Water bodies like lakes and rivers are also

favourable thermal reservoirs for 5GDHC. A further study could assess the potential of alternative thermal energy sources to reduce the cost of 5GDHC.

4.1.5.2 Strategic implications in planning 5GDHC

According to the case study, 5GDHC combined with BTES achieves lowest levelized cost for a wide range of cooling to heating ratios of 0.4 - 1.0. This result highlights the broad applicability of 5GDHC when used for combined heating and cooling purpose. In today's residential buildings, however, the energy demand is primarily heating and usually the cooling to heating ratio is below this optimal range. Adequate BHE capacity for heating would be oversized for cooling, meaning that the benefit of seasonal storage is not fully realized. Nevertheless, a more balanced heating and cooling structure which ensures sufficient borehole regeneration in the long-term could be realized by i) connecting other constructions that generally have large cooling requirement, such as data centres, hospitals, and offices, ii) by making better use of available waste heat like industrial excess heat and iii) by installing solar thermal collectors [55]. Furthermore, building retrofitting and climate change impact can increase the share of cooling demand in building energy demands [257]. All these aspects indicate that there will be increasing opportunities for 5GDHC.

4.1.5.3 Future market potential

As shown in the results, the high upfront cost of borehole drilling and heat pump installation is an economic barrier to investing in 5GDHC. However, according to [258], both ASHP and GSHP (water-source heat pump combined with BHEs) have a high potential for cost reduction, as they are in relatively early stages of market growth. Gas boilers, however, have limited cost reduction potential, given their high market volume by now. It is estimated that by 2050, the specific cost of ASHP will decrease by 29%, GSHP decrease by 20%, Gas boiler decrease only by 8% [258]. If the potential of efficiency improvement is further taking into account, both 5GDHC supplied by BHEs and stand-alone heat pump systems have a great potential in decarbonizing future thermal energy systems.

Another reason for considering 5GDHC combined with BHEs is that it improves the energy self-sufficiency of the district by facilitating the use of local energy sources, such as geothermal heat, waste heat, etc. Such a system would depend less on imported energy sources (e.g., gas, electricity) and would thus be less vulnerable to fluctuations in energy market prices.

4.1.5.4 Limitations and future work

This work is subject to several limitations, with one main limitation concerning the simulation of energy performance of geothermal borehole fields utilizing analytical finite line source solution. This modelling approach is essential to facilitate the scalability of our proposed

5GDHC model. Ongoing efforts are focusing on the development of a dynamic system model for 5GDHC coupled with BTES based on Modelica [259], aiming to achieve a more comprehensive understanding of 5GDHC dynamics and performance. In this study we focus on the impact of cooling to heating ratio on the performance of 5GDHC. Hence, we keep other parameters constant, such as heat pump efficiency, temperature requirement, cost of equipment, discount rate, energy prices, etc. They are main sources of uncertainty in the 5GDHC model. Further research is necessary to establish a better understanding of the potential impact of uncertainties on the competitiveness of 5GDHC. Another drawback of this study is that when comparing the proposed 5GDHC with the reference systems, the embodied emission of equipment is not considered. Research on the life cycle assessment of 5GDHC is encouraged to justify the feasibility of 5GDHC to supply low-carbon thermal energy.

4.1.6 Conclusion

This paper investigates the potential of integrating 5GDHC with BHEs to decarbonise future thermal energy systems. A novel model is developed for designing and evaluating 5GDHC combined with BTES in respect to levelized cost of energy, upfront cost, greenhouse gas emission, exergy efficiency, and the electricity peak power. The performance of 5GDHC is assessed against two alternatives: the Electrification option (electricity driven heat pump systems) and the BAU option (traditional gas boilers and compression chillers). The proposed model is demonstrated on a case study of 305 buildings in a dense residential district.

We demonstrated that 5GDHC with BHEs can achieve lower levelized costs of energy, less greenhouse gas emission, higher exergy efficiency, and lower electricity peak load compared to decarbonisation of heat through individual heat pumps/air conditioning units in each building (electrification scenario) in the case study area. Our results demonstrated that the cooling to heating ratio substantially influences the economic performance of 5GDHC with BHEs, with it being the most cost competitive option when cooling to heating ratio is within the range of 0.4 - 1.0. Levelized costs can be up to 30% lower compared to the Electrification option and up to 19% lower compared to the BAU option with gas boilers. This is enabled by a long-term thermal equilibrium of the ground (in terms of heat extraction and injection) when used for balanced heating and cooling demands.

Our results underscored the benefits of integrating BTES to 5GDHC as a seasonal storage, creating a synergy between heating and cooling demands despite the low simultaneity between them. In effect summer cooling loads become a thermal resource for supplying winter cooling needs and the installed capacity of BHEs is fully exploited for both heating and cooling purpose. Stable ground temperatures maximise the efficiency of heat pumps driving the system, resulting in less final energy consumption and reduced greenhouse gas emissions.

We highlighted that the main barrier of adoption is high upfront cost from borehole drilling and BHP installation, even though the long service life and low maintenance needs allow to achieve a competitive levelized cost of energy. Given the attractiveness of the technology, policies should therefore address upfront costs for example through subsidies or measures to promote technical learning and cost reductions for borehole and HP.

The proposed model may be applied for the early planning stage of 5GDHC in candidate areas. It can further be utilized to carry out techno-economic analysis to identify the best suited future thermal energy systems. This work is being applied in the context of a technology transfer project to make use of previously generated data for all of Switzerland [160] to support energy suppliers in exploring of the potential of 5GDHC with BTES, helping to realize Switzerland's energy strategy for 2050. Another research direction is to better understand the role of other impact factors, such as temperature control and alternative renewable energy sources in improving the competitiveness of 5GDHC.

5 Applicability of 5GDHC

Research question 4: What are the main factors that influence the applicability of 5GDHC integrated with shallow geothermal energy?

To answer this question, I investigated the broader applicability of 5GDHC when integrated with BTES under uncertainty, especially in the context of rising cooling loads relative to heating due to climate change. To systematically assess the impact of uncertainties, a variance-based global sensitivity analysis is conducted. This analysis allows to rank the uncertain parameters based on their impact on the economic performance of 5GDHC. Furthermore, factors mapping is performed to determine the specific parameters responsible for driving 5GDHC's superior economic performance compared to the reference systems.

I have prepared one conference paper based on this work, which was presented at CISBAT 2023: the built environment in transition - Energy Efficiency & Renewables in the Digital Era, Lausanne, 13-14 September 2023.

Conference paper 3:

Xiang Li, Jonathan Chambers, Selin Yilmaz, and Martin K. Patel. "Sensitivity Analysis of Fifth Generation District Heating and Cooling Coupled with Borehole Thermal Energy Storage with Respect to Cooling Adoption." *Accepted by Journal of Physics: Conference Series*.

5.1 Sensitivity analysis of fifth generation district heating and cooling coupled with borehole thermal energy storage with respect to cooling adoption

5.1.1 Introduction

Decarbonising the heating and cooling sector is a crucial component of the European Union's strategy to achieve climate neutrality by 2050 [2]. In recent years, a new type of bi-directional network for simultaneous heating and cooling is emerging, named as fifth generation district heating and cooling (5GDHC) [35]. Previous studies [240,241] have focused on optimal design of 5GDHC for specific cases with balanced heating and cooling demands, which creates favourable conditions for 5GDHC development. However, they often overlook the diverse conditions encountered in more general case [260]. These uncertainties poses both challenges and opportunities for the development of 5GDHC. Specifically, our interest lies in exploring the potential opportunities for 5GDHC development arising from the growth in space cooling demands [46], fluctuation in prices [234], and advancements in technology [10]. This paper aims to address the following research questions: 1) How much is the 5GDHC performance affected by uncertainty? 2) Which parameters have the greatest impact on the economic performance of 5GDHC? 3) When does 5GDHC outperform its alternatives?

5.1.2 Methods

The proposed framework starts by introducing a model for designing and evaluating 5GDHC. Subsequently, studied uncertain parameters in the 5GDHC model are described. Finally, sensitivity analysis is performed to prioritize the model parameters by their influence and to test the robustness of the 5GDHC performance. The framework is demonstrated on a case study of a densely populated district in the Canton of Geneva, Switzerland, with a total floor area of 1.05 km^2.

5.1.2.1 5GDHC model

The 5GDHC model is presented in detail in [261]. The 5GDHC consists of three main components: 1) building substations equipped with booster heat pumps (BHP) for heating and heat exchangers for direct cooling, 2) a 2-pipe thermal network operating within a range of 4°C - 21°C, and 3) borehole thermal energy storage (BTES) that supply the thermal demands after compensation of simultaneous heating and cooling demands. The performance of the designed 5GDHC is evaluated in terms of economic, technical, and environmental indicators and compared to two reference systems. The first reference system, the Electrification option,

represents stand-alone building substations with air-source heat pumps (ASHP) and chillers. The Business-As-Usual (BAU) option represents present-day building substations with gas boilers and chillers.

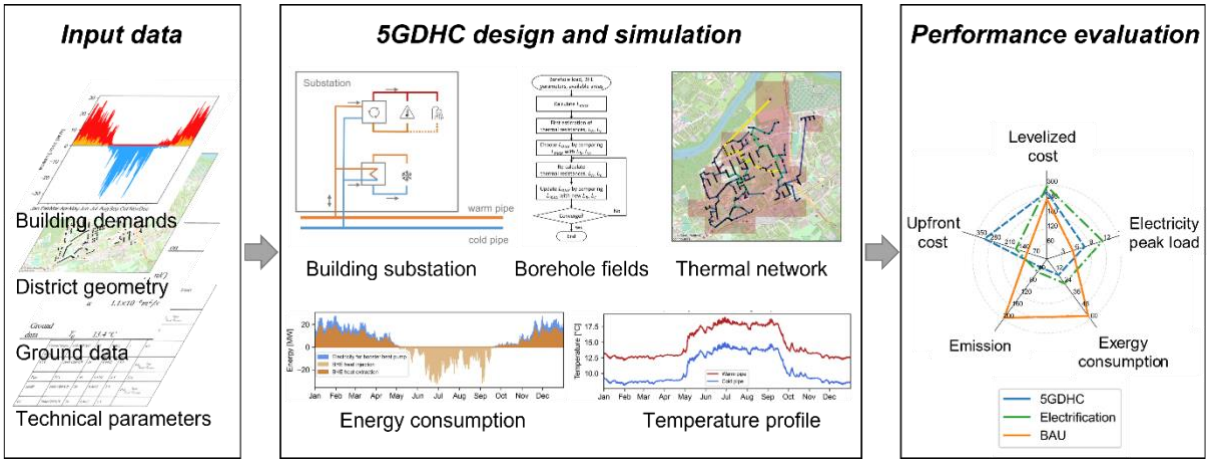

Figure 5.1 - Overview of the 5GDHC model.

5.1.2.2 Uncertainty analysis

This study investigated the impact of uncertainties in demand profiles, cost and emission of final energy, equipment costs, and equipment efficiencies. The probability distributions of uncertain parameters are summarized in Table **5.1**. In order to capture the growth in cooling demand, specifically the proportion of heating demands to cooling demands, we consider the cooling adoption rate from 0% to 100%. This variation represents the transition from negligible cooling demands in the present to fully cooled districts in the future. Other parameters are modelled by adapting the approach in [262]. To assess the level of uncertainty in the key performance indicators (KPI) of 5GDHC, Monte Carlo (MC) simulation is conducted. Sobol low discrepancy sequences are used to generate 2048 samples of each uncertain parameter, which were then fed into the 5GDHC model to obtain the KPIs of 5GDHC and the reference systems.

Table 5.1 - Probability distribution of input parameters.

Uncertain parameter	Symbol	Probability distribution
Cooling adoption rate	p_c	$U(0\%, 100\%)$
Carnot effectiveness[1] of BHP	$\eta_{CE,BHP}$	$0.5 * N(1, 0.2)$
Carnot effectiveness of ASHP	$\eta_{CE,ASHP}$	$0.4 * N(1, 0.2)$
Efficiency of gas boiler	η_{boiler}	$0.9 * N(1, 0.2)$
Price of electricity [CHF/kWh]	P_{elec}	$0.283 * U(0.5, 1.5)$
Price of gas [CHF/kWh]	P_{gas}	$0.120 * U(0.5, 1.5)$
Emission factor of electricity [kg CO_2/kWh]	EM_{elec}	$0.125 * U(0.5, 1.5)$
Unit price of BHP [CHF/kW]	P_{BHP}	$1200 * N(1, 0.2)$
Unit price of BHE [CHF/BHE]	P_{BHE}	$18500 * N(1, 0.2)$
Scale factor of pipe cost	SF_{pipe}	$N(1, 0.2)$
Price of ASHP [CHF/kW]	P_{ASHP}	$2000 * N(1, 0.2)$
Price of chiller [CHF/kW]	$P_{chiller}$	$2000 * N(1, 0.2)$
Price of gas boiler [CHF/kW]	P_{boiler}	$470 * N(1, 0.2)$
O&M[2] factor of BHP [%]	OM_{BHP}	$2.5 * N(1, 0.2)$
O&M factor of BHE [%]	OM_{BHE}	$0.5 * N(1, 0.2)$
O&M factor of pipe [%]	OM_{pipe}	$1.0 * N(1, 0.2)$
O&M factor of ASHP [%]	OM_{ASHP}	$3.5 * N(1, 0.2)$
O&M factor of chiller [%]	$OM_{chiller}$	$2.5 * N(1, 0.2)$
O&M factor of gas boiler [%]	OM_{boiler}	$3.0 * N(1, 0.2)$
Discount rate [%]	r	$U(0, 5)$

[1]Equels the efficiency of BHP divided by the Carnot efficiency.
[2]Operation and maintenance.

5.1.2.3 Global sensitivity analysis

We focus on identifying the most important parameters influencing the upfront cost and levelized cost of energy of 5GDHC, since they are the main barriers for 5GDHC adoption. Sobol analysis [263], a variance-based global sensitivity analysis technique, is used to decompose the variance of model output into contributions from uncertain parameters and their interactions. We calculate the first-order Sobol indices, which quantify the effect of each parameter alone, and total-order Sobol indices, which measures the variance caused by each parameter, including interactions with other parameters. This approach requires 22,000 MC runs.

5.1.2.4 Factors mapping

The objective of factors mapping is to determine the parameters responsible for 5GDHC's superior economic performance compared to the reference systems. Monte Carlo filtering (MCF) [264] has been performed by following these steps: 1) we define a criterion as '5GDHC has lower levelized cost of energy than the alternative'; 2) we divide all MC runs into two subsets based on this criterion; 3) we conduct two-sample Kolmogorov-Smirnov (K-S) [265] tests to compare the probability distributions of each parameter in the two subsets.

5.1.3 Results

5.1.3.1 Variation in 5GDHC performance

Figure **5.2** illustrates the variation in KPIs of 5GDHC and the reference systems. The levelized cost of energy of 5GDHC ranges from 170 to 430 CHF/MWh (5^{th} and 95^{th} percentiles), with approximately half of the MC runs indicating a smaller levelized cost of energy than the Electrification option, while only one-third of the cases indicate that 5GDHC outperforms the BAU option. The upfront cost of 5GDHC ranges from 150 – 610 million CHF, which is substantially larger than the reference systems. Borehole heat exchangers (BHE, which constitutes BTES) and BHP contribute the most. In contrast, 5GDHC show better results in terms of environmental and technical performance. In the majority of MC runs, 5GDHC results in fewer emissions and less exergy consumption than the reference systems. This can be attributed to the higher efficiency of heat pumps when connected to a low-temperature energy source from BTES. Although the BAU option typically has the lowest electricity peak load, 5GDHC generally reduces the electricity peak load when compared with the Electrification option.

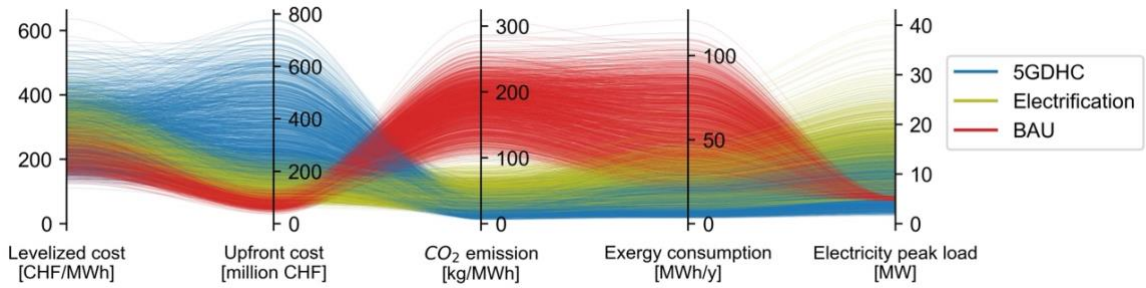

Figure 5.2 - Variation of KPIs of 5GDHC and the reference systems based on the MC runs.

5.1.3.2 Sources of uncertainty

The results of Sobol analysis for the economic indicator ratio between 5GDHC and the Electrification option are presented in Figure **5.3**, showing the three most important parameters.

Starting with the comparison of upfront cost, cooling adoption rate is the most influential parameter, as it is closely related to the total building energy demand and therefore the required capacity of device. It is followed by the price of BHE and ASHP. BHE is the largest contributor to the upfront cost of 5GHDC, while ASHP is the largest contributor in the Electrification option. It's worth mentioning that the scaling factor of pipe cost has insignificant impact on the total investment cost. These influential parameters also have the greatest impact on the levelized cost of energy, as annualized investment cost outweighs fuel and O&M costs in 5GDHC. In addition, discount rate is influential in determining the annualize factor for investment cost. Parameters related to fuel and O&M costs, such as equipment efficiency and O&M cost, have less impact.

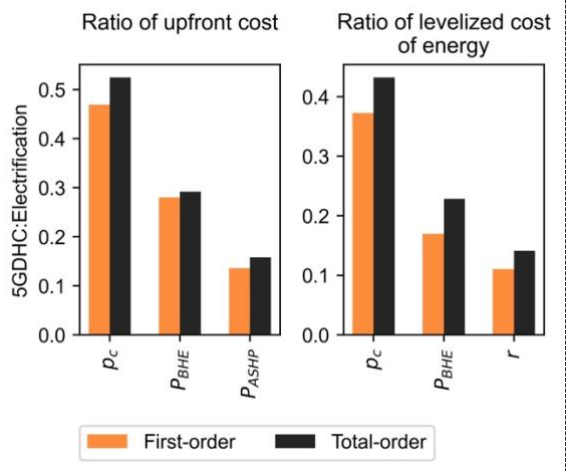

Figure 5.3 - Sobol indices for the ratio of economic indicators between 5GDHC and the Electrification option.

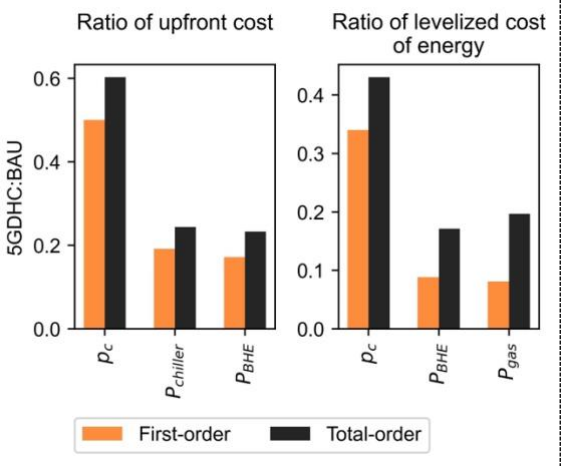

Figure 5.4 - Sobol indices for the ratio of economic indicators between 5GDHC and the BAU option.

Figure **5.4** presents the Sobol analysis results of the economic indicator ratios between 5GDHC and the BAU option. The results reveal that cooling adoption rate and equipment price are the most significant sources of uncertainty in comparing economic performance indicators. In addition, price of gas also ranked high as the fuel cost holds the largest share of the levelized cost of energy in the BAU option.

5.1.3.3 Critical parameters driving 5GDHC adoption

Figure **5.5** and Figure **5.6** present the critical parameters that determine whether 5GDHC outperform the reference systems economically. These parameters largely coincide with the most influential parameters identified by the Sobol analysis. However, with the results of factor mapping, we can analyse how these parameters affect the relative attractiveness of 5GDHC. When cooling adoption rate falls in the range of 0.4-0.9, 5GDHC is more likely to outperform

the reference systems from a cost perspective. This is attributed to the fact that maintaining an appropriate ratio of cooling to heating demands facilitates an optimal regeneration of the ground, making it favorable for the use of BTES. Lower BHE price also benefits the adoption of 5GDHC. However, a high discount rate is unfavorable for 5GDHC, as it weakens the benefit of reduced fuel cost over time. Furthermore, high gas prices will drive the shift from the BAU option to 5GDHC.

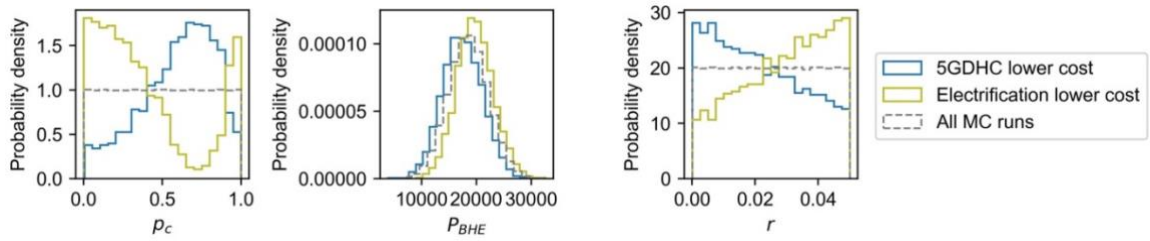

Figure 5.5 - Probability distribution of critical parameters that result in lower levelized cost of 5GDHC than the Electrification option.

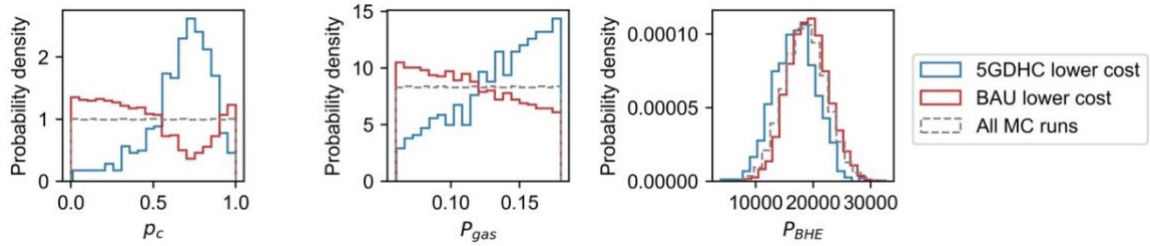

Figure 5.6 - Probability distribution of critical parameters that result in lower levelized cost of 5GDHC than the BAU option.

5.1.4 Discussion

The results indicate significant uncertainty in the relative performance of 5GDHC. The attractiveness of 5GDHC is closely linked to the cooling adoption rate, which affects the balance between cooling and heating demands. 5GDHC is a promising technology for combined heating and cooling and could realize potential synergies between them. Gas significantly impacts the economic performance of the BAU option, however its uncertainty is more difficult to address than other sources of uncertainties in 5GDHC, such as equipment price. Adopting 5GDHC has the potential to reduce uncertainty in energy costs. All these aspects indicate growing opportunities for 5GDHC.

Several factors that could potentially impact the results of the case study have not been addressed in this study. The uncertainty associated with building energy demands due to climate change has not been considered. Additionally, the partial load efficiency of heat pumps has not

been accounted. To offer more reliable suggestions for decision-makers, further investigation is needed to address these factors more comprehensively.

5.1.5 Conclusion

Sensitivity analysis is employed in this study to evaluate a model for designing and evaluating 5GDHC coupled with BTES. The proposed workflow integrates MC simulation, Sobol analysis, and MCF to investigate the performance of 5GDHC in general cases and factors driving its economic attractiveness. The results demonstrate that accounting for uncertainty is crucial when designing 5GDHC, as it can result in significant variations in its performance. Furthermore, the study highlights cooling adoption rate, price of equipment, and discount rate as the most influential parameters, which significantly influence the economic performance of 5GDHC. The proposed method can be used to assess the effectiveness and competitiveness of alterative thermal energy systems by considering relevant uncertainties, thus assist in identifying attractive options for decarbonising the thermal energy sector.

6 Conclusions

This chapter presents the conclusions of the thesis, summarising its contributions to the knowledge gap (Section 6.1) and the methodological contributions (Section 6.2). The chapter further presents the policy implications derived from the findings (Section 6.3). Finally, recommendations for future research are provided (Section 6.4).

6.1 Contribution to the knowledge gap

This thesis presents significant contributions to addressing the knowledge gaps. It contributes to a spatially detailed mapping of future cooling demand and its main drivers. Furthermore, it has evaluated the potential role of DHC and shallow geothermal energy in meeting this rising cooling demand alongside heating demand. The contributions of this thesis are presented and summarised in alignment with the four research questions addressed in the previous chapters:

6.1.1 To what extent will the cooling demand of the Swiss service sector increase, and what are the main drivers of this increase?

A data-driven Monte Carlo model of the building stock is developed and applied in order to investigate RQ1 under IPCC climate scenarios for 2050. The space cooling demand in the Swiss service sector with the current adoption of cooling systems of 9% based on the cooling permits is 900 ± 200 GWh/year in 2015. Considering the increasing adoption of cooling systems and cooling energy intensity due to climate change, as well as changes in the dynamics of the building stock, I estimate that space cooling will increase to 4100 ± 300 GWh/year (+ 400%) in RCP 2.6, 5300 ± 400 GWh/year (+ 500%) in RCP 4.5, and 6000 ± 500 GWh/year (+ 600%) in RCP 8.5 by 2050. The analysis further highlights that it is the increase in saturation rate (+ 180-200%) that is the most significant driver of the growth in space cooling demand which refers to the adoption of cooling triggered by climate change. It is followed by the increase in total service area (+ 35%) due to construction of new buildings and cooling energy intensity (+ 30-70%) due to the warming climate.

6.1.2 What are the technical potentials of shallow geothermal energy usable by DHC?

To answer RQ2, a novel framework is proposed to investigate and quantify the technical potential of shallow geothermal energy. In this framework, the spatial allocation of the shallow geothermal energy is addressed in more detail, taking into account the spatial constraints in scenarios for DHC and for direct heat exchange (No DHC. Shallow geothermal energy is only supplied on-site building). Additionally, seasonal regeneration of boreholes by waste heat from space cooling is addressed to investigate synergetic use of boreholes for combined heating and cooling in a district network. The framework is applied to a case study in western Switzerland, specifically the Geneva and Vaud canton, to estimate the shallow geothermal potential for both heating and cooling. I found that the utilization of DHC significantly improves the useful potential by allowing the integration of surplus thermal energy in neighbouring areas as potential supply sources of the DHC. Results show that if DHC is employed, the useful geothermal potential may cover up to 87% of service-sector cooling demand and up to 85% of heat demand in 2050, which decreases to 71% and 55% for direct heat exchange when DHC is not employed. The findings revealed that using the excess heat from space cooling for seasonal regeneration of ground may significantly reduce thermal interference between boreholes. This allows to increase the maximum technical geothermal potential density from 15 kWh/m² without heat injection to above 300 kWh/m² in pixels with heat injection densities above 330 kWh/m².

6.1.3 What is the technical and economic performance of a 5GDHC integrated with shallow geothermal energy?

When addressing the RQ3, I take an energy system modelling approach and conduct a techno-economic analysis of the performance of the 5GDHC system supplied by shallow geothermal based on 5 KPIs (namely levelized cost of energy, upfront cost, CO_2 emission, exergy efficiency, and electricity peak load) in a case study in Geneva**.** In this system I considered integrating the borehole heat exchanger (BHE) in 5GDHC which can serve as both the thermal energy source and the seasonal thermal storage to explore synergy for combined heating and cooling. This is referred to as borehole thermal energy storage (BTES). I bring attention to the benefit of 5GDHC with BTES in the context of balanced yet asynchronous heating and cooling loads and assess future prospects with regards to increasing cooling load relative to heating, which is likely to occur due to climate change and increased demand for thermal comfort. The findings reveal that indeed thanks to the fact that 5GDHC integrated with BTES facilitates the seasonal balancing of heating and cooling demands, this leads to lower levelized cost of energy (272 CHF/MWh vs. 294 CHF/MWh), less greenhouse gas emission (28 kg CO_2 eq./MWh vs. 43 CO_2 eq./MWh), less

exergy consumption (16 MWh/y vs. 24 MWh/y), and lower electricity peak load (8 MW vs. 12 MW) compared to the stand-alone heat pump system that is being currently considered in districts. However, the higher upfront cost of 5GDHC integrated with BTES (309 million CHF vs. 153 million CHF), mainly attributed to BHE drilling and heat pump installation, might be a barrier to the adoption of such systems. It is therefore very important for decision-makers and investors to highlight the sustainable environmental benefits and operational savings over the system's long lifecycle under climate change, rather than solely focusing on the substantial upfront investment.

6.1.4 What are the main factors that influence the applicability of 5GDHC integrated with shallow geothermal energy?

Sensitivity analysis was employed to answer the question of what main factors influence the applicability of 5GDHC with BTES. This analysis contributes to advance knowledge and understanding on the performance of 5GDHC with BTES across a range of conditions, including adoption rates where multiple configurations come out in different districts. This analysis revealed significant variations in the performance of 5GDHC with BTES. The cooling adoption rate emerged as the most influential parameter affecting its economic performance, followed by the price of equipment, and discount rate. I point out that when the cooling adoption rate is in the range of 0.4-0.9, 5GDHC with BTES is more likely to outperform other alternative systems such as stand-alone heat pump system and traditional gas-driven systems from a cost perspective, again underscoring the wide applicability of such system for cooling and heating combined. This is attributed to a long-term equilibrium of the ground when used for well-balanced heating and cooling demands. An important finding is that a low discount rate is favourable for 5GDHC as it strengthens the benefit of operational savings over time. This implies that low-interest loans can help to reduce the financial risk of investment in 5GDHC projects.

6.2 Methodological contribution

In addition to the contribution to the body of empirical research, this study also aimed to improve methods of district heating and cooling system modelling to make it become a practical tool in the decision-making process. This has been achieved by the completion of development of modelling frameworks to consider under-researched spatial and temporal aspects, and methodological enhancements for integration of techno-economic assessment. These methodological enhancements encompass the capability of DHC models to be reflective of reality, their scalability to larger-scale applications and the speed of the model whilst providing a comprehensive evaluation for making better informed planning decisions.

To estimate the space cooling demand at building level, I have introduced a data-driven Monte Carlo model of the service building stock based on empirical cooling data (chapter 2.1). When predicting the presence of space cooling equipment, the model takes a bottom-up approach and integrates a logistic regression to take into account building characteristics and climate conditions. This offers a more accurate estimation of the diffusion of space cooling equipment under climate change, advancing the capabilities of building energy demand modelling in future. While the model was applied to Swiss building stock in this study, the bottom-up approach makes it possible to apply to national building stocks of other countries with comparable social and economic conditions, in case of paucity of required data.

A scalable methodology to consider efficient allocation of resources subject to spatial constraints was under-developed. In this thesis, I have proposed a spatial allocation with optimisation (SAO) method that integrates geospatial data pre-processing, a graph theory-based cluster partition technique, and an optimal allocation algorithm adapted from transportation theory (Chapter 3.1). The SAO addresses the shortcoming of lack of scalability of previous methodologies and enhances the applicability of these methodologies to large-scale problems by disaggregating the large-scale problem into smaller units through graph theory. The computational efficiency allows for it to be broadly applied, due to the lower computational power needed and the potential of automated analysis. The SAO method further improves the accuracy in computing allocable resources in comparison to a reference model without optimisation, allowing to avoid planning errors in systems design for districts and cities. This was a shortcoming of the previous research, which has led to overestimation of the potential of energy resources. The developed SAO method is applicable to the allocation of diverse geospatially bounded resources, such as industrial excess heat and geothermal energy which were shown as the two applications in this thesis as well as other resources such as lakes and rivers as thermal reservoirs.

By expanding upon the SAO method, I further propose a modelling framework to quantify the potential of shallow geothermal for DHC (Chapter 3.2) which is capable of representing seasonal regeneration through re-injection of waste heat from space cooling. This enables accounting synergies between heating and cooling usage of shallow geothermal in a consistent manner and therefore accurately estimates the improved potential of shallow geothermal.

I propose a comprehensive modelling framework that integrates the spatial-temporal analysis of DHC systems and techno-economic assessment, providing a full output of cost and environmental performance indicators (Chapter 4.1). This integration not only advances the understanding of local context and temporal variations within the context of DHC systems but also provides a fast evaluation of their feasibility and economic viability. These outputs provide essential information for the early stage of DHC design and planning in different sites with spatial and technical and economic characteristics. This leads to holistic perspectives that may not be achievable through single-discipline methods.

6.3 Policy implications

To achieve Switzerland's pledge of climate neutrality by 2050, current energy policy focuses on abating emissions from space heating and hot water since it currently dominates the total energy consumption [13]. Little attention has been paid to cooling demand in the energy policy framework compared with heating, despite concerns about projections of warming temperature and more frequent and more intense heatwaves [100]. This work highlights a rapid growth of space cooling demand in the Swiss service sector in the coming decades, especially in cantons with insignificant space cooling demand today (Chapter 2). Therefore, it is essential for policy makers to incorporate the decarbonisation of cooling when formulating long-term energy strategies for meeting climate-neutral targets. The government should propose stronger measures to regulate the use of air conditioners in advance and to promote passive cooling and renewable-based cooling solutions. An example of good practices is the Green Mark Scheme implemented in Singapore, which assess the environmental performance of buildings including cooling systems [266]. This scheme incentivises the adoption of energy efficient solutions for cooling, such as solar-driven cooling systems and district cooling.

Shallow geothermal energy and 5GDHC are identified by this thesis as the key solutions to unlock the synergistic effects of combined heating and cooling. My study found that there is a huge potential for shallow geothermal for both heating and cooling. When excess heat from cooling application is used to regenerate the ground, such systems provide two-fold benefits: the shallow geothermal offers increased potential for heating while cooling demand is met through renewables (Chapter 3). Despite its substantial potential for both heating and cooling, shallow geothermal remains under-exploited. To promote the utilisation of this potential, high-resolution datasets and maps of shallow geothermal potential should be available to different stakeholders such as municipalities, utility companies, and the public.

The integration of shallow geothermal significantly enhances the efficiency of DHC. I compared the KPIs of 5GDHC combined with BTES to alternative decarbonisation scenarios. Remarkably, 5GDHC with BTES provide stable environmental benefits and reduction in operation costs, outweighing the high investment costs in the construction stage (Chapter 4). Policy measures such as subsidy programmes offsetting the financial barrier of high upfront cost should therefore be introduced to encourage investment in DHC projects, in light of their long-term benefits.

I further show that 5GDHC integrated with BTES is a promising solution especially in areas with a mixed heating and cooling demand (Chapter 5). Although space cooling is rarely considered with the current climate, heating demand and cooling demand will become more and more balanced with climate change, indicating growing opportunities for 5GDHC. Another important practical implication is therefore that policy makers should support pilot and demonstration

(P&D) projects in order to gain knowledge and insights from experience through measures such as local innovation funds.

In summary, the future deployment of DHC based on shallow geothermal energy requires comprehensive policies and regulations to support awareness-building initiatives, financial incentives, workforce development, and continued research and development. As the benefits of these systems become more widely recognised, it is possible that they become an integrated part of the future sustainable energy system.

6.4 Future research

Building upon the work presented in this thesis, several directions for further research are identified.

Currently, a pilot and demonstration (P&D) project is underway in real-life conditions to validate the performance of the 5GDHC based on shallow geothermal energy as a solution for building heating and cooling. During the initial phase of the P&D project, the methods and tools developed in this thesis will be applied to assess the feasibility of the system. The implementation phase will include installation, operation, monitoring, and benchmarking to confirm the capability of the system to meet sustainability goals. This project is expected to provide deeper insights into critical aspects such as system integration, economic viability, social acceptance, and regulatory challenges. The successful implementation of this project can potentially serve as a case study to encourage the widespread adoption of such systems.

Future work could aim to investigate the geographical distribution of future heating and cooling demands, and to identify potential areas that are suitable for the development of 5GDHC on a large-scale (e.g., across Europe). Such an investigation should consider factors like climate change, building retrofits, and urbanisation, etc. By employing the assessment framework proposed in this thesis on a broader scale, typical conditions can be summarised for areas where the combination of heating and cooling demands are promising for successful 5GDHC deployment.

Another potential direction for future research is the exploration of sector coupling. Heat pump is an integral part of 5GDHC, presenting an opportunity to couple the thermal sector with the power sector. Integrated thermal storage within 5GDHC could potentially reduce the need for battery storage for storing surplus electricity generation from volatile renewable sources, e.g., solar and wind energy, thus facilitating renewable and decentralized electricity generation.

Appendix A Estimation of Space cooling demand

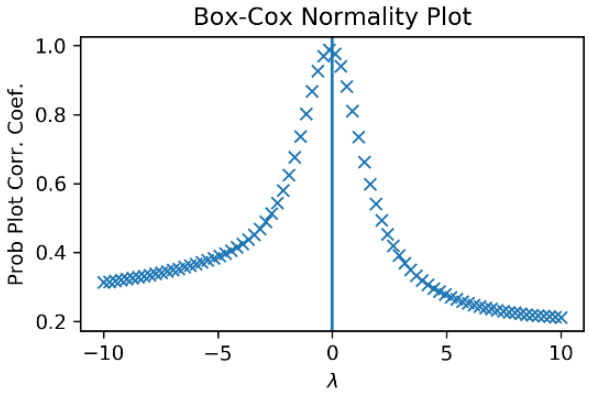

Figure A.1 - The Box-Cox normality plot of cooling power intensity.

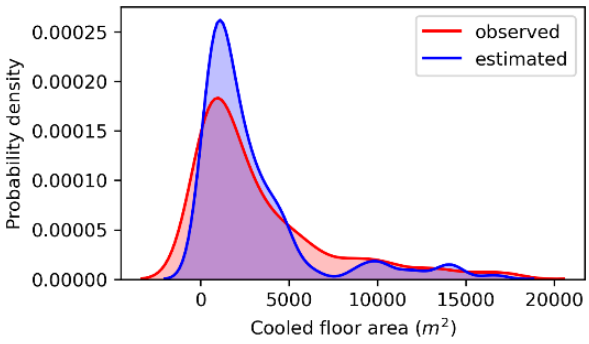

Figure A.2 - Comparison of the kernel density estimate (KDE) of the probability distributions of observed and simulated cooled floor area in office buildings in Geneva.

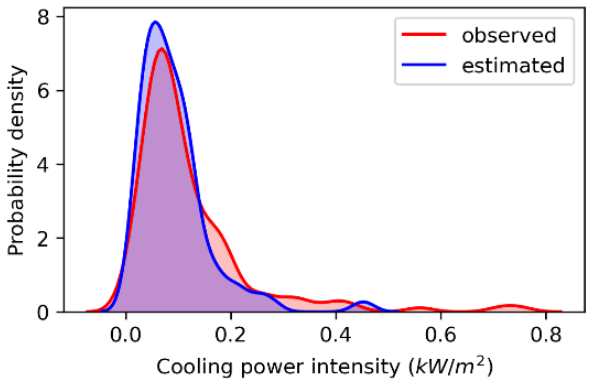

Figure A.3 - Comparison of the kernel density estimate (KDE) of the probability distributions of observed and simulated cooling power intensity in office buildings in Geneva.

Appendix B Availability of shallow geothermal energy

B.1 Heating and cooling degree days

The heating and cooling degree days (HDD/CDD) are computed from daily mean ambient temperature (T_{amb}) [64]. For HDD, we use the formula provided in the Swiss norm SIA 2028 [217]:

$$HDD = \sum_{d=1}^{d_m} \left(20°C - T_{amb}(d,m)\right) \quad \forall T_{amb}(d,m) \leq 12°C \qquad (B.1)$$

where d, m denote the day and month and d_m is the number of days in each month. As no Swiss norm exists for CDD, we obtain the CDD from [64] using a reference temperature of 18°C:

$$CDD = \sum_{d=1}^{d_m} (T_{amb}(d,m) - 18°C) \quad \forall T_{amb}(d,m) \geq 18°C \qquad (B.2)$$

The maximum monthly heating/cooling weights ($w_{hdd/cdd,max}$) are obtained as [159]:

$$w_{hdd/cdd,max} = 1.05 \, \frac{HDD/CDD_{max}}{\sum HDD/CDD} \qquad (B.3)$$

where the HDD/CDD_{max} are the maximum monthly HDD/CDD.

B.2 Data availability beyond the case study area

To replicate the proposed methods outside of the case study area, the input datasets summarized in Table **3.4** must be obtained for the area of interest. While many of the required input datasets are available at European scale or beyond, other datasets would have to be approximated. Notably, maps of the thermal ground properties are rarely available. For large-scale studies, these can be mapped from literature data based on geological characteristics, as performed for example in [169,172,191,267]. Such mapping is a crude approximation, and the results must be

interpreted in this context. However, related work has shown that the thermal ground properties are not the most important features impacting GSHP performance [268], so this approach may be acceptable for large-scale studies.

Furthermore, the quality and resolution of the input data have to be suitable for the target application. The proposed analytical model is applied at individual parcel scale, which can be derived for example from OpenStreetMap data. For analyses at country scale or at pan-European scale, for example, even low-resolution inputs, for example using heat demand pixels at km-scale, may be acceptable for the replication of the proposed framework. At city scale, data is often available at higher quality and higher spatial resolution, allowing to obtain more accurate results. An overview of the required input datasets, there potential availability in the European context and suggestions of references are provided in Table B.**1**. References are provided for the European scale where possible, but they are not exhaustive.

Table B.1 - Suggestions of methods and datasets to obtain the required input data for the replicability of the proposed framework beyond the case study region.

	Input dataset	Potential availability	References (Europe)
Spatial constraints	Available area for BHEs	Can be obtained from national topographic data or OpenStreetMap (OSM) following the method in [159]	OSM [269]
	DHC zones	Can be obtained from the Heat Roadmap Europe[1] or derived using the method proposed in [161]	Heat Roadmap Europe [270]
	GSHP restrictions	Can be neglected for a rough potential estimate, or estimated from national hydrogeological data	SwissTopo [271] (Switzerland)
Geothermal input data	Thermal ground properties	If no 3D underground models or measurements are available, mapping of literature values to geological data may be performed in analogy to related studies [169,172,191,267]	SIA [201], VDI [272]
	Surface temperature	Can be derived from air temperature (see below) following [201,273]	COSMO[2]
	Air temperature	Reanalysis (e.g., COSMO REA) or other gridded data can be used	
	Full-load heating hours	Can be obtained from literature/norms	SIA [201], Kavanaugh [204]
Building energy demands	Building heating demand	Can be obtained from the Heat Roadmap Europe[1] for the reference year 2015. Future penetration of cooling equipment must be assessed in further work.	Heat Roadmap Europe [23], Hotmaps [274]
	Building cooling demand		Heat Roadmap Europe [51]

[1] https://heatroadmap.eu/peta4/.
[2] https://reanalysis.meteo.uni-bonn.de/.

Appendix C Performance of 5GDHC

Table C.**1** lists the investment cost (when installed in pair) and maximum allowed velocity of thermal network pipes. The data are obtained from FLEXYNETS [275], an European Project focusing on 5GDHC. A conversion rate of 1 (1 Euro = 1 CHF) is used.

Table C.1 - Maximum allowed velocity and investment cost of thermal network pipes.

Nominal diameter (DN) [mm]	Maximum allowed velocity [m/s]	Investment cost [euro/m]
20	1	68
25	1	88
32	1	119
40	1	138
50	1.5	186
65	1.5	229
80	1.5	282
100	1.5	380
125	1.5	454
150	1.5	558
200	2	783
250	2	952
300	2.5	1122
350	2.8	1203
400	3	1255
450	3	1266
500	3	1480
600	3	1794
700	3	2116
800	3	2527

List of publications

Journal articles

- Xiang Li, Jonathan Chambers, Selin Yilmaz, and Martin K Patel. 'A Monte Carlo Building Stock Model of Space Cooling Demand in the Swiss Service Sector under Climate Change'. *Energy & Buildings* 233 (2021). https://doi.org/10.1016/j.enbuild.2020.110662.
- Alina Walch*, Xiang Li*, Jonathan Chambers, Nahid Mohajeri, Selin Yilmaz, Martin Patel, and Jean-Louis Scartezzini. 'Shallow Geothermal Energy Potential for Heating and Cooling of Buildings with Regeneration under Climate Change Scenarios'. *Energy* 244 (April 2022): 123086. https://doi.org/10.1016/j.energy.2021.123086. (shared first authorship)
- Xiang Li, Alina Walch, Selin Yilmaz, Martin Patel, and Jonathan Chambers. 'Optimal Spatial Resource Allocation in Networks: Application to District Heating and Cooling'. *Computers & Industrial Engineering* 171 (2022): 108448. https://doi.org/10.1016/j.cie.2022.108448.
- Xiang Li, Selin Yilmaz, Martin K. Patel, and Jonathan Chambers. 'Techno-Economic Analysis of Fifth-Generation District Heating and Cooling Combined with Seasonal Borehole Thermal Energy Storage'. *Energy* 285 (December 2023): 129382. https://doi.org/10.1016/j.energy.2023.129382.

Conference articles

- Xiang Li, Jonathan Chambers, Selin Yilmaz, and Martin K Patel. 'GIS-Based Analysis of Space Cooling Demand in the Swiss Service Sector'. *21. Status-Seminar*, no. September 2020 (2020): 112–18. https://doi.org/10.5281/zenodo.3900180.
- Xiang Li, Jonathan Chambers, Selin Yilmaz, and Martin K. Patel. 'An Optimisation Approach for Spatial Allocation of Energy Sources to District Heating Networks'. *Journal of Physics: Conference Series* 2042, no. 1 (2021). https://doi.org/10.1088/1742-6596/2042/1/012038.
- Selin Yilmaz, Jonathan Chambers, Xiang Li, and Martin K. Patel. 'A Comparative Analysis of Patterns of Electricity Use and Flexibility Potential of Domestic and Non-Domestic Building Archetypes through Data Mining Techniques'. *Journal of Physics: Conference Series* 2042, no. 1 (1 November 2021): 012021. https://doi.org/10.1088/1742-6596/2042/1/012021.
- Xiang Li, Jonathan Chambers, Selin Yilmaz, and Martin K. Patel. "Sensitivity Analysis of Fifth Generation District Heating and Cooling Coupled with Borehole Thermal

Energy Storage with Respect to Cooling Adoption." *Accepted by Journal of Physics: Conference Series*.

Reports

- Xiang Li, Jonathan Chambers, Selin Yilmaz, and Martin K. Patel. 'Current Cooling Demand in the City of Zurich'. Geneva: Energy Efficiency Group, University of Geneva, 2022.

Bibliography

[1] Agreement P. Paris agreement. vol. 4, HeinOnline; 2015, p. 2017.

[2] European Commission. The European Green Deal. 2019.

[3] Federal Council aims for a climate-neutral Switzerland by 2050 n.d. https://www.admin.ch/gov/en/start/documentation/media-releases.msg-id-76206.html (accessed March 11, 2021).

[4] European Commission. An EU Strategy on Heating and Cooling. 2016.

[5] Kemmler A, Spillmann T, Piégsa A, Notter B, Cox B, Jakob M, et al. Analyse des schweizerischen Energieverbrauchs 2000 - 2019 nach Verwendungszwecken. Bern: Bundesamt für Energie; 2020.

[6] International Energy Agency. The Future of Cooling. Paris: IEA; 2018.

[7] REN21. Renewables 2022 Global Status Report. Paris: 2022.

[8] IRENA, Aalborg University. Integrating low-temperature renewables in district energy systems: Guidelines for policy makers. Abu Dhabi, Copenhagen: IRENA, Aalborg University; 2021.

[9] Rezaie B, Rosen MA. District heating and cooling: Review of technology and potential enhancements. Applied Energy 2012;93:2–10. https://doi.org/10.1016/j.apenergy.2011.04.020.

[10] IRENA, IEA, REN21. Renewable energy policies in a time of transition: Heating and Cooling. IRENA, OECD/IEA and REN21; 2020.

[11] Werner S. International review of district heating and cooling. Energy 2017;137:617–31. https://doi.org/10.1016/j.energy.2017.04.045.

[12] Bundesministerium für Wirtschaft und Energie. Integrierter Nationaler Energie- und Klimaplan. 2019.

[13] Energieperspektiven 2050+. Zusammenfassung der wichtigsten Ergebnisse. n.d.

[14] IRENA. Renewable energy in district heating and cooling. 2017.

[15] International Energy Agency. Renewables 2019: Analysis and forecasts to 2024. 2019. https://doi.org/10.1787/b3911209-en.

[16] Paardekooper S, Lund H, Chang M, Nielsen S, Moreno D, Thellufsen JZ. Heat Roadmap Chile: A national district heating plan for air pollution decontamination and decarbonisation. Journal of Cleaner Production 2020;272:122744. https://doi.org/10.1016/j.jclepro.2020.122744.

[17] Lake A, Rezaie B, Beyerlein S. Review of district heating and cooling systems for a sustainable future. Renewable and Sustainable Energy Reviews 2017;67:417–25. https://doi.org/10.1016/j.rser.2016.09.061.

[18] Perez-Mora N, Bava F, Andersen M, Bales C, Lennermo G, Nielsen C, et al. Solar district heating and cooling: A review. International Journal of Energy Research 2018;42:1419–41. https://doi.org/10.1002/er.3888.

[19] Axelsson G, Gunnlaugsson E, Jónasson T, Ólafsson M. Low-temperature geothermal utilization in Iceland – Decades of experience. Geothermics 2010;39:329–38. https://doi.org/10.1016/j.geothermics.2010.09.002.

[20] Østergaard PA, Werner S, Dyrelund A, Lund H, Arabkoohsar A, Sorknæs P, et al. The four generations of district cooling - A categorization of the development in district cooling from origin to future prospect. Energy 2022;253:124098. https://doi.org/10.1016/j.energy.2022.124098.

[21] Malla F. Enjeux et développement des réseaux thermiques basse température à Genève. Geneva: SIG; 2020.

[22] Pezzutto S, Zambotti S, Croce S, Zambelli P, Scaramuzzino C, Pascuas RP, et al. HOTMAPS D2.3 WP2 Report – Open Data Set for the EU28. 2019.

[23] Möller B, Wiechers E, Persson U, Grundahl L, Connolly D. Heat Roadmap Europe: Identifying local heat demand and supply areas with a European thermal atlas. Energy 2018;158:281–92. https://doi.org/10.1016/j.energy.2018.06.025.

[24] Paardekooper S, Lund RS, Mathiesen BV, Chang M, Petersen UR, Grundahl L, et al. Heat Roadmap Europe 4: Quantifying the Impact of Low-Carbon Heating and Cooling Roadmaps. Aalborg Universitetsforlag 2018.

[25] Lund H, Werner S, Wiltshire R, Svendsen S, Thorsen JE, Hvelplund F, et al. 4th Generation District Heating (4GDH). Integrating smart thermal grids into future sustainable energy systems. Energy 2014;68:1–11. https://doi.org/10.1016/j.energy.2014.02.089.

[26] Lund H, Østergaard PA, Chang M, Werner S, Svendsen S, Sorknæs P, et al. The status of 4th generation district heating: Research and results. Energy 2018;164:147–59. https://doi.org/10.1016/j.energy.2018.08.206.

[27] Østergaard D, Svendsen S. Space heating with ultra-low-temperature district heating – a case study of four single-family houses from the 1980s. Energy Procedia 2017;116:226–35. https://doi.org/10.1016/j.egypro.2017.05.070.

[28] Sulzer M, Werner S, Mennel S, Wetter M. Vocabulary for the fourth generation of district heating and cooling. Smart Energy 2021;1:100003. https://doi.org/10.1016/j.segy.2021.100003.

[29] Buffa S, Cozzini M, D'Antoni M, Baratieri M, Fedrizzi R. 5th generation district heating and cooling systems: A review of existing cases in Europe. Renewable and Sustainable Energy Reviews 2019;104:504–22. https://doi.org/10.1016/j.rser.2018.12.059.

[30] Vetterli N, Thaler E, Sulzer M, Ryser P. Monitoring Suurstoffi Auswertung Okt . 2013 – Sep . 2016 2017.

[31] Pellegrini M, Bianchini A. The innovative concept of cold district heating networks: A literature review. Energies 2018;11. https://doi.org/10.3390/en11010236.

[32] Gabrielli P, Acquilino A, Siri S, Bracco S, Sansavini G, Mazzotti M. Optimization of low-carbon multi-energy systems with seasonal geothermal energy storage: The Anergy Grid of ETH Zurich. Energy Conversion and Management: X 2020;8:100052. https://doi.org/10.1016/j.ecmx.2020.100052.

[33] Caputo P, Ferla G, Belliardi M, Cereghetti N. District thermal systems: State of the art and promising evolutive scenarios. A focus on Italy and Switzerland. Sustainable Cities and Society 2021;65:102579. https://doi.org/10.1016/j.scs.2020.102579.

[34] Wirtz M, Schreiber T, Müller D. Survey of 53 Fifth-Generation District Heating and Cooling (5GDHC) Networks in Germany. Energy Tech 2022;10:2200749. https://doi.org/10.1002/ente.202200749.

[35] Lund H, Østergaard PA, Nielsen TB, Werner S, Thorsen JE, Gudmundsson O, et al. Perspectives on fourth and fifth generation district heating. Energy 2021;227:120520. https://doi.org/10.1016/j.energy.2021.120520.

[36] Rosen MA, Koohi-Fayegh S. Geothermal energy: sustainable heating and cooling using the ground. John Wiley & Sons; 2017.

[37] Falcone G, Liu X, Okech RR, Seyidov F, Teodoriu C. Assessment of deep geothermal energy exploitation methods: The need for novel single-well solutions. Energy 2018;160:54–63.

[38] Vieira A, Alberdi-Pagola M, Christodoulides P, Javed S, Loveridge F, Nguyen F, et al. Characterisation of ground thermal and thermo-mechanical behaviour for shallow geothermal energy applications. Energies 2017;10:2044.

[39] Sarbu I, Sebarchievici C. General review of ground-source heat pump systems for heating and cooling of buildings. Energy and Buildings 2014;70:441–54. https://doi.org/10.1016/j.enbuild.2013.11.068.

[40] Rosiek S, Batlles F. Shallow geothermal energy applied to a solar-assisted air-conditioning system in southern Spain: Two-year experience. Applied Energy 2012;100:267–76.

[41] Allaerts K, Coomans M, Salenbien R. Hybrid ground-source heat pump system with active air source regeneration. Energy Conversion and Management 2015;90:230–7.

[42] Reuss M. The use of borehole thermal energy storage (BTES) systems. Advances in thermal energy storage systems, Elsevier; 2015, p. 117–47.

[43] Ciampi G, Rosato A, Sibilio S. Thermo-economic sensitivity analysis by dynamic simulations of a small Italian solar district heating system with a seasonal borehole thermal energy storage. Energy 2018;143:757–71. https://doi.org/10.1016/j.energy.2017.11.029.

[44] Francesco Calise, Cappiello FL, Dentice d'Accadia M, Petrakopoulou F, Vicidomini M. A solar-driven 5th generation district heating and cooling network with ground-source heat pumps: a thermo-economic analysis. Sustainable Cities and Society 2022;76:103438. https://doi.org/10.1016/j.scs.2021.103438.

[45] Santamouris M. Cooling the buildings – past, present and future. Energy and Buildings 2016;128:617–38. https://doi.org/10.1016/j.enbuild.2016.07.034.

[46] Wirtz M, Kivilip L, Remmen P, Müller D. Quantifying Demand Balancing in Bidirectional Low Temperature Networks. Energy and Buildings 2020;224:110245. https://doi.org/10.1016/j.enbuild.2020.110245.

[47] Team CW, Pachauri RK, Meyer LA. IPCC, 2014: Climate Change 2014: Synthesis Report. Contribution of Working Groups I, II and III to the Fifth Assessment Report of the Intergovernmental Panel on Climate Change. IPCC; 2014. https://doi.org/10.1046/j.1365-2559.2002.1340a.x.

[48] Ürge-Vorsatz D, Cabeza LF, Serrano S, Barreneche C, Petrichenko K. Heating and cooling energy trends and drivers in buildings. Renewable and Sustainable Energy Reviews 2015;41:85–98. https://doi.org/10.1016/j.rser.2014.08.039.

[49] Dalin P, Nilsson J, Rubenhag A. The European Cold Market. Ecoheatcool, Work Package 2006.

[50] Aebischer B, Henderson G, Catenazzi G. Impact of climate change on energy demand in the Swiss service sector - and application to Europe. Improving Energy Efficiency in Commercial Buildings: Proceeding of the International Conference IEECB'06: Frankfurt,

Germany, 26-27 April 2006, European Commission, Institute for Environment and Sustainability; 2006, p. 205–18.

[51] Werner S. European space cooling demands. Energy 2016;110:148–56. https://doi.org/10.1016/j.energy.2015.11.028.

[52] Connolly D. Heat Roadmap Europe: Quantitative comparison between the electricity, heating, and cooling sectors for different European countries. Energy 2017;139:580–93. https://doi.org/10.1016/j.energy.2017.07.037.

[53] Bertoldi P, Atanasiu B. Electricity consumption and efficiency trends in European Union-Status Report 2009. JRC-IE, Ispra, Italy 2009.

[54] Pezzutto S, De Felice M, Fazeli R, Kranzl L, Zambotti S. Status quo of the air-conditioning market in europe: Assessment of the building stock. Energies 2017;10:1253. https://doi.org/10.3390/en10091253.

[55] Jakubcionis M, Carlsson J. Estimation of European Union service sector space cooling potential. Energy Policy 2017;113:223–31. https://doi.org/10.1016/j.enpol.2017.11.012.

[56] Pardo N, Vatopoulos K, Riekkola AK, Perez A. Methodology to estimate the energy flows of the European Union heating and cooling market. Energy 2013;52:339–52. https://doi.org/10.1016/j.energy.2013.01.062.

[57] Heinrich C, Wittig S, Albring P, Richter L, Safarik M, Böhm U, et al. Sustainable cooling supply for building air conditioning and industry in Germany. Umweltbundesamt; 2015.

[58] Dumortier R, Lang T, Schmutz B. Elektrizitätsbedarf fürs Kühlen in der Schweiz. Schweizerischen Vereins für Kälte- technik, Bundesamts für Energie; 2012.

[59] Fleiter T, Herbst A, Hirzel S, Krail M, Frassine C, Aydemir A, et al. Mapping and analyses of the current and future (2020 - 2030) heating/cooling fuel deployment (fossil/renewables) - Work package 1: Final energy consumption for the year 2012. 2016.

[60] Mauree D, Coccolo S, Perera ATD, Nik V, Scartezzini JL, Naboni E. A new framework to evaluate urban design using urban microclimatic modeling in future climatic conditions. Sustainability 2018;10:1134. https://doi.org/10.3390/su10041134.

[61] Frank T. Climate change impacts on building heating and cooling energy demand in Switzerland. Energy and Buildings 2005;37:1175–85. https://doi.org/10.1016/j.enbuild.2005.06.019.

[62] Subhes C. Bhattacharyya. Energy economics: concepts, issues, markets and governance. 2019. https://doi.org/10.4324/9781315114064.

[63] Europe to America: Your love of air-conditioning is stupid - The Washington Post n.d. https://www.washingtonpost.com/news/worldviews/wp/2015/07/22/europe-to-america-your-love-of-air-conditioning-is-stupid/ (accessed January 6, 2020).

[64] Christenson M, Manz H, Gyalistras D. Climate warming impact on degree-days and building energy demand in Switzerland. Energy Conversion and Management 2006;47:671–86. https://doi.org/10.1016/j.enconman.2005.06.009.

[65] Swan LG, Ugursal VI. Modeling of end-use energy consumption in the residential sector: A review of modeling techniques. Renewable and Sustainable Energy Reviews 2009;13:1819–35. https://doi.org/10.1016/j.rser.2008.09.033.

[66] Corrado V, Fabrizio E. Assessment of building cooling energy need through a quasi-steady state model: Simplified correlation for gain-loss mismatch. Energy and Buildings 2007;39:569–79. https://doi.org/10.1016/j.enbuild.2006.09.012.

[67] Zucker G, Judex F, Blöchle M, Köstl M, Widl E, Hauer S, et al. A new method for optimizing operation of large neighborhoods of buildings using thermal simulation. Energy and Buildings 2016;125:153–60. https://doi.org/10.1016/j.enbuild.2016.04.081.

[68] Wang D, Landolt J, Mavromatidis G, Orehounig K, Carmeliet J. CESAR: A bottom-up building stock modelling tool for Switzerland to address sustainable energy transformation strategies. Energy and Buildings 2018;169:9–26. https://doi.org/10.1016/j.enbuild.2018.03.020.

[69] Afshari A. A new model of urban cooling demand and heat island—application to vertical greenery systems (VGS). Energy and Buildings 2017;157:204–17. https://doi.org/10.1016/j.enbuild.2017.01.008.

[70] Yamaguchi Y, Miyachi Y, Shimoda Y. Stock modelling of HVAC systems in Japanese commercial building sector using logistic regression. Energy and Buildings 2017;152:458–71. https://doi.org/10.1016/j.enbuild.2017.07.007.

[71] Rafsanjani HN, Ahn CR, Alahmad M. A review of approaches for sensing, understanding, and improving occupancy-related energy-use behaviors in commercial buildings. vol. 8. 2015. https://doi.org/10.3390/en81010996.

[72] Burleyson CD, Iyer G, Hejazi M, Kim S, Kyle P, Rice JS, et al. Future western U.S. building electricity consumption in response to climate and population drivers: A comparative study of the impact of model structure. Energy 2020;208:118312. https://doi.org/10.1016/j.energy.2020.118312.

[73] Kwok SSK, Lee EWM. A study of the importance of occupancy to building cooling load in prediction by intelligent approach. Energy Conversion and Management 2011;52:2555–64. https://doi.org/10.1016/j.enconman.2011.02.002.

[74] Guerra Santin O, Itard L, Visscher H. The effect of occupancy and building characteristics on energy use for space and water heating in Dutch residential stock. Energy and Buildings 2009;41:1223–32. https://doi.org/10.1016/j.enbuild.2009.07.002.

[75] Huebner GM, Hamilton I, Chalabi Z, Shipworth D, Oreszczyn T. Explaining domestic energy consumption - The comparative contribution of building factors, socio-demographics, behaviours and attitudes. Applied Energy 2015;159:589–600. https://doi.org/10.1016/j.apenergy.2015.09.028.

[76] Oh SJ, Ng KC, Thu K, Chun W, Chua KJE. Forecasting long-term electricity demand for cooling of Singapore's buildings incorporating an innovative air-conditioning technology. Energy and Buildings 2016;127:183–93. https://doi.org/10.1016/j.enbuild.2016.05.073.

[77] Sailor DJ, Pavlova AA. Air conditioning market saturation and long-term response of residential cooling energy demand to climate change. Energy 2003;28:941–51. https://doi.org/10.1016/S0360-5442(03)00033-1.

[78] Zhao H, Magoulès F. A review on the prediction of building energy consumption. Renewable and Sustainable Energy Reviews 2012;16:3586–92. https://doi.org/10.1016/j.rser.2012.02.049.

[79] Chambers J, Hollmuller P, Bouvard O, Schueler A, Scartezzini J-L, Azar E, et al. Evaluating the electricity saving potential of electrochromic glazing for cooling and lighting at the scale of the non-residential national building stock using a Monte Carlo model. Energy 2019;185:136–47. https://doi.org/10.1016/j.energy.2019.07.037.

[80] Kavgic M, Mavrogianni A, Mumovic D, Summerfield A, Stevanovic Z, Djurovic-Petrovic M. A review of bottom-up building stock models for energy consumption in the residential sector. Building and Environment 2010;45:1683–97. https://doi.org/10.1016/j.buildenv.2010.01.021.

[81] Schneider S, Hollmuller P, Le Strat P, Khoury J, Patel M, Lachal B. Spatial–Temporal Analysis of the Heat and Electricity Demand of the Swiss Building Stock. Frontiers in Built Environment 2017;3:53. https://doi.org/10.3389/fbuil.2017.00063.

[82] Streicher KN, Padey P, Parra D, Bürer MC, Patel MK. Assessment of the current thermal performance level of the Swiss residential building stock: Statistical analysis of energy performance certificates. Energy and Buildings 2018;178:360–78. https://doi.org/10.1016/j.enbuild.2018.08.032.

[83] Schneider S, Hollmuller P, Chambers J, Patel M. A Heat Demand Load Curve Model of the Swiss National Territory. IOP Conference Series: Earth and Environmental Science 2019;290:012107. https://doi.org/10.1088/1755-1315/290/1/012107.

[84] Buffat R, Froemelt A, Heeren N, Raubal M, Hellweg S. Big data GIS analysis for novel approaches in building stock modelling. Applied Energy 2017;208:277–90. https://doi.org/10.1016/j.apenergy.2017.10.041.

[85] Heidari M, Majcen D, van der Lans N, Floret I, Patel MK. Analysis of the energy efficiency potential of household lighting in Switzerland using a stock model. Energy and Buildings 2018;158:536–48. https://doi.org/10.1016/j.enbuild.2017.08.091.

[86] Yilmaz S, Majcen D, Heidari M, Mahmoodi J, Brosch T, Patel MK. Analysis of the impact of energy efficiency labelling and potential changes on electricity demand reduction of white goods using a stock model: The case of Switzerland. Applied Energy 2019;239:117–32. https://doi.org/10.1016/j.apenergy.2019.01.137.

[87] Sartori I, Sandberg NH, Brattebø H. Dynamic building stock modelling: General algorithm and exemplification for Norway. Energy and Buildings 2016;132:13–25. https://doi.org/10.1016/j.enbuild.2016.05.098.

[88] Sandberg NH, Sartori I, Heidrich O, Dawson R, Dascalaki E, Dimitriou S, et al. Dynamic building stock modelling: Application to 11 European countries to support the energy efficiency and retrofit ambitions of the EU. Energy and Buildings 2016;132:26–38. https://doi.org/10.1016/j.enbuild.2016.05.100.

[89] Spinoni J, Vogt JV, Barbosa P, Dosio A, McCormick N, Bigano A, et al. Changes of heating and cooling degree-days in Europe from 1981 to 2100. International Journal of Climatology 2018;38:e191–208. https://doi.org/10.1002/joc.5362.

[90] Day AR, Jones PG, Maidment GG. Forecasting future cooling demand in London. Energy and Buildings 2009;41:942–8. https://doi.org/10.1016/j.enbuild.2009.04.001.

[91] Cox RA, Drews M, Rode C, Nielsen SB. Simple future weather files for estimating heating and cooling demand. Building and Environment 2015;83:104–14. https://doi.org/10.1016/j.buildenv.2014.04.006.

[92] Kolokotroni M, Davies M, Croxford B, Bhuiyan S, Mavrogianni A. A validated methodology for the prediction of heating and cooling energy demand for buildings within the Urban Heat Island: Case-study of London. Solar Energy 2010;84:2246–55. https://doi.org/10.1016/j.solener.2010.08.002.

[93] Borah P, Singh MK, Mahapatra S. Estimation of degree-days for different climatic zones of North-East India. Sustainable Cities and Society 2015;14:70–81. https://doi.org/10.1016/j.scs.2014.08.001.

[94] Berger M, Worlitschek J. The link between climate and thermal energy demand on national level: A case study on Switzerland. Energy and Buildings 2019;202:109372. https://doi.org/10.1016/j.enbuild.2019.109372.

[95] Larsen MAD, Petrović S, Radoszynski AM, McKenna R, Balyk O. Climate change impacts on trends and extremes in future heating and cooling demands over Europe. Energy and Buildings 2020;226. https://doi.org/10.1016/j.enbuild.2020.110397.

[96] Asloune H, Riviere P, Dittmann F, Berthou T, Asloune H, Riviere P, et al. Prospective Modelling of Residential Space Cooling Diffusion in France 2019.

[97] Bird DN, de Wit R, Schwaiger HP, Andre K, Beermann M, Žuvela-Aloise M. Estimating the daily peak and annual total electricity demand for cooling in Vienna, Austria by 2050. Urban Climate 2019;28:100452. https://doi.org/10.1016/j.uclim.2019.100452.

[98] Isaac M, van Vuuren DP. Modeling global residential sector energy demand for heating and air conditioning in the context of climate change. Energy Policy 2009;37:507–21. https://doi.org/10.1016/j.enpol.2008.09.051.

[99] RegBL | Federal Register of Buildings and Dwellings n.d. https://www.housing-stat.ch/fr/accueil.html (accessed September 30, 2019).

[100] CH2018. CH2018 – Climate Scenarios for Switzerland, Technical Report. 2018.

[101] Kinerrch A, Bredow D, Ess F, Grebel habil T, Hofer P, Kemmler A, et al. Die Energieperspektiven für die Schweiz bis 2050 Anhang 3. Basel: Bundesamt für Energie; 2012.

[102] Climatisation de confort | GE.CH – République et canton de Genève n.d. https://www.ge.ch/rafraichir-climatiser-batiment/climatisation-confort (accessed November 6, 2019).

[103] SIA N. 180:2014 Wärmeschutz, Feuchteschutz und Raumklima in Gebäuden. 2014.

[104] Norm SIA. 382/1: Lüftungs-und Klimaanlagen–Allgemeine Grundlagen und Anforderungen 2007.

[105] Air conditioning systems - City of Zurich n.d. https://www.stadt-zuerich.ch/gud/de/index/beratungen_bewilligungen/ugz/bauberatung/baubewilligung/fachthemen/lueftungen-klima/klimaanlagen.html (accessed October 23, 2020).

[106] Energy forms | State of Vaud n.d. https://www.vd.ch/themes/environnement/energie/formulaires-energie-pour-demandes-dautorisation-et-autres-formulaires-dannonce/formulaires-energie/ (accessed November 6, 2019).

[107] ASHRAE. ASHRAE handbook: Fundamentals. American Society of Heating, Refrigerating, and Air-Conditioning Engineers; 2005.

[108] Virtanen P, Gommers R, Oliphant TE, Haberland M, Reddy T, Cournapeau D, et al. SciPy 1.0--Fundamental Algorithms for Scientific Computing in Python 2019.

[109] Seabold, Skipper, Perktold J. Statsmodels: Econometric and statistical modeling with python. 9th Python in Science Conference 2010.

[110] Montgomery DC, Peck EA, Vining GG, Vining GG. Introduction to linear regression analysis, 2012, p. 171–210.

[111] Urge-Vorsatz D, Petrichenko K, Antal M, Staniec M, Labelle M, Ozden E, et al. Best Practice Policies for Low Energy and Carbon Buildings. A Scenario Analysis. Research report prepared by the Center for Climate Change and Sustainable Policy (3CSEP) for the Global Buildings Performance Network. Global Buildings Performance Network; 2012.

[112] Vu DH, Muttaqi KM, Agalgaonkar AP. A variance inflation factor and backward elimination based robust regression model for forecasting monthly electricity demand using climatic variables. Applied Energy 2015;140:385–94. https://doi.org/10.1016/j.apenergy.2014.12.011.

[113] Alin A. Multicollinearity. Wiley Interdisciplinary Reviews: Computational Statistics 2010;2:370–4. https://doi.org/10.1002/wics.84.

[114] O'Brien RM. A caution regarding rules of thumb for variance inflation factors. Quality and Quantity 2007;41:673–90. https://doi.org/10.1007/s11135-006-9018-6.

[115] Marill KA. Advanced Statistics: Linear Regression, Part II: Multiple Linear Regression. Acad Emerg Med 2004;11:94–102. https://doi.org/10.1197/S1069-6563(03)00601-8.

[116] Liddament M. A Guide to Energy Efficienct Ventilation. Air Infiltration and Ventilation Centre Coventry; 1996.

[117] Gratia E, De Herde A. Greenhouse effect in double-skin facade. Energy and Buildings 2007;39:199–211. https://doi.org/10.1016/j.enbuild.2006.06.004.

[118] Dittmann F, Rivière P, Stabat P. Heat Roadmap Europe WP3 - Space Cooling Technology in Europe. Deliverable 3.2: Cooling technology datasheets in the 14 MSs in the EU28. 2017.

[119] Huang B, Hansen PMS, Viegand J, Riviere P, Asloune H, Dittmann F. Air conditioners and comfort fans , Review of Regulation 206 / 2012 and 626 / 2011 Final report. European Commission, DG Energy; 2018.

[120] Cook M, Short A. Natural Ventilation and Low Energy Cooling of Large, Non-Domestic Buildings – Four Case Studies. International Journal of Ventilation 2005;3:283–94. https://doi.org/10.1080/14733315.2005.11683923.

[121] Rohat G, Goyette S. On the Use of the Climate Twins Approach to Pose the Challenges of Urban Adaptation. 16th Swiss Global Change Day: Book of Abstracts, Bern: 2015. https://doi.org/10.1002/joc.3804.4.

[122] Fleiter T, Elsland R, Rehfeldt M, Steinbach J, Reiter U, Catenazzi G, et al. EU Profile of heating and cooling demand in 2015. Heat Roadmap Europe project 2017:70.

[123] Ramachandran Kannan, Turton H. Switzerland Energy Transition Scenarios – Development and Application of the Swiss TIMES Energy System Model (STEM). 2014. https://doi.org/10.1094/PHYTO.2003.93.9.1068.

[124] Totschnig G, Hirner R, Müller A, Kranzl L, Hummel M, Nachtnebel HP, et al. Climate change impact and resilience in the electricity sector: The example of Austria and Germany. Energy Policy 2017;103:238–48. https://doi.org/10.1016/j.enpol.2017.01.019.

[125] Li X, Chambers J, Yilmaz S, Patel MK. A Monte Carlo building stock model of space cooling demand in the Swiss service sector under climate change. Energy & Buildings 2021;233. https://doi.org/10.1016/j.enbuild.2020.110662.

[126] Internaltional Energy Agency. Net Zero by 2050. IEA; 2021.

[127] European Commission. Amendment to the Renewable Energy Directive to implement the ambition of the new 2030 climate target. Brussels: 2021.

[128] European Commission. Proposal for a Directive on energy efficiency (recast). Brussels: 2021.

[129]International Energy Agency. World Energy Statistics and Balances 2020 (Database). Paris: IEA; 2020.

[130] Bianco E, Brown A, Hafner M, Eicke A, Eicke L, Uherova Hasbani K. Renewable Energy Market Analysis: Southeast Europe. International Renewable Energy Agency (IRENA); 2019.

[131] Andrews D, Pardo-garcia N, Krook-Riekkola A, Tzimas E, Serpa J, Carlsson J, et al. Background Report on EU-27 District Heating and Cooling Potentials, Barriers, Best Practice and Measures of Promotion. 2012. https://doi.org/10.2790/47209.

[132] Haiwen S, Lin D, Xiangli L, Yingxin Z. Quasi-dynamic energy-saving judgment of electric-driven seawater source heat pump district heating system over boiler house district heating system. Energy and Buildings 2010;42:2424–30. https://doi.org/10.1016/j.enbuild.2010.08.012.

[133] Bühler F, Petrović S, Holm FM, Karlsson K, Elmegaard B. Spatiotemporal and economic analysis of industrial excess heat as a resource for district heating. Energy 2018;151:715–28. https://doi.org/10.1016/j.energy.2018.03.059.

[134] Lund R, Persson U. Mapping of potential heat sources for heat pumps for district heating in Denmark. Energy 2016;110:129–38. https://doi.org/10.1016/j.energy.2015.12.127.

[135] Rismanchi B. District energy network (DEN), current global status and future development. Renewable and Sustainable Energy Reviews 2017;75:571–9. https://doi.org/10.1016/j.rser.2016.11.025.

[136] Chambers J, Zuberi S, Jibran M, Narula K, Patel MK. Spatiotemporal analysis of industrial excess heat supply for district heat networks in Switzerland. Energy 2020;192:116705. https://doi.org/10.1016/j.energy.2019.116705.

[137] West DB. Introduction to graph theory. vol. 2. Prentice hall Upper Saddle River; 2001.

[138] He L, Chalil Madathil S, Oberoi A, Servis G, Khasawneh MT. A systematic review of research design and modeling techniques in inpatient bed management. Computers and Industrial Engineering 2019;127:451–66. https://doi.org/10.1016/j.cie.2018.10.033.

[139] de Oliveira PB, de Camargo RS, de Miranda Júnior G, Martins AX. A computational study of a decomposition approach for the dynamic two-level uncapacitated facility location problem with single and multiple allocation. Computers and Industrial Engineering 2021;151:106964. https://doi.org/10.1016/j.cie.2020.106964.

[140] Dasgupta S, Papadimitriou C, Vazirani U. Algorithms 2006.

[141] Moore EF. The shortest path through a maze. Proc. Int. Symp. Switching Theory, 1959, 1959, p. 285–92.

[142] Hopcroft J, Tarjan R. Algorithm 447: efficient algorithms for graph manipulation. Communications of the ACM 1973;16:372–8.

[143] Kuhn HW. The Hungarian method for the assignment problem. Naval Research Logistics Quarterly 1955;2:83–97.

[144] Boloori Arabani A, Farahani RZ. Facility location dynamics: An overview of classifications and applications. Computers and Industrial Engineering 2012;62:408–20. https://doi.org/10.1016/j.cie.2011.09.018.

[145] Sarkar S, Pramanik A, Maiti J, Reniers G. COVID-19 outbreak: A data-driven optimization model for allocation of patients. Computers and Industrial Engineering 2021;161:107675. https://doi.org/10.1016/j.cie.2021.107675.

[146] Sarma D, Bera UK, Das A. A mathematical model for resource allocation in emergency situations with the co-operation of NGOs under uncertainty. Computers and Industrial Engineering 2019;137:106000. https://doi.org/10.1016/j.cie.2019.106000.

[147] Hitchcock FL. The distribution of a product from several sources to numerous localities. Journal of Mathematics and Physics 1941;20:224–30.

[148] Koopmans TC. Exchange ratios between cargoes on various routes (non-refrigerating dry cargoes). Memorandum for the Combined Shipping Adjustment Board, Washington DC 1942:1–12.

[149] Dantzig GB. Linear programming and extensions. Princeton university press; 1963.

[150] Khachiyan LG. A polynomial algorithm in linear programming. Doklady Akademii Nauk, vol. 244, Russian Academy of Sciences; 1979, p. 1093–6.

[151] Tucker AW. Symposium on Modern Techniques for Extremum Problems—Linear and Nonlinear Programming. Operations Research 1957;5:244–57.

[152] Jordahl K. GeoPandas: Python tools for geographic data. URL: Https://Github Com/Geopandas/Geopandas 2014.

[153] Hagberg A, Swart P, S Chult D. Exploring network structure, dynamics, and function using NetworkX. Los Alamos National Lab.(LANL), Los Alamos, NM (United States); 2008.

[154] Mitchell S, OSullivan M, Dunning I. PuLP: a linear programming toolkit for python. The University of Auckland, Auckland, New Zealand 2011.

[155] Hoyer S, Hamman J. xarray: ND labeled arrays and datasets in Python. Journal of Open Research Software 2017;5.

[156] Gillies S, Ward B, Petersen AS. Rasterio: geospatial raster I/O for Python programmers. URL Https://Github Com/Mapbox/Rasterio 2013.

[157] Walt S van der, Colbert SC, Varoquaux G. The NumPy array: a structure for efficient numerical computation. Computing in Science & Engineering 2011;13:22–30.

[158] McKinney W. pandas: a foundational Python library for data analysis and statistics. Python for High Performance and Scientific Computing 2011;14.

[159] Walch A, Mohajeri N, Gudmundsson A, Scartezzini JL. Quantifying the technical geothermal potential from shallow borehole heat exchangers at regional scale. Renewable Energy 2021;165:369–80. https://doi.org/10.1016/j.renene.2020.11.019.

[160] Walch A, Li X, Chambers J, Mohajeri N, Yilmaz S, Patel M, et al. Shallow geothermal energy potential for heating and cooling of buildings with regeneration under climate change scenarios. Energy 2022;244:123086. https://doi.org/10.1016/j.energy.2021.123086.

[161] Chambers J, Narula K, Sulzer M, Patel MK. Mapping district heating potential under evolving thermal demand scenarios and technologies: A case study for Switzerland. Energy 2019;176:682–92. https://doi.org/10.1016/j.energy.2019.04.044.

[162] Lund JW, Toth A. Direct Utilization of Geothermal Energy 2020 Worldwide Review. Proceedings World Geothermal Congress 2020, Reykjavik, Iceland: 2020.

[163] Florides G, Kalogirou S. Ground heat exchangers—A review of systems, models and applications. Renewable Energy 2007;32:2461–78. https://doi.org/10.1016/j.renene.2006.12.014.

[164] Soltani M, M. Kashkooli F, Dehghani-Sanij AR, Kazemi AR, Bordbar N, Farshchi MJ, et al. A comprehensive study of geothermal heating and cooling systems. Sustainable Cities and Society 2019;44:793–818. https://doi.org/10.1016/j.scs.2018.09.036.

[165] Vienken T, Kreck M, Dietrich P. Monitoring the impact of intensive shallow geothermal energy use on groundwater temperatures in a residential neighborhood. Geothermal Energy 2019;7:8. https://doi.org/10.1186/s40517-019-0123-x.

[166] Hähnlein S, Bayer P, Ferguson G, Blum P. Sustainability and policy for the thermal use of shallow geothermal energy. Energy Policy 2013;59:914–25. https://doi.org/10.1016/j.enpol.2013.04.040.

[167] Garabetian T, Dumas P, Serrano C, Mazzagatti V, Kumar S, Dimitrisina R, et al. EGEC Geothermal Market Report. EGEC - European Geothermal Energy Council; 2020.

[168] Casasso A, Sethi R. Assessment and mapping of the shallow geothermal potential in the province of Cuneo (Piedmont, NW Italy). Renewable Energy 2017;102:306–15. https://doi.org/10.1016/j.renene.2016.10.045.

[169] Galgaro A, Di Sipio E, Teza G, Destro E, De Carli M, Chiesa S, et al. Empirical modeling of maps of geo-exchange potential for shallow geothermal energy at regional scale. Geothermics 2015;57:173–84. https://doi.org/10.1016/j.geothermics.2015.06.017.

[170] García-Gil A, Vázquez-Suñe E, Alcaraz MM, Juan AS, Sánchez-Navarro JA, Montlleó M, et al. GIS-supported mapping of low-temperature geothermal potential taking groundwater flow into account. Renewable Energy 2015;77:268–78. https://doi.org/10.1016/j.renene.2014.11.096.

[171] Muñoz M, Garat P, Flores-Aqueveque V, Vargas G, Rebolledo S, Sepúlveda S, et al. Estimating low-enthalpy geothermal energy potential for district heating in Santiago

basin–Chile (33.5 °S). Renewable Energy 2015;76:186–95. https://doi.org/10.1016/j.renene.2014.11.019.

[172] Perego R, Pera S, Galgaro A. Techno-Economic Mapping for the Improvement of Shallow Geothermal Management in Southern Switzerland. Energies 2019;12:279. https://doi.org/10.3390/en12020279.

[173] Tissen C, Menberg K, Bayer P, Blum P. Meeting the demand: geothermal heat supply rates for an urban quarter in Germany. Geotherm Energy 2019;7:9. https://doi.org/10.1186/s40517-019-0125-8.

[174] Zhang Y, Soga K, Choudhary R. Shallow geothermal energy application with GSHPs at city scale: study on the City of Westminster. Géotechnique Letters 2014;4:125–31. https://doi.org/10.1680/geolett.13.00061.

[175] Miglani S, Orehounig K, Carmeliet J. A methodology to calculate long-term shallow geothermal energy potential for an urban neighbourhood. Energy and Buildings 2018;159:462–73. https://doi.org/10.1016/j.enbuild.2017.10.100.

[176] Bayer P, Attard G, Blum P, Menberg K. The geothermal potential of cities. Renewable and Sustainable Energy Reviews 2019;106:17–30. https://doi.org/10.1016/j.rser.2019.02.019.

[177] Rivera JA, Blum P, Bayer P. Increased ground temperatures in urban areas: Estimation of the technical geothermal potential. Renewable Energy 2017;103:388–400. https://doi.org/10.1016/j.renene.2016.11.005.

[178] FascÌ ML, Lazzarotto A, Acuna J, Claesson J. Analysis of the thermal interference between ground source heat pump systems in dense neighborhoods. Science and Technology for the Built Environment 2019;25:1069–80. https://doi.org/10.1080/23744731.2019.1648130.

[179] Attard G, Bayer P, Rossier Y, Blum P, Eisenlohr L. A novel concept for managing thermal interference between geothermal systems in cities. Renewable Energy 2020;145:914–24. https://doi.org/10.1016/j.renene.2019.06.095.

[180] Alcaraz M, Vives L, Vázquez-Suñé E. The T-I-GER method: A graphical alternative to support the design and management of shallow geothermal energy exploitations at the metropolitan scale. Renewable Energy 2017;109:213–21. https://doi.org/10.1016/j.renene.2017.03.022.

[181] Wagner R, Weisskopf T. Erdsondenpotenzial in der Stadt Zürich. Amt für Hochbauten Stadt Zürich; 2014.

[182] Kriesi R. Methoden der Erdsonden-Regeneration mit Sekundärnutzen oder tiefen Wärmekosten. Amt für Hochbauten Stadt Zürich; 2017.

[183] Miglani S, Orehounig K, Carmeliet J. Integrating a thermal model of ground source heat pumps and solar regeneration within building energy system optimization. Applied Energy 2018;218:78–94. https://doi.org/10.1016/j.apenergy.2018.02.173.

[184] Liu Z, Xu W, Zhai X, Qian C, Chen X. Feasibility and performance study of the hybrid ground-source heat pump system for one office building in Chinese heating dominated areas. Renewable Energy 2017;101:1131–40. https://doi.org/10.1016/j.renene.2016.10.006.

[185] Pahud D. A Case Study: The Dock Midfield of Zurich Airport. Energy Geostructures, John Wiley & Sons, Ltd; 2013, p. 281–96. https://doi.org/10.1002/9781118761809.ch14.

[186] Girard A, Gago EJ, Muneer T, Caceres G. Higher ground source heat pump COP in a residential building through the use of solar thermal collectors. Renewable Energy 2015;80:26–39. https://doi.org/10.1016/j.renene.2015.01.063.

[187] Michopoulos A, Papakostas KT, Kyriakis N. Potential of autonomous ground-coupled heat pump system installations in Greece. Applied Energy 2011;88:2122–9. https://doi.org/10.1016/j.apenergy.2010.12.061.

[188] Aditya GR, Narsilio GA. Environmental assessment of hybrid ground source heat pump systems. Geothermics 2020;87:101868. https://doi.org/10.1016/j.geothermics.2020.101868.

[189] Nguyen HV, Law YLE, Alavy M, Walsh PR, Leong WH, Dworkin SB. An analysis of the factors affecting hybrid ground-source heat pump installation potential in North America. Applied Energy 2014;125:28–38. https://doi.org/10.1016/j.apenergy.2014.03.044.

[190] Rad FM, Fung AS, Leong WH. Feasibility of combined solar thermal and ground source heat pump systems in cold climate, Canada. Energy and Buildings 2013;61:224–32. https://doi.org/10.1016/j.enbuild.2013.02.036.

[191] Casasso A, Sethi R. G . POT : A quantitative method for the assessment and mapping of the shallow geothermal potential. Energy 2016;106:765–73. https://doi.org/10.1016/j.energy.2016.03.091.

[192] Schiel K, Baume O, Caruso G, Leopold U. GIS-based modelling of shallow geothermal energy potential for CO 2 emission mitigation in urban areas. Renewable Energy 2016;86:1023–36. https://doi.org/10.1016/j.renene.2015.09.017.

[193] Kljajić MV, Anđelković AS, Hasik V, Munćan VM, Bilec M. Shallow geothermal energy integration in district heating system: An example from Serbia. Renewable Energy 2020;147:2791–800. https://doi.org/10.1016/j.renene.2018.11.103.

[194] Jensen JK, Ommen T, Markussen WB, Elmegaard B. Design of serially connected district heating heat pumps utilising a geothermal heat source. Energy 2017;137:865–77. https://doi.org/10.1016/j.energy.2017.03.164.

[195] Alberg Østergaard P, Mathiesen BV, Möller B, Lund H. A renewable energy scenario for Aalborg Municipality based on low-temperature geothermal heat, wind power and biomass. Energy 2010;35:4892–901. https://doi.org/10.1016/j.energy.2010.08.041.

[196] Carotenuto A, Figaj RD, Vanoli L. A novel solar-geothermal district heating, cooling and domestic hot water system: Dynamic simulation and energy-economic analysis. Energy 2017;141:2652–69. https://doi.org/10.1016/j.energy.2017.08.084.

[197] Formhals J, Feike F, Hemmatabady H, Welsch B, Sass I. Strategies for a transition towards a solar district heating grid with integrated seasonal geothermal energy storage. Energy 2021;228:120662. https://doi.org/10.1016/j.energy.2021.120662.

[198] Unternährer J, Moret S, Joost S, Maréchal F. Spatial clustering for district heating integration in urban energy systems: Application to geothermal energy. Applied Energy 2017;190:749–63. https://doi.org/10.1016/j.apenergy.2016.12.136.

[199] Stegnar G, Staničić D, Česen M, Čižman J, Pestotnik S, Prestor J, et al. A framework for assessing the technical and economic potential of shallow geothermal energy in individual and district heating systems: A case study of Slovenia. Energy 2019;180:405–20. https://doi.org/10.1016/j.energy.2019.05.121.

[200] Blum A, Wyss R. Statistik der geothermischen Nutzung in der Schweiz – Ausgabe 2016. Bern, Switzerland: EnergieSchweiz; 2016.

[201] SIA. Sondes géothermiques (SIA384/6). Swiss Society of Engineers and Architects; 2010.

[202] Pahud D. Geothermal energy and heat storage. 2002.

[203] Eskilson P. Thermal analysis of heat extraction boreholes. University of Lund, 1987.

[204] Stephen P Kavanaugh, Kevin D Rafferty. Geothermal heating and cooling: design of ground-source heat pump systems. ASHRAE; 2014.

[205] Alavy M, Dworkin SB, Leong WH. A design methodology and analysis of combining multiple buildings onto a single district hybrid ground source heat pump system. Renewable Energy 2014;66:515–22. https://doi.org/10.1016/j.renene.2013.12.030.

[206] Foster S, Love J, Walker I, Crane M. Heat pumps in district heating. Final report. Department of Energy & Climate Change 2016.

[207] Li X, Walch A, Yilmaz S, Patel MK, Chambers J. Optimal spatial resource allocation in networks: application to district heating and cooling. Submitted to Computers & Industrial Engineering 2021.

[208] Mohajeri N, Perera ATD, Coccolo S, Mosca L, Le Guen M, Scartezzini J-L. Integrating urban form and distributed energy systems: Assessment of sustainable development

scenarios for a Swiss village to 2050. Renewable Energy 2019;143:810–26. https://doi.org/10.1016/j.renene.2019.05.033.

[209] ASIT VD. Cadastre - MO et NPCS - Thème Biens-fonds 2019. www.asitvd.ch/md/03d4716b-66af-f4d4-99a2-83406987ad32 (accessed January 22, 2020).

[210] SITG. Parcelles de la mensuration 2020. https://ge.ch/sitg/fiche/8450 (accessed March 23, 2020).

[211] Swisstopo. swissTLM3D Version 1.6. Swisstopo; 2018.

[212] ASIT VD. Cadastre de géothermie basse température 2019. www.asitvd.ch/md/f8c427d3-dc9e-4864-c593-f763b122e824 (accessed February 4, 2020).

[213] SITG. Cadastre technique du sous-sol 2019. https://ge.ch/sitg/fiche/6435 (accessed March 25, 2020).

[214] Assouline D, Mohajeri N, Gudmundsson A, Scartezzini J-L. A machine learning approach for mapping the very shallow theoretical geothermal potential. Geothermal Energy 2019;7:19. https://doi.org/10.1186/s40517-019-0135-6.

[215] MeteoSwiss. Daily Mean, Minimum and Maximum Temperature. Federal Office of Meteorology and Climatology MeteoSwiss; 2017.

[216] Swisstopo. swissALTI3D - The high precision digital elevation model of Switzerland 2017. https://shop.swisstopo.admin.ch/en/products/height_models/alti3D (accessed August 13, 2019).

[217] SIA. Klimadaten für Bauphysik, Energie- und Gebäudetechnik (SIA 2028). Swiss Society of Engineers and Architects; 2010.

[218] BFE. Energiestrategie 2050: Erstes Massnahmenpaket. Switzerland: Bundesamt für Energie BFE; 2012.

[219] Kim Y, Lee JS, Jeon SW. Hybrid ground-source heat pump systems. Advances in Ground-Source Heat Pump Systems, Elsevier; 2016, p. 331–57. https://doi.org/10.1016/B978-0-08-100311-4.00012-1.

[220] Ondreka J, Rüsgen MI, Stober I, Czurda K. GIS-supported mapping of shallow geothermal potential of representative areas in south-western Germany—Possibilities and limitations. Renewable Energy 2007;32:2186–200. https://doi.org/10.1016/j.renene.2006.11.009.

[221] Bühler F, Petrović S, Karlsson K, Elmegaard B. Industrial excess heat for district heating in Denmark. Applied Energy 2017;205:991–1001. https://doi.org/10.1016/j.apenergy.2017.08.032.

[222] Tian Z, Zhang S, Deng J, Fan J, Huang J, Kong W, et al. Large-scale solar district heating plants in Danish smart thermal grid: Developments and recent trends. Energy Conversion and Management 2019;189:67–80. https://doi.org/10.1016/j.enconman.2019.03.071.

[223] Zuberi MJS, Bless F, Chambers J, Arpagaus C, Bertsch SS, Patel MK. Excess heat recovery: An invisible energy resource for the Swiss industry sector. Applied Energy 2018;228:390–408. https://doi.org/10.1016/j.apenergy.2018.06.070.

[224] Streicher KN, Mennel S, Chambers J, Parra D, Patel MK. Cost-effectiveness of large-scale deep energy retrofit packages for residential buildings under different economic assessment approaches. Energy and Buildings 2020;215:109870. https://doi.org/10.1016/j.enbuild.2020.109870.

[225] Möller B, Wiechers E, Persson U, Grundahl L, Lund RS, Mathiesen BV. Heat Roadmap Europe: Towards EU-Wide, local heat supply strategies. Energy 2019;177:554–64. https://doi.org/10.1016/j.energy.2019.04.098.

[226] Galindo Fernández M, Roger-Lacan C, Gährs, U, Aumaitre V. Efficient district heating and cooling markets in the EU: Case studies analysis, replicable key success factors and potential policy implications. JRC; 2016. https://doi.org/10.2760/371045.

[227] Sommer T, Sulzer M, Wetter M, Sotnikov A, Mennel S, Stettler C. The reservoir network: A new network topology for district heating and cooling. Energy 2020;199:117418. https://doi.org/10.1016/j.energy.2020.117418.

[228] Boesten S, Ivens W, Dekker SC, Eijdems H. 5Th Generation District Heating and Cooling Systems As a Solution for Renewable Urban Thermal Energy Supply. Advances in Geosciences 2019;49:129–36. https://doi.org/10.5194/adgeo-49-129-2019.

[229] Wirtz M, Neumaier L, Remmen P, Müller D. Temperature control in 5th generation district heating and cooling networks: An MILP-based operation optimization. Applied Energy 2021;288:116608. https://doi.org/10.1016/j.apenergy.2021.116608.

[230] Ahmadisedigh H, Gosselin L. How can combined heating and cooling networks benefit from thermal energy storage? Minimizing lifetime cost for different scenarios. Energy 2022;243:123112. https://doi.org/10.1016/j.energy.2022.123112.

[231] Tunzi M, Ruysschaert M, Svendsen S, Smith KM. Double loop network for combined heating and cooling in low heat density areas. Energies 2020;13. https://doi.org/10.3390/en13226091.

[232] Calixto S, Köseoğlu C, Cozzini M, Manzolini G. Monitoring and aggregate modelling of an existing neutral temperature district heating network. Energy Reports 2021;7:140–9. https://doi.org/10.1016/j.egyr.2021.08.162.

[233] Persson U, Möller B, Werner S. Heat Roadmap Europe : Identifying strategic heat synergy regions. Energy Policy 2014;74:663–81. https://doi.org/10.1016/j.enpol.2014.07.015.

[234] Persson U, Wiechers E, Möller B, Werner S. Heat Roadmap Europe: Heat distribution costs. Energy 2019;176:604–22. https://doi.org/10.1016/j.energy.2019.03.189.

[235] Patureau R, Tran CT, Gavan V, Stabat P. The new generation of District heating & cooling networks and their potential development in France. Energy 2021;236. https://doi.org/10.1016/j.energy.2021.121477.

[236] Østergaard PA, Andersen AN. Booster heat pumps and central heat pumps in district heating. Applied Energy 2016;184:1374–88. https://doi.org/10.1016/j.apenergy.2016.02.144.

[237] Averfalk H, Werner S. Economic benefits of fourth generation district heating. Energy 2020;193:116727. https://doi.org/10.1016/j.energy.2019.116727.

[238] Lund R, Østergaard DS, Yang X, Mathiesen BV. Comparison of low-temperature district heating concepts in a long-term energy system perspective. International Journal of Sustainable Energy Planning and Management 2017;12:5–18. https://doi.org/10.5278/ijsepm.2017.12.2.

[239] Meesenburg W, Ommen T, Thorsen JE, Elmegaard B. Economic feasibility of ultra-low temperature district heating systems in newly built areas supplied by renewable energy. Energy 2020;191:116496. https://doi.org/10.1016/j.energy.2019.116496.

[240] Zarin Pass R, Wetter M, Piette MA. A thermodynamic analysis of a novel bidirectional district heating and cooling network. Energy 2018;144:20–30. https://doi.org/10.1016/j.energy.2017.11.122.

[241] Wirtz M, Kivilip L, Remmen P, Müller D. 5th Generation District Heating: A novel design approach based on mathematical optimization. Applied Energy 2020;260:114158. https://doi.org/10.1016/j.apenergy.2019.114158.

[242] Millar M-A, Yu Z, Burnside N, Jones G, Elrick B. Identification of key performance indicators and complimentary load profiles for 5th generation district energy networks. Applied Energy 2021;291:116672. https://doi.org/10.1016/j.apenergy.2021.116672.

[243] Cimmino M, Bernier M. A semi-analytical method to generate g-functions for geothermal bore fields. International Journal of Heat and Mass Transfer 2014;70:641–50. https://doi.org/10.1016/j.ijheatmasstransfer.2013.11.037.

[244] Claesson J, Eskilson P. Conductive heat extraction to a deep borehole: Thermal analyses and dimensioning rules. Energy 1988;13:509–27.

[245] Chambers J. Computationally scalable geospatial network and routing analysis through multi-level spatial clustering. MethodsX 2020;7:101072. https://doi.org/10.1016/j.mex.2020.101072.

[246] Cimmino M. A finite line source simulation model for geothermal systems with series- and parallel-connected boreholes and independent fluid loops. Journal of Building Performance Simulation 2018;11:414–32. https://doi.org/10.1080/19401493.2017.1381993.

[247] Zarrella A, Emmi G, De Carli M. A simulation-based analysis of variable flow pumping in ground source heat pump systems with different types of borehole heat exchangers: A case study. Energy Conversion and Management 2017;131:135–50. https://doi.org/10.1016/j.enconman.2016.10.061.

[248] Cimmino M, Thorne D, Langevin CD, Sukop MC. Pygfunction : an Open-Source Toolbox for the Evaluation of Thermal Response Factors for Geothermal Borehole Fields. eSim 2018 - IBPSA Canada 2018;32:492–501.

[249] Cimmino M. Fluid and borehole wall temperature profiles in vertical geothermal boreholes with multiple U-tubes. Renewable Energy 2016;96:137–47. https://doi.org/10.1016/j.renene.2016.04.067.

[250] Petkov I, Mavromatidis G, Knoeri C, Allan J, Hoffmann VH. MANGOret: An optimization framework for the long-term investment planning of building multi-energy system and envelope retrofits. Applied Energy 2022;314. https://doi.org/10.1016/j.apenergy.2022.118901.

[251] Meuer J, Lamaro F, Vetterli N. Embedding energy optimization in organizations: A case study of a Swiss decentralized renewable energy system. Energy and Buildings 2021;235:110710. https://doi.org/10.1016/j.enbuild.2020.110710.

[252] Pahud D, Belliardi M, Caputo P. Geocooling potential of borehole heat exchangers' systems applied to low energy office buildings. Renewable Energy 2012;45:197–204. https://doi.org/10.1016/j.renene.2012.03.008.

[253] Belliardi M. Applied analysis of geocooling technology for a residential building in Lugano. Swiss Federal Office of Energy SFOE; 2020.

[254] Lucerne University of Applied Sciences and Arts (HSLU). Heizkostenvergleichsrechner 2.0 [Heating Costs Comparison Calculator] 2019.

[255] Koordinationskonferenz der Bau- und Liegenschaftsorgane der öffentlichen Bauherren KBOB, ecobau, Interessengemeinschaft privater, professioneller Bauherren (IPB). Ökobilanzdaten im Baubereich 2009/1:2022. 2022.

[256] Tarifs et règlements | SIG n.d. https://ww2.sig-ge.ch/particuliers/offres/tarifs-reglements (accessed November 21, 2022).

[257] Streicher KN, Berger M, Panos E, Narula K, Soini MC, Patel MK. Optimal building retrofit pathways considering stock dynamics and climate change impacts. Energy Policy 2021;152:112220. https://doi.org/10.1016/j.enpol.2021.112220.

[258] Köhler B, Moser C, Garzia F, Stobbe M. D4.1: Guideline II: nZEB Technologies: Report on cost reduction potentials for technical nZEB solution sets. 2018.

[259] Tiller M. Introduction to physical modeling with Modelica. vol. 615. Springer Science & Business Media; 2012.

[260] Usher W. The Value of Learning about Critical Energy System Uncertainties. 2016.

[261] Xiang Li, Selin Yilmaz, Martin K. Patel, Jonathan Chambers. Techno-economic analysis of fifth-generation district heating and cooling combined with seasonal borehole thermal energy storage. Under Review 2023.

[262] Mavromatidis G, Orehounig K, Carmeliet J. Uncertainty and global sensitivity analysis for the optimal design of distributed energy systems. Applied Energy 2018;214:219–38. https://doi.org/10.1016/j.apenergy.2018.01.062.

[263] Saltelli A, Ratto M, Andres T, Campolongo F, Cariboni J, Gatelli D, et al. Global sensitivity analysis: the primer. John Wiley & Sons; 2008.

[264] Saltelli A, editor. Sensitivity analysis in practice: a guide to assessing scientific models. Hoboken, NJ: Wiley; 2004.

[265] Massey Jr FJ. The Kolmogorov-Smirnov test for goodness of fit. Journal of the American Statistical Association 1951;46:68–78.

[266] Deng Y, Li Z, Quigley JM. Economic returns to energy-efficient investments in the housing market: Evidence from Singapore. Regional Science and Urban Economics 2012;42:506–15. https://doi.org/10.1016/j.regsciurbeco.2011.04.004.

[267] Gemelli A, Mancini A, Longhi S. GIS-based energy-economic model of low temperature geothermal resources: A case study in the Italian Marche region. Renewable Energy 2011;36:2474–83. https://doi.org/10.1016/j.renene.2011.02.014.

[268] Walch A, Castello R, Mohajeri N, Gudmundsson A, Scartetzzini J-L. Using Machine Learning to estimate the technical potential of shallow ground-source heat pumps with thermal interference. CISBAT 2021 (Accepted for presentation), Lausanne, Switzerland: 2021.

[269] OpenStreetMap Wiki. Elements 2021. https://wiki.openstreetmap.org/wiki/Elements.

[270] Möller B, Persson U. Updated Peta atlas for each MS with the final level of district heating recommended in WP6. 2018.

[271] swisstopo. GeoMaps 500 - Vector. Federal Office of Topography Swisstopo n.d. https://www.swisstopo.admin.ch/en/geodata/geology/maps/gk500/vector.html (accessed June 22, 2021).

[272] VDI. VDI 4640 Blatt 2 - Thermische Nutzung des Untergrunds - Erdgekoppelte Wärmepumpenanlagen. Verein Deutscher Ingenieure; 2019.

[273] Signorelli S, Kohl T. Regional ground surface temperature mapping from meteorological data. Global and Planetary Change 2004;40:267–84. https://doi.org/10.1016/j.gloplacha.2003.08.003.

[274] Müller A, Hummel M, Kranzl L, Fallahnejad M, Büchele R. Open Source Data for Gross Floor Area and Heat Demand Density on the Hectare Level for EU 28. Energies 2019;12:4789. https://doi.org/10.3390/en12244789.

[275] Cozzini M, Trier D, Bava F, Fedrizzi R, Buffa S, Jensen LL, et al. FLEXYNETS Guide Book. FLEXYNETS; 2018.